TUDelft

Delft University of Technology

Downstream Process Development for Bio-based Production of Phenolics

Henriques da Silva, Marcelo

DOI
10.4233/uuid:70c2b43b-e2c0-43e1-9bcf-117703e9b23a

Publication date
2019

Important note
To cite this publication, please use the final published version (if applicable).
Please check the document version above.

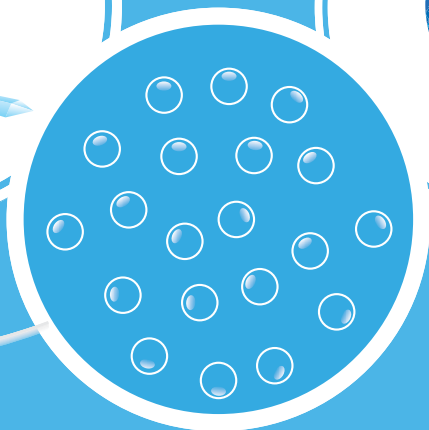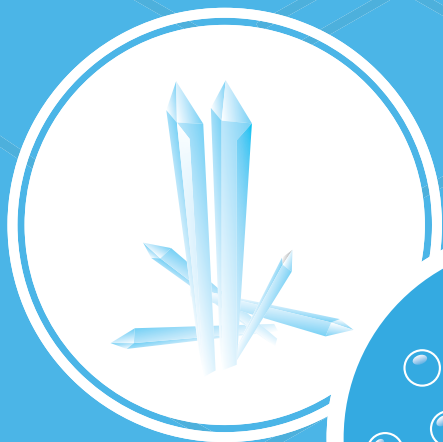# DOWNSTREAM PROCESS DEVELOPMENT FOR BIO-BASED PRODUCTION OF PHENOLICS

MARCELO DAVID HENRIQUES DA SILVA

Downstream Process Development for Bio-Based Production of Phenolics

Dissertation

for the purpose of obtaining the degree of doctor at Delft University
of Technology by the authority of the Rector Magnificus prof.dr.ir.
T.H.J.J. van der Hagen chair of the Board for Doctorates
to be defended publicly on Monday 15 April 2019 at 10:00 o'clock

by

Marcelo David HENRIQUES DA SILVA

Master of Science in Biological Engineering,

University of Lisbon, Portugal

born in Lisbon, Portugal

This dissertation has been approved by the promotors.

Composition of the doctoral committee:

Rector Magnificus	chairman
Prof dr. L.A.M. van der Wielen	promotor
Dr. ir Marcel Ottens	Delft University of Technology, promotor
Prof. dr. L.A.M. van der Wielen	Delft University of Technology, promotor

Independent members:

Prof. dr. M.H.M. Eppink	Wageningen University Synthon Biopharmaceuticals B.V.
Prof J.H. ter Horst	University of Strathclyde
Prof. dr. H.J. Noorman	DSM Biotechnology Center Delft University of Technology
Prof. dr. J.R. van Ommen	Delft University of Technology
Prof. dr. M.R.M.S. Aires-Barros	University of Lisbon

Table of Contents

Chapter 6 Downstream process synthesis for the recovery and purification of polyphenols from afermentation broth **159**

Summary

Polyphenols are molecules with a wide range of bioactive properties. They are being applied as nutraceuticals or natural colorants. The growing interest in these molecules has led to the creation of projects such as the BacHBerry project (www.bachberry.eu), with the main goal of discovering novel polyphenols and tapping their commercial application **(Chapter 1)**. Moreover, the same project targets the synthesis of those secondary metabolites by fermentation, in order to increase process yield and decrease the environmental impact. That shift in the current paradigm, based on the recovery of polyphenols by plant extraction requires the development of different downstream process strategies.

Since the compounds of interest are highly hydrophobic, one of the most logical ways of purifying them from a broth containing mostly polar compounds is by liquid-liquid extraction. The main challenge relies, however, in dealing with the modelling the equilibrium properties of complex molecules as polyphenols. By coupling a semi-predictive thermodynamic model as NRTL-SAC with the well-known Kremser equation, different liquid-liquid extraction scenarios can be developed even for the complex purification of similar hydrophobic polyphenols like naringenin and *trans*-resveratrol **(Chapter 2)**.

Given their application in the food industry, specific requirements might be imposed on the type of chemicals that can contact with polyphenols during the downstream process. Since one of the most commonly accepted food-grade solvents is ethanol, it makes sense to investigate the potential of adsorption for the capture and purification of polyphenols. As most of these compounds are characterized for having a hydrophobic core, hydrophobic adsorption is the clearest option concerning the choice of the resin chemistry. However, the most challenging problem is selectivity, given the low concentration these compounds normally present in aqueous solutions. Using food-grade functionalized resins is one of the ways selectivity can be improved. By using imidazole and pyridine groups attached to hydrophobic resins, the recently developed RENSA resins show adsorption capacities and affinities not seen previously for these

compounds. Moreover, by acidifying the medium (water/ethanol mixture), desorption also proves to be possible despite the strong affinity **(Chapter 3)**.

The development and optimization of a downstream process should obviously take the upstream process into account. For the case of polyphenols, it is suggested that not only they tend to partition into the more lipophilic cell membrane, but they also tend to inhibit cell growth and, consequently, the product titer (*trans*-resveratrol production is growth associated). Thus, a continuous product removal setup from the fermentation broth may not only allow for process intensification, but also to increase production and improve excretion by passive diffusion. Due to several constraints associated with an integrated liquid-liquid extraction process (e.g., solvent corrosion, cell toxicity), the application of hydrophobic macroporous resins is a promising strategy to improve the yield of resveratrol in a fermentation using *C. glutamicum* **(Chapter 4)**.

Since the synthesis of polyphenols proceed through similar metabolic pathways, it is expected the fermentation broth to contain similar, related polyphenols as *trans*-resveratrol and pinosylvin. The presence of chemically related polyphenols that have to be recovered and purified, can highly increase the complexity of the downstream process train. Despite the fact that more selective solvent mixtures might be used in a liquid-liquid extraction step or more selective resins in an adsorption step, the associated cost might be too large to sell these products as food additives, for example. One of the possible solutions can be the application of preferential crystallization, a concept that has been mainly applied to the resolution of enantiomers. This step would be applied after a preliminary purification step using, for example, adsorption. Each of the two crystallizers would contain a solution slightly richer in one of two polyphenols (e.g., naringenin and *trans*-resveratrol) and would contain crystal seeds of that same polyphenol. By controlling the temperature profiles in each vessel and allowing them to exchange their liquid phase, supersaturation is controlled along time in order to maximize the yield of each polyphenol in each reactor, obeying to a minimal required purity of 95% **(Chapter 5)**.

Throughout this thesis different downstream process strategies for hydrophobic polyphenols are proposed. Their advantages and disadvantages are discussed in each chapter, as well as from a techno-economical perspective **(Chapter 6)**.

Samenvatting

Polyfenolen zijn moleculen met een breed scala aan bioactieve eigenschappen. Ze worden o.a. gebruikt als *nutraceuticals* of natuurlijke kleurstoffen. De groeiende interesse in deze moleculen heeft geleid tot het opzetten van onderzoeks- en ontwikkelingsprojecten zoals het "BacHBerry" project (www.bachberry.eu), met als doel het vervaardigen van nieuwe polyfenolen en hun toepassing commercieel te exploiteren **(Hoofdstuk 1)**. Verder heeft het project als doel de synthese van polyfenol gerelateerde secundaire metabolieten door middel van fermentatie, om de opbrengst van het proces te vergroten en de impact op het milieu te verminderen. Dat is een verandering in het heersende paradigma, wat gebaseerd is op het verkrijgen van polyfenolen door plantenextractie, en vereist de ontwikkeling van verschillende innovatieve opwerkingenstrategieën.

De polyfenolen van interesse zijn zeer hydrofoob, en een van de meest logische manieren ze van een fermentatieoplossing (dat voornamelijk polaire moleculen bevat) te scheiden, is door middel van vloeistof-vloeistofextractie. De grootste uitdaging hier is het verkrijgen en goed modelleren van de thermodynamische eigenschappen. Door het samenvoegen van een semi-voorspellend thermodynamisch model zoals NRTL-SAC met de welbekende "Kremser" vergelijking, kunnen verschillende vloeistof-vloeistofextractie scenario's worden ontwikkeld, zelfs voor de complexe isolatie van soortgelijke hydrofobe polyfenolen zoals naringenin en *trans*-resveratrol **(Hoofdstuk 2)**.

Omdat de polyfenolen worden toegepast in de voedingsindustrie worden specifieke eisen gesteld aan chemicaliën die worden gebruikt tijdens de opwerking. Een van de meest bekend "food-grade" oplosmiddelen is ethanol, en het is dan ook logisch om ethanol te gebruiken als oplosmiddel bij het onderzoeken van adsorptie voor de zuivering van polyfenolen. Omdat de meeste van deze moleculen hydrofoob zijn, is hydrofobe adsorptie de meest logische optie, en bepaalt het type hars dat gebruikt wordt. Het meest uitdagende probleem is de selectiviteit van scheiding van de polyphenolen, die een lage concentratie in waterige oplossingen hebben. "Food-grade" gefunctionaliseerde harsen zijn een van de opties om de selectiviteit te verbeteren. Door gebruik te maken van imidazole en pyridine die aan de harsen zijn geimobiliseerd, tonen recent ontwikkelde

"RENSA" harsen niet eerder waargenomen adsorptie capaciteiten en affiniteiten voor polyfenolen. Bovendien kan door de aanzuring van de oplossing (water/ethanolmengsel) desorptie van polyfenolen eenvoudig bewerkstelligd worden **(Hoofdstuk 3)**.

De ontwikkeling en optimalisatie van een opwerkingsproces moet rekening houden met het *upstream* proces (fermentatie). Polyfenolen hebben ze de neiging zich te vestigen in het meer lipofiele celmembraan, en hebben ook de neiging om celgroei te remmen. Bijgevolg remmen zij ook de concentratie van het eindproduct (de productie van o.a. *trans*-resveratrol is geassocieerd met de celgroei). Dus een continue productverwijderingsstap gedurende de fermentatie, zal de productie verhogen en de uitscheiding van polyfenolen uit de cellen door passieve diffusie verbeteren. Dit is een vorm van procesintensificatie. Vanwege verschillende beperkingen in verband met een geïntegreerd vloeistof-vloeistof-extractieproces (b.v. corrosie, celtoxiciteit), is gekeken naar adsorptie. De toepassing van hydrofobe macroporeuze harsen in continue productverwijderingsstap gedurende de fermentatie, blijkt een veelbelovende strategie om de opbrengst aan *trans*-resveratrol in een *C. glutamicum* fermentatie te verbeteren **(Hoofdstuk 4)**.

Omdat de synthese van polyfenolen via vergelijkbare metabole routes verloopt, wordt verwacht dat de fermentatie oplossing soortgelijke en gerelateerde polyfenolen bevat (e.g., *trans*-resveratrol, pinosylvin). De aanwezigheid van chemisch verwante polyfenolen die moeten worden gezuiverd, kan de complexiteit van het opwerkingprocesproces verhogen. Ondanks dat meer selectieve oplosmiddelmengsels in een vloeistof-vloeistof-extractiestap, of meer selectieve harsen in een adsorptiestap kunnen worden gebruikt, kunnen de bijbehorende kosten te hoog worden om deze producten bijvoorbeeld als voedseladditieven te verkopen. Een van de mogelijke oplossingen kan preferentiële kristallisatie zijn, een proces dat hoofdzakelijk is toegepast op de resolutie van enantiomeren. Deze processtap zou kunnen worden toegepast na een zuiveringsstap met behulp van adsorptie. Elk van de twee kristallisatoren zou een oplossing bevatten die enigszins rijker is in een van de twee polyfenolen (b.v. naringenin, *trans*-resveratrol) en zou kristalkiemen van dezelfde polyfenol bevatten.

Door de temperatuurprofielen in elk vat te regelen en door de vloeibare inhoud uit te wisselen, kan oververzadiging continu worden gehandhaafd om de kristal opbrengst van elk polyfenol in de respectieve kristallisator te maximeren zodat een minimaal vereiste zuiverheid van 95% kan worden bereikt (**Hoofdstuk 5**).

In dit proefschrift zijn verschillende opwerkingprocesstrategieën voor hydrofobe polyfenolen voorgesteld. Voor- en nadelen van elke strategie worden in elk hoofdstuk besproken. Een gedetailleerd technisch-economisch perspectief wordt uiteindelijk geschetst in een separaat hoofdstuk **(Hoofdstuk 6)**.

1

INTRODUCTION

1.1 BACKGROUND AND MOTIVATION

In the last years, interest on the bioactive properties of polyphenols has been growing.[1, 2] These aromatic molecules usually have a significant number of relatively stable resonance structures, making them known radical scavengers.[3] This property has been associated, for example, with their protecting activity against neurological and cardiovascular diseases.[4] One of most well-known cases is the one of *trans*-resveratrol (Figure 1.1a).

Besides their antioxidant properties, some polyphenols are also be used as colorants. Molecules like delphinidin (Figure 1.1b) and pelargonidin (Figure 1.1c) are examples of anthochyanins that span different colors, making them a promising replacement for synthetic dyes.[5]
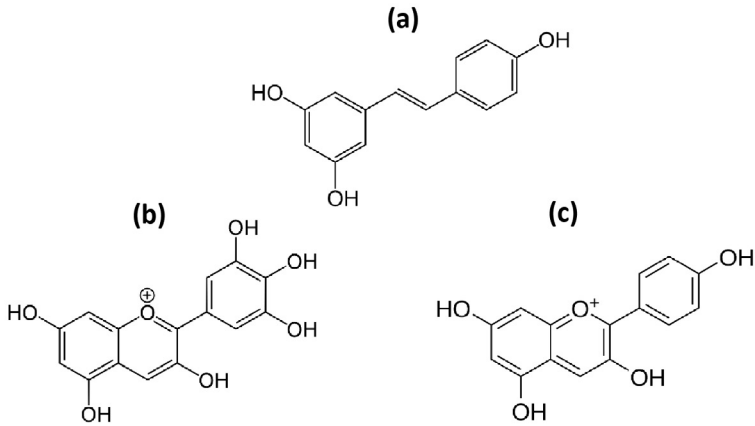
Figure 1.1 – Several polyphenols that have properties of interest for the biotechnological industry. *Trans*-resveratrol (a) has been associated with protective health effects. Delphinidin (b) and pelargonidin (c) are used as natural colorants.

Due to the increasing awareness of the average consumer, the market for polyphenols has been growing over the last years and it is expected to reach 850 Million USD by 2018.[6] Universities and companies are involved in projects that further explore the properties of polyphenols and implement processes that can be both profitable and environmentally-friendly. One of such projects is the European funded BacHBerry (BACterial Hosts for production of Bioactive phenolics from bERRY fruits) project (http://www.bachberry.eu). This project was split into different packages that focused on every step from bioprospecting to production process implementation at a large-scale (Figure 1.2).
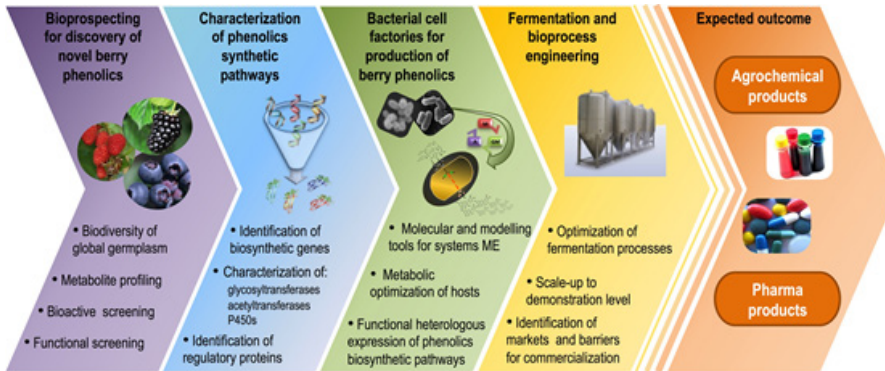
Figure 1.2 – Illustration of the different steps involved in the BacHBerry project, from the bioprospecting of novel phenols to their large-scale production.[7]

In its activities, the BacHBerry consortium had the following objectives in mind:[4] (i) to systematically analyze the phenolic contents in the large berry germplasm collections available from consortium members, (ii) to establish a publicly-available database of transcriptomic and metabolic data obtained from berry bioprospecting within, as well as outside of the project, (iii) to discover novel bioactivities in berry extracts against a range of human pathologies, such as Alzheimer's disease and Amyotrophic Lateral Sclerosis (ALS), by high-throughput screening with subsequent identification of functional biomolecules, (iv) to identify the corresponding biosynthetic genes and perform functional characterization of the respective gene products, (v) to assay a selection of the biosynthetic genes for functionality in Gram-positive bacterial hosts and use those to construct bacterial cell factories for phenolic production, (vi) to improve the production efficiency further by introducing modifications to the host metabolic networks predicted via rational design or computational tools developed within the project, (vii) to design and optimize cost-effective food-grade methods for extraction of phenolic compounds from bacterial fermentation broth, and (viii) to optimize fermentation conditions and subsequently upscale the production to pilot plant levels. All these activities are detailed in Table 1.1.

The main task of the Technical University of Delft (TU Delft) within the BacHBerry project, was the development of a downstream process

strategy for the recovery and purification of different polyphenols, produced by fermentation. In that sense, the project partners with which TU Delft was most actively involved were the Technical University of Denmark (DTU) and the Jülich Research Center, which were developing the microbial strains for the fermentation process and Biotempo, a company located in Portugal that was responsible for the process scale-up and the optimization of the fermentation conditions. The cooperation between those project partners allowed to address some of the most important questions when developing the downstream process, which are addressed in the following sections:

- What is the exact composition of the fermentation medium and how can it affect the downstream process design?

- What are the expected fermentation by-products?

- Are there multiple co-produced polyphenols?

1

Table 1.1 - Summary of the outcomes of the BacHBerry project.[4]

Specific application area in project	Bioprospecting for discovery of novel berry phenolics	Characterization of phenolics biosynthetic pathways
General aims of BacHBerry	**To tap into the biodiversity of berries from around the globe and of their phenolics content**	**Identification and characterization of berry phenolics biosynthetic pathways**
Achievements of the project	Standardization of methodologies for harvesting, extract preparation, phenolics content assessment and fractionation Metabolomics data from berry species originating from UK, mainland Europe, Russia, Chile, and China was obtained and made available in form of an online database Implementation of robust assays based on the SMART platform for discovery of bioactivity and functionality. Obtained berry extracts were assayed for bioactivity against several human diseases, and additionally evaluated for other functional uses (eq. food additives, antimicrobials). Bioactivities against Alzheimer's, Parkinson's and Huntington's diseases, Amyotrophic Lateral Sclerosis and inflammation were detected. Several pure bioactive effector compounds were identified and validated	Transcriptomes of 13 germplasms spanning eight genera, seven families and seven orders were generated and analyzed New algorithms for functional genomics and improved computational methods for pathway identification were established Over 4000 candidate genes for various biosynthetic steps, transport and regulation of polyphenol production were identified Biochemical activities of some of the gene candidates were tested, thus validating the predictions

1

Specific application area in project	Bacterial cell factories for production of berry phenolics	Fermentation and bioprocess engineering
General aims of BacHBerry	**Design and generation of bacterial cell factories for production of high-value berry phenolics**	**Implementation of production of high-value phenolics in fermenters up to demonstration scale**
Achievements of the project	*L. lactis* strains were engineered for stilbene (*trans*-resveratrol and pterostilbene) and anthocyanin production Production of various stilbenes (*trans*-resveratrol, pinosylvin, and piceatannol), methylated stilbenes (pinostilbene and pterostilbene), flavanones (naringenin, pinocembrin, and eryodictiol), and flavonols (kaempferol and quercetin) was achieved in *C. glutamicum* with yields comparable to those obtained in the model organism *E. coli*. Production titers for the produced flavonols are the highest titers obtained in engineered microorganism until today Polyphenol production was further improved by engineering enhanced precursor supply (eq. L-tyrosine, malonyl-CoA) via rational design, modeling-based prediction, and use of biosensors Alternative biosynthetic routes were explored though engineering of *trans*-resveratrol production from 4-hydroxybenzoic acid (HBA) in *C. glutamicum* Computational models were developed allowing predicting a minimal set of modifications needed for improved polyphenol production in both a single-strain population and a consortium of two or more species	Cultivation conditions for improved productivity were developed for both *L. lactis* and *C. glutamicum* through optimization of fermentation parameters (batch versus fed-batch operation, substrate and dissolved oxygen concentration, etc.) Whey was evaluated as an alternative carbon source for polyphenol production in *L lactis* Multiple bioseparation methods for extraction of produced polyphenols from fermentation broth were evaluated Two possible designs for a system for continuous product removal from the fermentation broth were implemented Resveratrol production in *C. glutamicum* was scaled up from shake flask to 5 l fermenter to demonstration scale (250 l)

1

1.2 Synthesis of polyphenols using Gram-positive bacteria: *Corynebacterium glutamicum*

The current state of the art for the production of secondary metabolites relies mostly on plant extraction or, to a less extent, on chemical synthesis.[8, 9] However, both strategies present some hurdles difficult to overcome. Plant extraction strategies are limited by factors such as low natural abundance, seasonal conditions or complex downstream processing. Chemical synthesis, on the other hand, requires harsh or toxic solvents and can be difficult to apply to more complex molecules.[8] One of the goals of the BacHBerry project was then to be able to produce the desired polyphenols by microbial fermentation. With this strategy, not only a more environmentally-friendly process could be obtained as a simpler downstream process could be devised.[9]

When selecting the host organisms to produce bio-based polyphenols, two criteria were taken into account: (1) they had to be robust, well-studied organisms with a long-standing history of industrial use and (2) the bacteria must have a generally regarded as safe (GRAS) status and/or be recognized as food-grade.[4] One of possibilities that was then considered was *Corynebacterium glutamicum*. This microorganism is used in industrial biotechnology for the production of bulk chemicals (namely aminoacids) and is very robust, showing high resistance to the presence of small aromatic compounds like polyphenols.[4]

During the BacHBerry project, *C. glutamicum* was engineered in order to be able to synthesize polyphenols of interest such as *trans*-resveratrol or naringenin. Eventually a strain, *C. glutamicum* DelAro[4], was developed that could produce those compounds directly from glucose (Figure 1.3).[4]

1
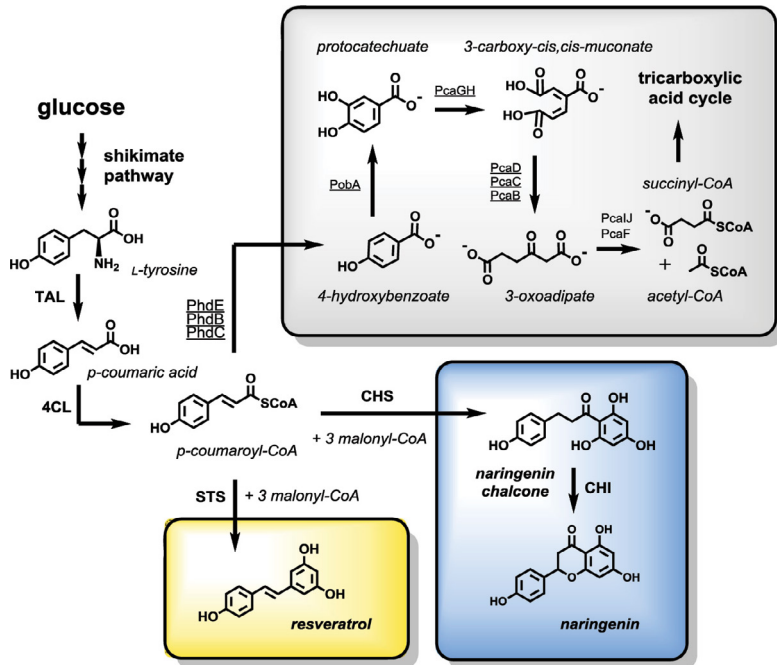
Figure 1.3 - Overview of the endogenous phenylpropanoid degradation and the engineered pathway for polyphenol synthesis in *C. glutamicum*. One of the precursors for the production of the stilbene *trans*-resveratrol (catalyzed by stilbene synthase, STS) or for naringenin chalcone (catalyzed by chalcone synthases, CHS) is *p*-coumaroyl-CoA. Naringenin chalcone isomerizes to the (2*S*)-flavanone naringenin either spontaneously or catalyzed by the activity of chalcone isomerase (CHI). In *C. glutamicum*, *p*-coumaric acid can be degraded to 4-hydroxybenzoate by a CoA-dependent, -oxidative deacetylation pathway. 4-Hydroxybenzoate is subsequently hydroxylated to protocatechuate, which is catabolized to succinyl-CoA and acetyl-CoA by the -ketoadipate pathway. Genes coding for the underlined enzymes were deleted in the course of the construction of the platform strain *C. glutamicum* DelAro⁴.[4]

In most cases still, the proper phenylpropanoid precursor (e.g., cinnamic acid, *p*-coumaric acid, caffeic acid) has to be added to the medium in order to obtain the desired final product.[10]

Given the diagram depicted in Figure 1.3, it is possible to have an idea of the expected impurities in the broth which are associated with the metabolic pathways for the production of polyphenols.

Some of them are, for example, 4-hydroxybenzoate and fatty acids such as linoleic or stearic acid (data from the project partners). Those result from the conversion of phenylpropanoids to succinyl-CoA and acetyl-CoA, which are ultimately used in the tricarboxylic acid cycle.[4] Other impurities are the non-consumed intermediates (e.g., *p*-coumaric acid) and other related polyphenols which might be co-produced. As depicted in Figure 3, if both STS and CHS enzymes are available, both *trans*-resveratrol and naringenin can be produced from *p*-coumaric acid.

1.2.1 Fermentation medium composition

Apart from knowing the molecules involved in the metabolic pathways that lead to the synthesis of polyphenols, the composition of the fermentation medium itself is as important for the downstream process design. During the BacHBerry project, the role of one of the project partners – Biotempo – was the development of an economically feasible and sustainable process. Therefore, one of their focus areas was on the minimization of the operation and investment cost,[4] which involves both upstream and downstream process costs. For that reason, the performed fermentation batches during the project when using *C. glutamicum* used only the CGXII defined medium, with pH control being done with automatic acid/base addition and without adding any cerulenin (a fatty acid synthesis inhibitor).

The composition of the CGXII medium, without any MOPS buffer (pH is automatically controlled), is mostly composed of glucose, salts and small concentrations of IPTG (heterologous gene expression inducer), biotin (vitamin) and protocatechuic acid. Since most of those compounds are highly hydrophilic, they should be relatively easy to separate from the polyphenols of interest, which are usually highly hydrophobic. Proteins and DNA, which are normally released to the medium during the fermentation, should be easily removed by ultrafiltration.

1.3 CHEMICAL PROPERTIES OF POLYPHENOLS

The knowledge of the chemical properties of polyphenols is of great importance to the downstream process development. Knowing which molecules they are and how do they differ from the remaining broth components, makes it easier to look for the best approach to their purification.

Polyphenols are, in most cases, molecules which are characterized by having multiple phenol rings (Figure 1.1). This not only provides them with a significant hydrophobic area, making them almost water-insoluble, but also with a varying number of hydroxyl groups, which can participate in hydrogen bonding.

Another relevant aspect is that most of the polyphenols of interest are neutral molecules, at least in their pH range of stability (usually acidic pH). The same does not happen, for example, with the polyphenol precursors such as caffeic acid or *p*-coumaric acid, which are weak acids and can be negatively charged at neutral pH.

As mentioned previously, most of the impurities present in the fermentation broth are hydrophilic molecules (with the exception of fatty acids and possible similar polyphenols) or molecules, such as proteins and DNA, which differ greatly in size. For that reason, and considering the chemical properties of polyphenols, the following driving forces for separation were considered during this thesis:

- Size difference (removal of cells, proteins, DNA)

- Difference in hydrophobicity (possible capture and purification step)

- Difference in hydrophobicity and hydrogen bonding (possible capture and purification step)

- Difference in solubility (hydrophobicity) and crystallization kinetics (possible purification step)

1.4 Designing the recovery and purification process of polyphenols

The research question this thesis tries to address is: for different polyphenol purification scenarios, and considering the design constraints, what is the most economical and environmentally-friendly downstream process design?

This question was first addressed by sketching the different downstream process designs that could meet both technical feasibility and the process constraints. Those constraints are, in first place, defined by the product stability. Since polyphenols are usually more stable at low temperatures and low pH, the criteria in Table 1.3 were defined.

Table 1.2 – **Temperature and pH windows where polyphenols have higher stability.**

Parameter	Window
Temperature	< 45°C
pH	< 7

Given the above-mentioned criteria and taking into account the chemical characteristics of both polyphenols and the impurities, unit operations that could possibly be used in the downstream process are liquid-liquid extraction, reverse-phase adsorption and crystallization. Those were the only ones given, having assumed that cells could be removed by centrifugation or microfiltration and that larger molecules (e.g., protein, DNA) could be removed by ultrafiltration.

Having defined possible unit operations for the purification of the desired polyphenols, other constraints have also to be addressed and those are process constraints. Given that the produced polyphenols may find application in both pharma and food industries, it was checked in the literature what materials and solvents complied with either FDA rules or ICH guidelines (Table 1.3).

Table 1.3 – Legislation to which some of the resins and solvents mentioned in this chapter comply to.

Resin	Compliance
Reverse-phase resins	21 CFR 173.65
Ion exchange resins	21 CFR 173.25
Functionalized reverse-phase resins	-

Solvent	Compliance
Heptane	ICH Class 3
Ethyl acetate	ICH Class3 / 21 CFR 182.60
Isobutyl acetate	ICH 3
Ethanol	ICH Class 3 / 21 CFR 184.1293

From what is possible to observe in Table 1.3, downstream process strategies using only reverse-phase resins, ethanol and ethyl acetate are the ones that comply with more rules and guidelines. In case functionalized reverse-phase resins are used, preliminary acceptance from regulatory agencies such as the FDA has to be obtained. If solvents like heptane or isobutyl acetate need to be used, although their application in a pharma-oriented process might be feasible, their usage in a food-grade process might be limited.

Having stated the research question, the possible downstream process strategies (conceptually) and the project constraints (product and process), the following chapters of this thesis deal with the techno-economic feasibility study of different strategies, including liquid extraction (with one or two associated columns), reverse-phase adsorption (with possible integration with the fermentation and considering functionalized resins as well) and preferential crystallization. Not only this thesis addresses those points from a perspective of a process engineer, but also at a more fundamental level, with the goal of enabling the conclusions taken in this thesis to be extended to different polyphenols and even other chemically related compounds.

1.5 Thesis outline

The work developed during this thesis had in mind the development of feasible downstream process strategies for the purification of polyphenols found within the BacHBerry project (**Chapter 1**).

The fact that these polyphenolic compounds are much more hydrophobic than the remaining broth components, introduces liquid-liquid extraction as a possible purification unit operation (**Chapter 2**).

An effort has been put in finding food-grade microbial strains and developing a food-grade process. For that reason, a harsh constraint is put on the solvents that can be used in a liquid-liquid extraction process. An alternative might then be reverse-phase adsorption, which can use food-grade resins as selective adsorbents and water/ethanol mixtures as eluent (**Chapter 3**).

Polyphenols are known to act as anti-bacterial agents, thus inhibiting cell growth above a certain threshold. Moreover, hydrophobic polyphenols such as *trans*-resveratrol tend to partition towards the lipophilic cell membrane rather than to aqueous solutions. Those two factors combined can impart the obtained polyphenol yield in a fermentation process, when the desired molecule is expected to be recovered in the extracellular medium after passively diffusing through the cell membrane. The integration of reverse-phase adsorption with batch fermentation in a continuous removal set-up is described in **Chapter 4**.

As introduced in this chapter, the polyphenol biosynthetic pathways present in plants and now also introduced in microorganisms are inter-related. That means that in a typical fermentation broth, more than one polyphenol may be present (e.g., *trans*-resveratrol and naringenin) and the recovery and purification of them both might be desired. Although liquid-liquid extraction and reverse-phase adsorption might still consist in good options, the added complexity and cost (e.g., more expensive resins and higher energy consumption), might render the process economically unattractive. Preferential crystallization, a technique normally used for the resolution

of enantiomers, might then become a better option to take into consideration (**Chapter 5**).

One of the most important goals of the BacHBerry project was the construction and economical evaluation of different downstream processes for the purification of polyphenols. Given the wide diversity of polyphenols existent in nature and the difficulty in predicting their thermodynamic properties, process development was focused on hydrophobic polyphenols such as *trans*-resveratrol and naringenin. The reason being that most of the effort being put in the microbial pathway engineering, was being done for similar molecules (e.g., kaempferol, quercetin, pinostilbene and pterostilbene).

Having put together all the findings made throughout the previous chapters of this thesis and combining them into the Aspen Plus process simulator, made it possible to study and economically evaluate different downstream process alternatives for two scenarios of interest: the recovery of *trans*-resveratrol from a *C. glutamicum* broth (1); the recovery and purification of both *trans*-resveratrol and naringenin from a similar broth (2). Liquid-liquid extraction, reverse-phase adsorption and preferential crystallization were all studied and compared in this analysis (**Chapter 6**).

1

References

1 Rasouli, H.; Farzaei, M. H.; Khodarahmi, R., Polyphenols and their benefits: A review. *International Journal of Food Properties* **2017,** 20, 1700-1741.

2 Karam, J.; Bibiloni, M. D.; Tur, J. A., Polyphenol estimated intake and dietary sources among older adults from Mallorca Island. *Plos One* **2018,** 13, (1).

3 Higdon, J. V.; Frei, B., Tea catechins and polyphenols: health effects, metabolism, and antioxidant functions. *Crit Rev Food Sci Nutr* **2003,** 43, (1), 89-143.

4 Dudnik, A.; et al., BacHBerry: BACterial Hosts for production of Bioactive phenolics from bERRY fruits. *Phytochemistry Reviews* **2017,** 17, (2), 291-326.

5 Khoo, H. E.; Azlan, A.; Tang, S. T.; Lim, S. M., Anthocyanidins and anthocyanins: colored pigments as food, pharmaceutical ingredients, and the potential health benefits. *Food Nutr Res* **2017,** 61, (1), 1361779.

6 Aranaz, I.; Acosta, N.; N Mengíbar, M.; Calderón, L.; Harris, R.; Heras, Á., InFiQuS: Making the Best of Leftovers. In *Industrial Biorenewables: A Practical Viewpoint*, María, P. D. d., Ed. John Wiley & Sons, Inc.: 2016.

7 BacHBerry Project. http://www.bachberry.eu/ (06-07-2018).

8 Zhao, L.; Shao, Z.; V Shanks, J., Anticancer Drugs. In *Industrial Biotechnology: Products and Processes*, Wittmann, C.; C. Liao, J., Eds. Wiley VCH Verlag GmbH & Co. KGaA: 2016.

9 Chouhan, S.; Sharma, K.; Zha, J.; Guleria, S.; Koffas, M. A. G., Recent Advances in the Recombinant Biosynthesis of Polyphenols. *Front Microbiol* **2017,** 8, 2259.

(10) Milke, L.; Aschenbrenner, J.; Marienhagen, J.; Kallscheuer, N., Production of plant-derived polyphenols in microorganisms: current state and perspectives. *Appl Microbiol Biotechnol* **2018,** 102, (4), 1575-1585.

2

___

Liquid-liquid extraction for the recovery of polyphenols

Abstract

Liquid-liquid extraction (LLE) can be an effective strategy for the purification of polyphenols from a fermentation broth. However, a careful selection of the proper solvent is needed for an adequate process design. For that purpose, a systematic study is needed, including the prediction of polyphenol partition coefficients through thermodynamic models. In this work, four polyphenols were considered: naringin, naringenin, p-coumaric acid, and trans-resveratrol. Their partition coefficient in different solvents was measured and described using the Nonrandom Two-Liquid Segment Activity Coefficient model (NRTL-SAC). The average absolute deviation, based on the activity coefficient, was of 56%. For regressing the needed parameters, available solubility data was used. The obtained model made it possible to describe the adequate solvent, or solvent mixture, for two purification scenarios: the recovery of trans-resveratrol and the purification of both naringenin and trans-resveratrol from a typical broth. For those two scenarios, a conceptual downstream process was also proposed.

2.1 Introduction

Polyphenols are compounds that have interesting health benefits alongside other diverse (biotechnological) applications (e.g., colorants, nutraceuticals).[1] These molecules are secondary metabolites naturally produced by plants, which can act as radical scavengers due to the high stabilization provided by ring aromaticity.[2] Over the last years, research on their health properties has grown considerably,[3] with authors studying the properties of these molecules in the prevention of diseases such as Alzheimer and several types of cancer.[4]

Although these compounds are mostly obtained by plant extraction, there has been a growing interest in their production using fermentation processes, mainly due to sustainability issues.[5] The fact that the titers achieved for these molecules are usually low,[5] demands that efficient downstream process strategies are developed in order to attain economic feasibility. One of the possible strategies that might combine simplicity and lower costs is liquid-liquid extraction (LLE).

LLE can be a suitable option for the recovery and purification of polyphenols. Not only it can offer high flexibility, but it is also adequate when the product of interest is heat-sensitive and when the feed stream is dilute.[6] One of the critical issues in the design of a LLE process is solvent selection, which has to provide – among other characteristics –, extraction capacity, selectivity and good mass transfer.[7] For the particular case of polyphenols, there is no systematic study, to the best knowledge of the authors, concerning the adequacy of different solvent chemical classes for the recovery and purification of polyphenols. In order to perform that study, not only a reliable thermodynamic model is needed to describe their equilibrium properties, but this model also needs to have predictive capabilities.[8-10] Although some models have already been applied to describe the solubility of polyphenols in different solvents (e.g., NRTL-SAC, MPP-UNIFAC, etc.),[11, 12] they were scarcely applied to liquid-liquid equilibrium data. One of the possibilities is using a model like COSMO-RS,[13] but some of the disadvantages, though, is that its predictive quality is still inferior to other models as UNIFAC

or NRTL-SAC.[14] On the other hand, group contribution models like UNIFAC are attractive, but a drawback is that group contribution does not take proximity effects into account,[15] which are likely very important in molecules with multiple strong functional groups, like polyphenols.[16] Moreover, some chemical groups present in polyphenols are still not accurately modeled and the equilibrium data present in literature is not abundant. [12] Due to all the reasons mentioned above, the NRTL-SAC model[17] might be one of the best options available. It is an activity coefficient model that takes both excess enthalpy and excess entropy into account and that uses four molecular descriptors to characterize any molecule (X is a parameter related to hydrophobicity, Y^- and Y^+ to polarity and Z to hydrophilicity) and only a relative small amount of equilibrium data is needed to regress those parameters.[18] This model has already been applied to describe solubility of polyphenols, but rarely to liquid-liquid equilibrium, despite being widely used for that purpose. [7]

In this work, four model polyphenols were selected: naringenin (flavonoid), naringin (glycosylated flavonoid), *trans*-resveratrol (stilbene) and *p*-coumaric acid (phenolic acid) (Figure 2.1). Their partition coefficients in different solvents were predicted using NRTL-SAC and the results compared with obtained experimental data. The regressed molecular descriptors were then used to unveil which solvent properties were desirable (degree of hydrophobicity, polarity and hydrogen bonding) for the purification of the studied polyphenols from a fermentation broth. The obtained results were ultimately used to suggest possible process configurations that can be applied to the downstream process of those compounds in two proposed situations: recovery of *trans*-resveratrol from a stream containing hydrophilic components (including *p*-coumaric acid) and recovery and purification of two similar hydrophobic polyphenols: *trans*-resveratrol and naringenin, from a fermentation broth.

In the following section, a description of the used materials and methods is given, including a short description of the thermodynamic model employed. The main obtained results and their discussion is presented on section 2.3 and the conclusions are included in section 2.4.

(S)-naringin

(S)-naringenin

trans-resveratrol

_p_-coumaric acid
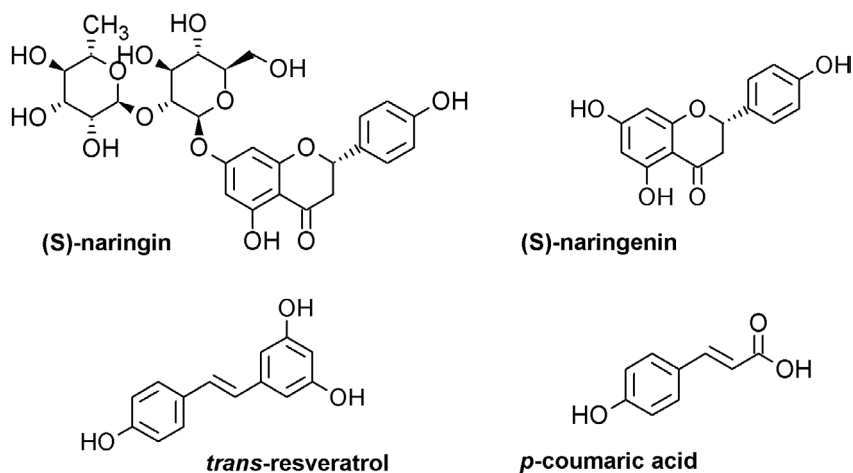
Figure 2.1 — Chemical structure of the polyphenols studied in this work.

2.2 MATERIALS AND METHODS

2.2.1 Chemicals

For the preparation of all the solutions, Milli-Q grade water was used. The polyphenol _trans_-resveratrol ≥98% was obtained from Olon S.P.A (Italy) for Evolva. Naringenin (natural (US), 98%, lot #MKBW8466V), naringin (≥95% (HPLC), lot #BCBM4171V) and _p_-coumaric acid ≥98% (lot #BCBR8319V) were purchased from Sigma-Aldrich. The used organic solvents are indicated in Table 2.1.

Table 2.1 – List of solvents used for the experiments performed in this work.

Solvent	Supplier	Purity
Heptane	Sigma-Aldrich	Anhydrous ≥ 99% (GC)
Acetonitrile	Sigma-Aldrich	HPLC Plus, ≥99.9%
Isobutyl acetate	Fluka	Puriss ≈ 99%
Butyl acetate	Fluka	Purum ≥ 98.5%
MTBE	Fluka	Anhydrous, 99.8%
1-Octanol	Sigma-Aldrich	ACS reagent ≥ 99%
HCl 37% w/w	Sigma-Aldrich	ACS reagent 37%

2.2.2 Partition coefficient determination

The partition coefficient of the used compounds was performed by the shake-flask method,[19] at the constant temperature of 25°C. The experiments were performed in 15 mL Falcon tubes, using a liquid volume between 9 to 10 mL. The phase ratios were selected based on a preliminary guess of the partition coefficient and, in most instances, a 1:1 ratio was used. The tubes were shaken for 1h30 in a Sartorius® Certomat BS-1 at 320 rpm (kinetic experiments were performed in order to check this was time enough to achieve equilibrium). Afterwards, the tubes were centrifuged at 4000 rpm and 25°C for 3 minutes. Samples were then taken from both phases and analyzed by UHPLC.

For the experiments with *p*-coumaric acid, due to its acidic character which might influence partition, the aqueous phase consisted of a 10 mM HCl aqueous solution, in order to assure that the molecule would be in its neutral form.

2.2.3 Polyphenol determination by UHPLC

The quantification of *p*-coumaric acid, *trans*-resveratrol and naringenin was carried out by UHPLC (Ultimate 3000, Thermo Scientific, USA) in a C18 column (Acquity UPLC HSS column, 1.8μm, 2.1mm x100 mm Waters, Milford, USA). Mobile phase A consisted of 10% formic acid in Milli-Q water and mobile phase B of 10% formic acid in acetonitrile. Every run was performed in isocratic mode, with the mobile phase containing 33.5% of B and 66.5% of A and flowing at 0.30 mL/min. The detection of *p*-coumaric acid was performed at 340 nm, that of *trans*-resveratrol at 304 nm, naringenin at 289 nm and naringin at 283 nm.

2.2.4 The NRTL-SAC model

The NRTL-SAC model is an excess Gibbs energy model, based on the polymer NRTL model. The activity coefficient of a given

compound is taken to be the sum of a combinatorial (enthalpic) contribution and a residual (entropic) contribution:

$$\ln(\gamma_i) = ln\left(\gamma_i^C\right) + ln\left(\gamma_i^R\right) \qquad (2.1)$$

The main difference from the original model is that instead of modeling the Van der Waals interactions in a *per molecule* basis, the molecules are represented by four conceptual segments: X, Y+, Y- and Z. Each of these segments represents the hydrophobic, polar and hydrophilic character of each molecule and the interaction energies between each segment are pre-defined.[17] The full mathematical treatment of this model can be found elsewhere.[17]

In this work, the four parameters (X, Y+, Y- and Z) were regressed using solid-liquid equilibrium (SLE) data, available on the literature.[20-24] To relate the activity coefficient of the molecule in solution to its solubility, a simplified equation of the solid-liquid equilibrium relation was used: [25, 26]

$$ln(\gamma_i \cdot x_i) = \frac{\Delta H_m}{RT_m}\left(\frac{T_m}{T} - 1\right) \qquad (2.2)$$

Using the previous equation to describe solid-liquid equilibrium carries some approximations, among them:[29]

- The melting temperature of a given compound is close enough to its triple point temperature;

- The solvent is insoluble in the crystal lattice;

- The difference between the liquid and the solid heat capacities is considered negligible when compared to the fusion enthalpy;

- It is assumes that the solid-liquid transition occurs at a defined temperature point (the triple point temperature).

As most of the above-mentioned approximations are not far from reality, eq. 2.2 has been applied before to the description of the solid-liquid equilibrium of polyphenols and found adequate.[28] For the case of naringin, however, one was confronted with a particular problem: some literature mentions that it is able to crystallize[30] (e.g., in water, as an octa-hydrate and with a melting temperature of 83°C); another study suggests that it does not solidify in a crystalline structure and does not have a defined melting point.[31] In both cases, the approximations contained in eq. 2.2 may no longer be valid (either the water of hydration is not taken into account or there is no defined melting point). Owing to that, two approaches were followed in this case: in one of them, an equation with the same structure as eq. 2.2 was used, but leaving the melting temperature and enthalpy as regressing parameters; in the other one, the relation between the liquid-liquid partition coefficient and the activity coefficient of the molecule in the aqueous and the organic phases was used instead:[19]

$$\frac{C_{i,org}}{C_{i,aq}} \cdot \frac{\overline{V}_{org}}{\overline{V}_{aq}} = P \cdot \frac{\overline{V}_{org}}{\overline{V}_{aq}} = \frac{\gamma_{i,aq}}{\gamma_{i,org}} \tag{2.3}$$

Where P is the volume-based partition coefficient, $\overline{V}_{org}$ the molar volume of the organic phase and V_{aq} the molar volume of the aqueous phase. Thus, the liquid-liquid equilibrium data obtained in this work for naringin was, in this last approach, not predicted using the NRTL-SAC model. Instead, it was only used for the purpose of parameter estimation.

2.3 Results and discussion

2.3.1 Model validation using SLE data and solvent screening for LLE

The analyzed molecules in this work were selected from different polyphenol chemical classes. In that way, different downstream processes could be pictured, and a more general overview of

the NRTL-SAC model prediction capabilities could be obtained. Both naringenin and naringin are flavonoids, although naringin has two additional sugar moieties, rendering it more hydrophilic. The molecule *trans*-resveratrol is a hydrophobic stilbenoid, while *p*-coumaric acid is a phenolic acid.

As previously mentioned, the data used for the regressed parameters for the NRTL-SAC model was obtained from different solid-liquid equilibrium data sets, which are available in the literature. The used references are described in Table A1 (Appendix).

For the case of *p*-coumaric acid, being a weak acid, it is important to confirm that, in the solubility measurements, its main molecular form is the neutral form. Otherwise, two different molecules should be taken into account in the thermodynamic model. Given the pKa of *p*-coumaric acid to be 4.6,[28] it was checked that for the measured solubility in water, the neutral species would account for 97% of the total concentration. Thus, it is considered that the estimated NRTL-SAC parameters are specified for the neutral molecule.

In order to apply eq. (2.2), melting properties of the considered polyphenols are needed. This data is provided in Table 2.2. For naringin, there is some published work which argues that the molecule may not have a solid crystalline structure.[29] In that case, the melting enthalpy and temperature were added as regressing parameters, as suggested in other references.[30]

Table 2.2 – Chemical properties of the polyphenols considered in this work. The melting temperature and the melting enthalpy were used to obtain the activity coefficient of each molecule in solution, using eq. 2-2.

Molecule	M_w (g mol^{-1})	T_m (K)	H_m (kJ mol^{-1})	Reference
trans-resveratrol	228.25	541.3	30.6	36
p-coumaric acid	164.15	494.35	34.3	37
Naringenin	272.26	523.15	39.8	20
Naringin*	580.54	432.3	58.1	This work

* For this case, the melting temperature and enthalpy were not measured, but rather estimated from SLE data, using eq. 2.2.

2.3.2 Parameter determination for NRTL-SAC

For the parameter determination, the following objective function was used: [31]

$$\min_{X,Y^-,Y^+,Z} \sum_i \left[ln(\gamma_i^{mod}) - ln(\gamma_i^{exp}) \right]^2 \qquad (2.4)$$

In the previous equation, X, Y⁺, Y⁻ and Z are the molecular descriptors used by NRTL-SAC, γ_i^{mod} is the activity coefficient predicted by the model and γ_i^{exp} the experimental activity coefficient, obtained using SLE data and by applying eq. 2.2.

The needed parameters for the employed solvents were taken from the original NRTL-SAC paper.[17] However, whenever updated parameters were present in other sources,[34] those were used instead.

In order to check the applicability of the NRTL-SAC model for describing the measured solubility data, its predictions were compared with the experimental measurements. In Table 2.3, the regressed molecular descriptors are indicated, together with the percentage absolute average deviation (% AAD) (eq. 2.5) associated with the determined activity coefficients:

$$\% \, AAD = 100 \cdot \frac{1}{N} \sum_{i=1}^{N} \left| \gamma_i^{mod} - \gamma_i^{exp} \right| \qquad (2.5)$$

This previous parameter measures how distant, on average, the predicted activity coefficients are from the experimentally determined ones.

Table 2.3 – Regressed molecular descriptor parameters for the NRTL-SAC model. It is also included the average absolute deviation between the experimentally determined activity coefficient and the one determined by NRTL-SAC.

Molecule	X	Y^-	Y^+	Z	% AAD in γ (SLE data)	Reference
trans-resveratrol	0.427	1.768	3.057	0.000	44.2	This work
p-coumaric acid	0.545	1.777	1.871	0.75	33.5	This work
Naringenin	0.674	1.271	1.53	0.000	94.6	This work
Naringin	0.190	0.000	2.016	0.748	49.3	This work

2

The correlation between experimental data and the predictions made by the NRTL-SAC model are also graphically represented in Figure 2.2:
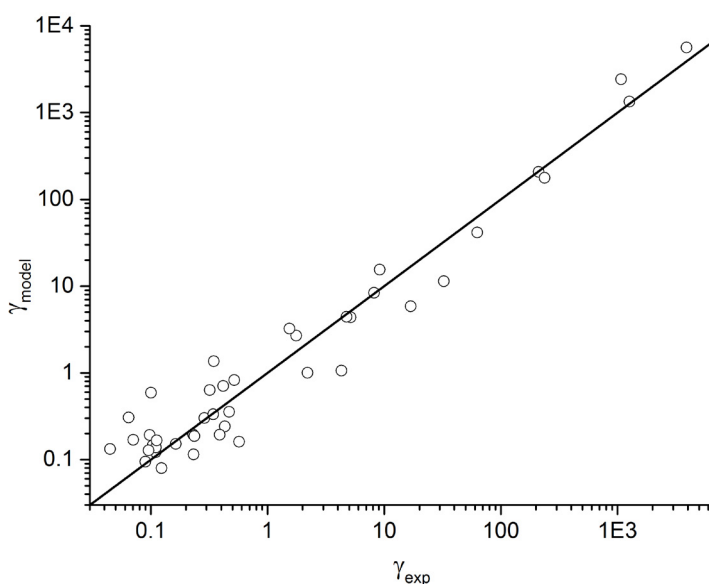
Figure 2.2 – Comparison between experimental SLE data and predictions by NRTL-SAC, after having regressed the parameters for each polyphenol.

As depicted in the Figure 2.2, and also corroborated by the obtained % AAD values, the NRTL-SAC was able to describe

the observed data satisfactorily for most of the cases. The obtained average deviation values are also in line with similar studies.[32]

2.3.3 Liquid-liquid extraction experiments

In order to prove that the predictions made by NRTL-SAC are concordant with the experimental values, liquid-liquid extraction experiments were performed and the obtained partition coefficients compared to those obtained from NRTL-SAC. From the analysis of the results obtained (see Figure 2.3), it was observed that for the case of naringin, although the model could describe the SLE data quite well (Table 2.3), the predictions for the LLE experiments were, in most of the cases, significantly higher than the experimental points. A possible explanation is related to the approximations contained in eq. 2.2 to the specific case of naringin. In some literature, this compound is said to crystallize in water as an octa-hydrate and in other solvents as a dihydrate.[30] However, for the solid-liquid equilibrium relation in eq. 2.2 to be valid, the energies of each dehydration step might have to be included.[36] In a different study, naringin has been observed not to have a defined melting point, possibly associated with having an amorphous rather than a crystalline form.[31] In this work, two approaches were followed in order to regress the molecular descriptor parameter for naringin: in the first one, the SLE dataset available in the literature (indicated in Table A1) was used for the parameter estimation (first row in Table 2.4). In the other one, the same parameters were regressed, but using only the obtained liquid-liquid partition data in this work (second row in Table 2.4).

Table 2.4 – Regressed molecular descriptor parameters for naringin, using the NRTL-SAC model. Due to the difficulty associated with describing the solid-liquid equilibrium data for the molecule, a new set of parameters was estimated, using only liquid-liquid partition data.

Molecule	X	Y^-	Y^+	Z
Naringin	0.190	0.000	2.016	0.748
Naringin*	0.000	1.462	0.000	0.238

* The parameters for this molecule were estimated using only LLE data.

The overall performance of the NRTL-SAC model in describing the obtained partition data is indicated in Figure 2.3.
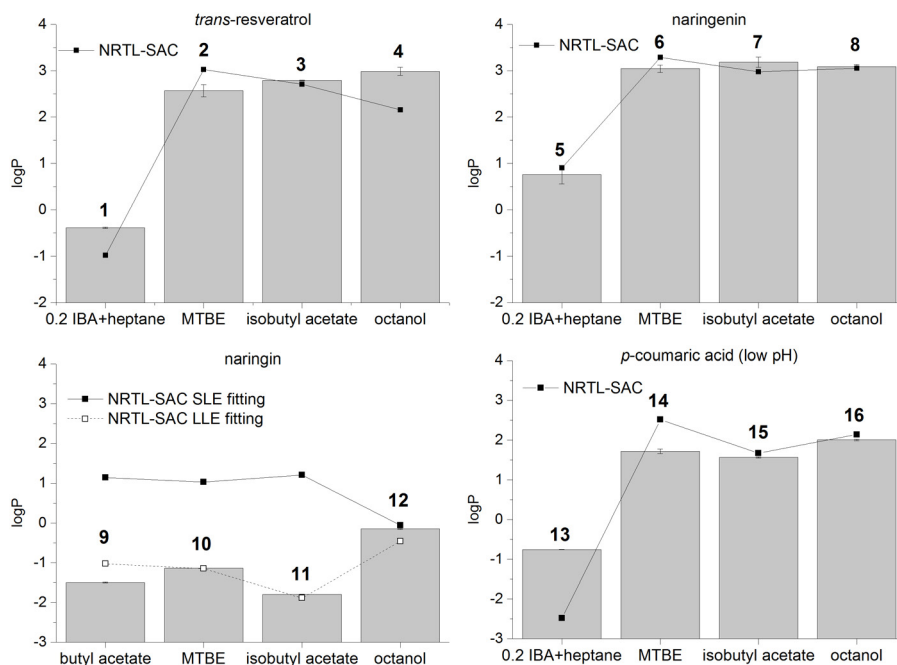
Figure 2.3 – Determined partition coefficients of the four different polyphenols considered in this work. The partition was measured in four different solvents, for which the NRTL-SAC parameters were already determined. The vertical bars are the obtained experimental values, and the lines connected by squares are the NRTL-SAC model predictions. Numbers were included in the graphic in order to reference each experimental condition throughout this article.

As shown in Figure 2.3, the naringin molecule was the one where the NRTL-SAC model had the worst performance, except when a different set of parameters was used, based on the obtained LLE data. In all of the remaining situations, the predictions were in line with the experiments.

The partition coefficients of *trans*-resveratrol and naringenin were not only measured in pure solvents, but also in different mixtures of heptane-isobutyl acetate (Figure 2.4). The goal with these experiments was to observe if by varying the amount of organic polar solvent (isobutyl acetate) to a hydrophobic solvent (heptane), the partition coefficient of two highly hydrophobic polyphenols could be fine-tuned. In this case as well, the NRTL-SAC is able to model the results almost quantitatively for every data point.
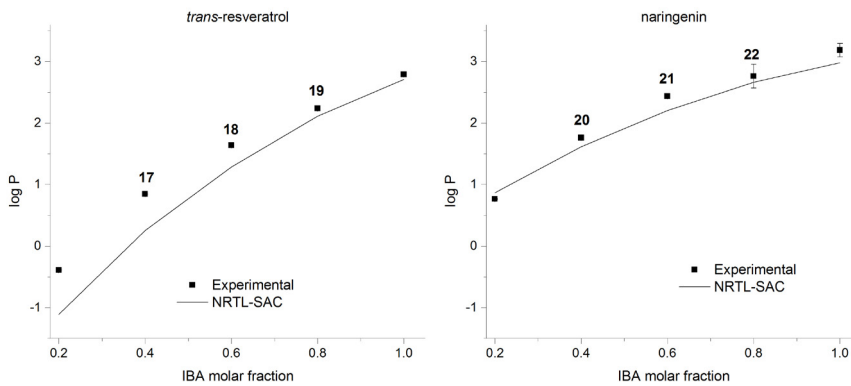
Figure 2.4 – Partition coefficients of *trans*-resveratrol and naringenin in different mixtures of isobutyl acetate-heptane. The experimental values (solid squares) are compared with the predictions by NRTL-SAC (solid line). Numbers were included in the graphic in order to reference each experimental condition throughout this article.

Like for the SLE predictions, the overall performance of the NRTL-SAC model was compared with the experimental liquid-liquid partition data. In Figure 2.5a, the results are shown when the parameters of naringin were obtained from SLE data. In Figure 2.5b, the parameters of naringin were obtained only using LLE data.
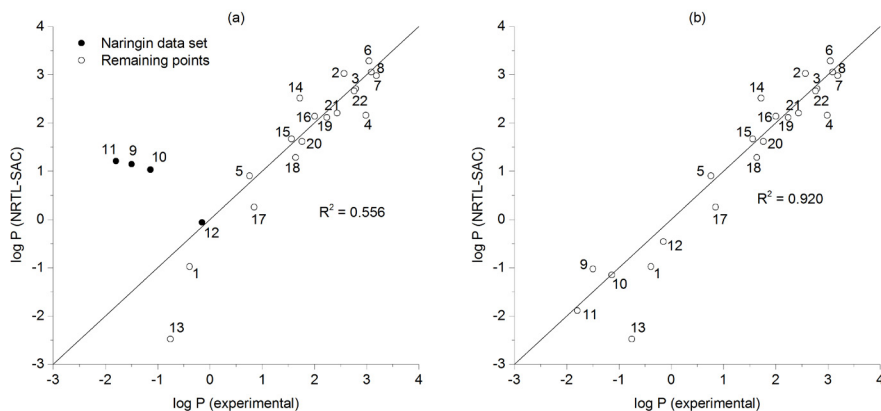
Figure 2.5 — Comparison between experimental LLE data and the predictions made by NRTL-SAC. In graphic (a), all the points were predicted using the molecular descriptors of naringin, when regressed using SLE data. In graphic (b), the naringin data points were predicted by using the molecular descriptors when regressed with the LLE data. Numbers were included in the graphic in order to reference each experimental condition throughout this article.

As indicated by the plots depicted in Figure 2.5, the NRTL-SAC predictions show a quite strong correlation with the experimental data, except for the case of naringin. However, the NRTL-SAC model itself is probably not the reason, but rather the possible simplified description of naringin solid-liquid equilibrium as previously mentioned. Either those details could be incorporated in a more complex thermodynamic model, or the molecular descriptors of naringin (and possibly other glycosylated polyphenols) may be fitted to experimental LLE data, as it was performed in Figure 2.5b. The average relative error for the situation depicted in Figure 2.5a was 56% (35% when discarding naringin) and 40% when naringin parameters were regressed using LLE data (Figure 2.5b).

The information obtained up until this point, together with the newly regressed NRTL-SAC parameters, was used to propose possible scenarios for the recovery and purification of the considered polyphenols.

2.3.4 Process design for liquid-liquid extraction of hydrophobic polyphenols

At this stage, it is important to determine the desired log P values for the different polyphenols, so that liquid-liquid extraction occurs as desired. For the recovery of hydrophobic polyphenols from a fermentation broth, the preferred log P values should be larger than 0. The reason is that, if the stream is going to be concentrated, the minimum solvent/aqueous feed ratio is of 1:1. Moreover, the solvent stream should be able to extract the polyphenols (recovery depending on the number of stages) while leaving sugars, proteins and organic acids behind, due to their low partition towards organic solvents. Because for those compounds the log P is lower than 0, purification is obtained if the log P $\geq$ 0 for the hydrophobic polyphenol. This statement is supported by obtained partition experimental data of glucose and proteins in a fermentation broth of *C. glutamicum* (data not shown) and on octanol/water partition data of organic acids present in literature.[37]

If purification of closely related polyphenols is intended (e.g., *trans*-resveratrol and naringenin), the log P values have to meet more specific criteria. First of all, if the log P is too large for both of them, even after one stage of extraction, complete recovery of both compounds can be achieved as indicated by the Kremser equation.[7]

In the following equations, V_r stands for solvent/aqueous feed volume ratio, P_i is the partition coefficient (volume based) of compound *i*, N is the number of column stages and Pur_i is the purity of compound *i*.

Assuming that the feed stream includes compounds 1 and 2 at 50% purity each and if both partition coefficients are so large that $V_r\,P_1$ and $V_r\,P_2$ become too large:

$$Pur_1 = \frac{1 - \dfrac{V_r P_1}{(V_r P_1)^{N+1} - 1}}{2 - \dfrac{V_r P_1}{(V_r P_1)^{N+1} - 1} - \dfrac{V_r P_2}{(V_r P_2)^{N+1} - 1}} \tag{2.6}$$

$$Pur_1 \approx \frac{1 - (V_r P_1)^{-N}}{2 - (V_r P_1)^{-N} - (V_r P_2)^{-N}} \rightarrow \frac{1}{2} \;, for\ N\ relatively\ small \qquad (2.7)$$

So, in the end, no purification occurs, as the purity of compound 1 remains at 50%. The ideal situation is when $V_r P_1 > 1$ and $V_r P_2 \approx 0$. Considering that maximum concentration factor is desired, that solubility of organic solvents in water is in the order of 50 g/L and their density is in the order of 0.8 g/mL, should be equal or larger than 0.0625. This is equivalent to saying that the feed stream should not be concentrated more than 16 times.

Assuming that the feed stream contains two compounds with 50% purity each and that the target is at least 70% purity, the log P of the impurity should be 0<log $P \leq 0.83$ and the log P for the desired compound has to be at least 0.4 units higher. This information was obtained using the Kremser equation.

In Figure 2.6, and based on the regressed parameters for NRTL-SAC, the partition coefficients of the studied polyphenols were predicted for a wide list of solvents present in the NRTL-SAC model database. For the case of *p*-coumaric acid, being a weak acid (pKa = 4.1), it is important to understand how the partition coefficient might vary with pH since, in some cases of interest, fermentations can occur at a pH considerably higher than its pKa (e.g., pH 7). Since the performed experiments for *p*-coumaric acid were performed at low pH, the partition coefficient at higher pH values (pH > pKa + 2) was calculated by assuming that the deprotonated species *p*-coumarate does not partition to the organic phase:

$$log\ D = log\left(\frac{[AH]_{org} + [A^-]_{org}}{[AH]_{aq} + [A^-]_{aq}}\right) \qquad (2.8)$$

$$\approx log\left(\frac{[AH]_{org}}{[AH]_{aq} + K_a[AH]_{aq}/[H^+]_{aq}}\right)$$

$$= log\left(\frac{[AH]_{org}}{[AH]_{aq}} \cdot \frac{1}{1 + K_a/[H^+]_{aq}}\right)$$

$$= log\ P - log(1 + 10^{pH-pKa})$$

In the previous equation, *D* is the partition coefficient of the weak acid *p*-coumaric acid that depends on pH. On the other hand, *P* is the partition coefficient of the neutral species.

Four hypothetical situations were considered. The first one considers a possible purification of *trans*-resveratrol and *p*-coumaric acid from a stream containing both compounds at low pH (approximately below 4, where most *p*-coumaric acid is in its protonated form). The second situation is equivalent, but at pH 7, where *p*-coumaric acid should be mostly deprotonated. The remaining two cases represent a hypothetical separation between naringenin and naringin (a glycosylated and non-glycosylated polyphenol) and between naringenin and *trans*-resveratrol (two hydrophobic polyphenols), respectively.

2
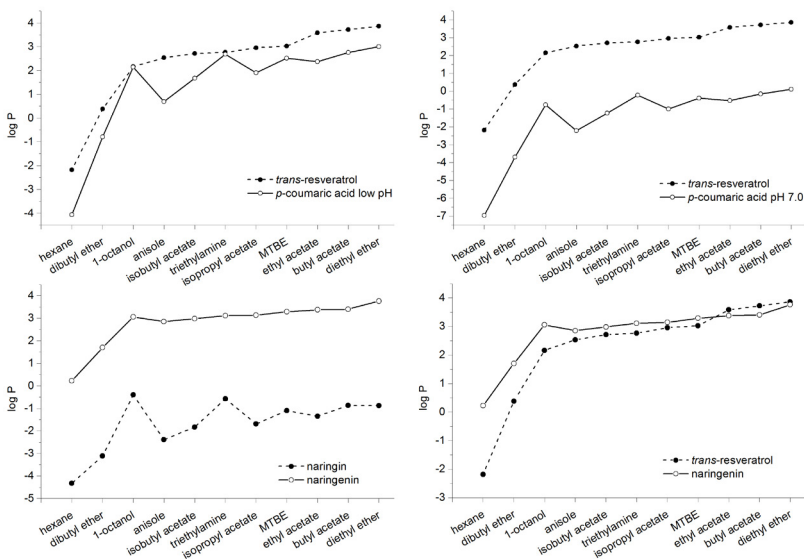
Figure 2.6 Predictions from NRTL-SAC for the partition coefficients of each polyphenol considered in this work. Each plot aims to compare the partition of two polyphenols that could be present in the same stream, and that would have to be purified.

Based on the results presented in Figure 2.6, one can expect the purification between naringenin and *trans*-resveratrol to be the most difficult one, as they have very similar partition profiles, the

major difference being when heptane is used. Another important case to mention is naringin. Because it exhibits negative log P values for the considered solvents, it might be easy to purify naringin from naringenin, but not to recover naringin from the remaining broth components such as sugars and proteins. As previously mentioned, a log P value lower than zero is not desired, because that means that the flow rate of extract phase would need to be larger than the one for the aqueous stream. Since that would lead to dilution of a possibly already dilute feed stream (considering the current low titers in fermentation), other recovery methods, based on adsorption, for example, would probably be a better option.

Taking into account the previous discussion, two purification cases will be analyzed in more depth in the following section. In the first place, the recovery of a hydrophobic polyphenol recovery from a typical fermentation broth (containing hydrophilic compounds as impurities) will be considered. Next, the recovery and purification of two similar hydrophobic polyphenols - naringenin and *trans*-resveratrol – from a fermentation broth, will also be tackled.

2.3.4 LLE process design for the recovery of *trans*-resveratrol

In this section, three different scenarios will be given for the recovery of *trans*-resveratrol from a hypothetical fermentation broth containing other, hydrophilic molecules: sugars, proteins and organic acids (pKa ≈ 4.5). As indicated in the previous section, the goal is to use a solvent to which the hydrophobic polyphenol can partition with a log P ≥ 0. For that, and has shown in Figure 2.6, almost any oxygenated organic solvent could meet the purpose.

2.3.4.1 First scenario: Liquid extraction with organic solvent

In the first scenario, a liquid-liquid extraction step is performed with ethyl acetate. The raffinate stream should contain the unextracted hydrophilic molecules, while the extract stream should carry the purified and concentrated *trans*-resveratrol. Because the solubility of this polyphenol in ethyl acetate is relatively high, it

should be concentrated in a multiple effect evaporator, before obtaining enough supersaturation to be crystallized. While the obtained crystals are filtered, washed with cold water and dried, the evaporated solvent is directed to a series of two distillation columns, where ethyl acetate is recovered and recycled to the extraction column.
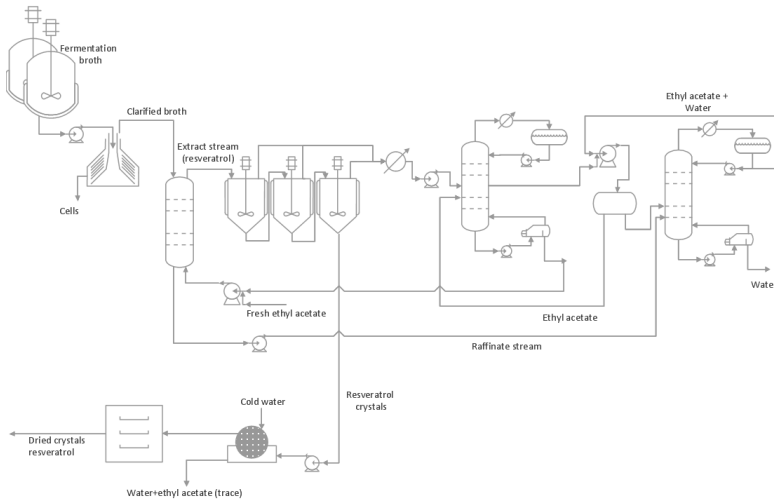
Figure 2.7 Conceptual downstream process train for the recovery of *trans*-resveratrol, a hydrophobic polyphenol, from a fermentation broth containing hydrophilic impurities. The clarified stream goes through a LLE step, where the polyphenol is preferentially extracted. Afterwards, the desired compound is crystallized, filtered, washed and dried to obtain the final formulation. The solvent used for the extraction, ethyl acetate, is distilled and recycled to the extraction column.

2.3.4.2 Second scenario: Using an anti-solvent for precipitation

In the second proposed scenario, a similar strategy to the one depicted in Figure 2.7 is proposed. The hydrophobic polyphenol is first extracted using an organic solvent, and the solution is then concentrated near solubility limit by evaporation. The solvent evaporated in this step is also recycled back to the process. The difference, in this case, is that depending on the solvent used

in the LLE step (if it can be made miscible with water or not), heptane or water can be added as an anti-solvent to make the polyphenol precipitate. This could reduce the amount of energy spent in evaporating the organic solvent (ethyl acetate in the previous case). As in the previous case, the organic solvents would be recycled back to the process by distillation.

2.3.4.3 Third scenario: Liquid extraction with switchable solvent

The last, third scenario, is also a small modification to the first one. For that reason, the same Figure 2.7 can be taken as a reference. In this case, the extraction is performed with a "green" solvent such as an ionic liquid or a switchable solvent. Assuming that this solvent might have a high boiling point, the preliminary concentration step by evaporation is skipped. The polyphenol is instead precipitated by adding water as anti-solvent. For the recovery, instead of using distillation, the used solvent would first be made immiscible with water either by adding CO_2, in the case of the switchable solvent or by adding an additive or changing the temperature for the case of the ionic liquid. The two phases would then be separated, for example, by centrifugation, before recycling them back to the process.

2.3.5 LLE process design for the recovery and purification of *trans*-resveratrol and naringenin

As previously mentioned, for the goal of purification, the objective is to have a large selectivity (log P difference of minimum 0.4), but also to have a relatively low partition coefficient for one of the compounds $(0 < \log P \leq 0.83)$.

One of the advantages of the NRTL-SAC model is that it represents each molecule to be composed of different segments: hydrophobic (X), polar (Y$^-$ and Y$^+$) and hydrophilic (Z). Due to that, it was investigated which value combination of X, Y$^-$, Y$^+$ and Z for a hypothetical solvent would lead to an optimal purification scenario, where optimal is defined as meeting the following constraints:

$$0 < (\log P)_1 \leqslant 0.83 \wedge (\log P)_2 \geq 1.23 \tag{2.9}$$

Or the other way around:

$$0 < (\log P)_2 \leqslant 0.83 \wedge (\log P)_1 \geq 1.23 \qquad (2.10)$$

For each of the molecular descriptors, their value was varied from 0 to 1 in 0.1 intervals, and the log P value evaluated. The result is present in Figure 2.8.
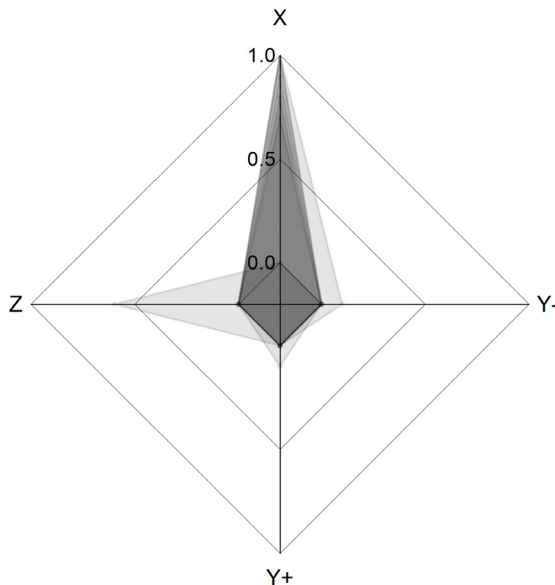
Figure 2.8 – Prediction made by NRTL-SAC for the set of molecular descriptors that would make the optimal solvent for the purification of naringenin from *trans*-resveratrol.

As it is possible to verify, the predictions made by the NRTL-SAC model, suggest using either a purely hydrophobic solvent (e.g., hexane) or a relatively hydrophilic solvent. The issue with the latter is that a solvent with high hydrophilic character will not be able to form two phases with a water-based fermentation broth. Thus, that hypothesis was disregarded. Because not always a solvent with the desired hydrophobicity may exist or be suitable (hexane, for example, has carcinogenic effects), one possible strategy for

purification is to use a hydrophobic solvent such as heptane together with an organic polar solvent (e.g., octyl acetate, methyl ethyl ketone) in order to adjust the partition coefficient of the desired molecule. This was demonstrated in the experimental data shown previously, where the partition coefficients of both naringenin and *trans*-resveratrol were obtained for different heptane/isobutyl acetate mixtures.

Another way of fine-tuning the desired solvent characteristics for the purification of this polyphenols is to use ionic liquids. For that reason, the possible applicability of ionic liquids to the extraction of the polyphenols studied in this work was also examined. However, due to the relatively small database of NRTL-SAC parameters available in the literature,[36] only some ionic liquids were considered. Those were, from the indicated reference, the ones that NRTL-SAC predicted to form a biphasic mixture with water. Their associated molecular descriptors are indicated in Table A2 (Appendix).
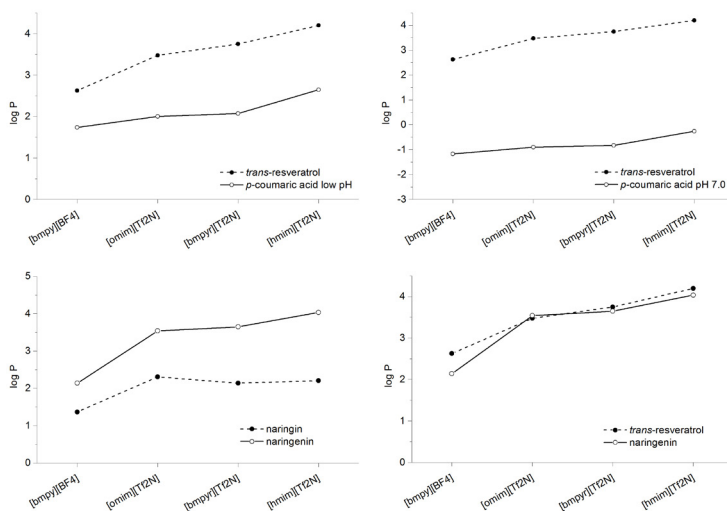
Figure 2.9 — Predictions from NRTL-SAC for the partition coefficients of each polyphenol considered in this work. Each plot aims to compare the partition of two polyphenols that could be present in the same stream, and that would have to be purified. The NRTL-SAC parameters for the considered ionic liquids are indicated in Table A2 (Appendix).

As it is possible to observe in Figure 2.9, the application of the examined ionic liquids seems to be only suitable for a possible purification scenario of *p*-coumaric acid and *trans*-resveratrol. For the other hypothetical purification steps, and as suggested by Figure 2.8, the applied solvents do not show sufficient hydrophobicity. For that reason, NRTL-SAC predicts hydrophobic polyphenols to have a log P value of equal to or larger than 1, which can make the purification task too challenging, since purification may not be obtained (polyphenols are co-extracted). Nonetheless, it is important to reinforce the idea that a very small set of ionic liquids were here evaluated, due to the lack of sufficient parameters for the NRTL-SAC model.

Similarly to the previously proposed polyphenol recovery scenarios, a possible purification sequence for polyphenols such as *trans*-resveratrol and naringenin is indicated in Figure 2.10. The suggested downstream process can be made almost completely similar to the previously indicated one (Figure 2.7), the only modification being the addition of another liquid-liquid extraction column, where a second organic solvent is used. The idea behind this strategy is first to use a solvent that is able to extract the most hydrophobic polyphenol, naringenin (e.g., 0.2 molar fraction ethyl acetate in heptane), while leaving the less hydrophobic, *trans*-resveratrol, behind. The latter would be extracted using a more polar solvent mixture (e.g., 0.6 molar fraction ethyl acetate in heptane).

2
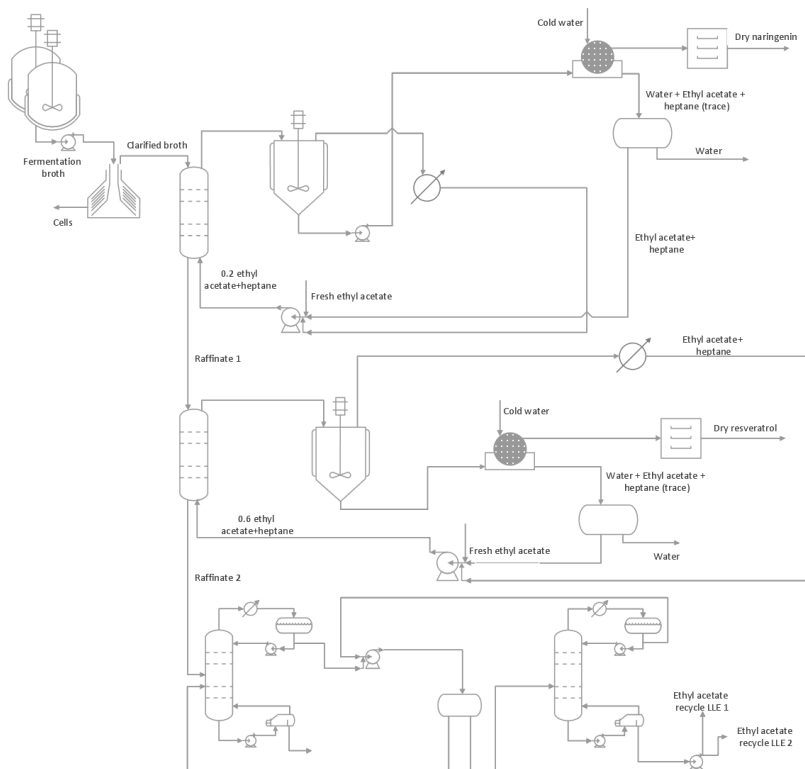
Figure 2.10 – Conceptual downstream process train for the recovery and purification of two similar polyphenols (e.g., *trans*-resveratrol and naringenin) from a fermentation broth. The clarified stream goes through a first LLE step, where naringenin is preferentially extracted by a relatively hydrophobic stream (0.2 molar fraction ethyl acetate in heptane). Connected to it, there is another LLE step where *trans*-resveratrol, present in the "raffinate 1" stream is recovered by using a more polar solvent mixture (0.6 molar fraction ethyl acetate in heptane). After liquid extraction is complete, both compounds are crystallized, filtered, washed and dried to obtain the final formulation. The organic solvents are recovered by using distillation and then recycled to the different extraction columns.

2.4 Conclusions

In this work, it was shown that the NRTL-SAC model could be applied to the description of liquid-liquid equilibrium data of complex molecules like polyphenols. Moreover, by only relying on pre-existent solubility data to regress the needed parameters, satisfactory predictions of the log P value were obtained (30% absolute average deviation), proving that the model is robust despite using a relatively small amount of data. The major exception occurred with naringin (56% AAD, when taking it into account), whose log P values were consistently over-predicted. The proposed explanation relies on the fact that the used solid-equilibrium equation is not applicable to amorphous substances, but rather to compounds with a defined melting point. Moreover, different naringin solvates (different hydrates) might exist in the solid phase, depending on the solvent where solubility was measured.

The molecular descriptors (X, Y⁻, Y⁺, and Z) obtained for the four polyphenols considered in this study, together with the Kremser equation, allowed to define and find suitable solvents or solvent mixtures for applying liquid-liquid extraction to the recovery and purification of those molecules. Although the purification of naringin from a water-based fermentation broth was not studied in detail, the obtained liquid-liquid equilibrium results suggested that reverse-phase adsorption might be a more suitable alternative, since its polarity is more similar to the remaining broth components than the other considered polyphenols.

Concerning the three remaining polyphenols (*trans*-resveratrol, naringin, and *p*-coumaric acid), two case-studies were addressed in this study. The first one concerned the recovery of *trans*-resveratrol from a fermentation broth containing hydrophilic molecules, namely *p*-coumaric acid. By relying on NRTL-SAC, it was shown that, at neutral pH, almost any polar organic solvent would be able to purify *trans*-resveratrol while leaving *p*-coumaric acid behind (taken as the most challenging molecule to be removed). The second scenario dealt with the purification of both naringenin and *trans*-resveratrol from the same fermentation broth. In this case, the biggest challenged relied

2

on the fact that both molecules are similar and highly hydrophobic. Thus, a binary solvent mixture which would combine a hydrophobic solvent (e.g., heptane) with a polar organic solvent (e.g., isobutyl acetate), was found to be one of the possible ways to fine-tune the partition value of each molecule in order to achieve separation.

The proposed conceptual downstream process designs for the two previously mentioned case-studies had in consideration the possible usage of green solvents as ionic liquids or switchable solvents. Their advantages, like using CO_2 to promote phase-splitting in water or the fact that ionic liquids are considered "designer" solvents are highly desired properties for the design of a liquid-liquid extraction process. Not only they present such advantages – among others -, but by using NRTL-SAC, the proper ionic liquid may now be developed with the right combination of hydrophobic-polar-hydrophilic character. Nonetheless, the lack of the needed parameters for NRTL-SAC in literature, made it impossible not only to scan a wide database of solvents but also to find ionic liquids that would present better properties (regarding extraction capacity and selectivity) than the considered organic solvents.

2

List of abbreviations

Abbreviation	Description
NRTL-SAC	Nonrandom Two-Liquid Segment Activity Coefficient
MPP-UNIFAC	Modified polyphenol UNIFAC
LLE	Liquid-liquid extraction
SLE	Solid-liquid equilibrium

Acknowledgements

Appendix A

Table A1 – Description of the solid-liquid equilibrium (SLE) dataset used for the NRTL-SAC parameter estimation for the four different polyphenols used in this work.

Polyphenol	Solvents	Number of data points	Reference
trans-resveratrol	Methanol, ethanol, 1-propanol, 2-propanol, 1-butanol, ethyl acetate, methyl acetate, acetone and water	10	26
p-coumaric acid	Methanol, ethanol, 1-propanol, 2-propanol, 1-butanol, acetone, ethyl acetate, methyl acetate and water	9	21
naringenin	Methanol, isopropanol, ethyl acetate, 1-butanol, hexane, water and ethanol	11	22, 23
naringin	Methanol, isopropanol, ethyl acetate, 1-butanol, hexane, water and ethanol	11	23, 24

Table A2 – Molecular descriptors parameters for ionic liquids already described in the literature.

Polyphenol	X	Y^+	Y^-	Z	Reference
[omim][Tf2N]	0.326	0.447	4.740	0.000	38
[bmpyr][Tf2N]	0.000	0.000	4.444	0.197	38
[hmim][Tf2N]	0.320	0.000	3.908	0.405	38
[bmpy][BF4]	0.000	0.062	1.224	0.158	38

References

1 Transparency Market Research, Polyphenols Market by Product (Grape Seed, Green Tea, Apple and Others), by Application (Functional Beverages, Functional Food, Dietary Supplements and Others): Global Industry Analysis, Size, Share, Growth, Trends and Forecast, 2012 - 2018. 2013.

2 Alov, P.; Tsakovska, I.; Pajeva, I., Computational Studies of Free Radical-Scavenging Properties of Phenolic Compounds. Current Topics in Medicinal Chemistry 2015, 15, (2), 85-104.

3 Scalbert, A.; Johnson, I. T.; Saltmarsh, M., Polyphenols: antioxidants and beyond. Am J Clin Nutr 2005, 81, (1 Suppl), 215S-217S.

4 Pandey, K. B.; Rizvi, S. I., Plant polyphenols as dietary antioxidants in human health and disease. Oxidative Medicine and Cellular Longevity 2009, 2, (5), 270-278.

5 Dudnik, A.; et al., BacHBerry: BACterial Hosts for production of Bioactive phenolics from bERRY fruits. Phytochemistry Reviews 2017.

6 Goldberg, E., Handbook of Downstream Processing. 1st Edition ed.; Springer Netherlands: 1997.

7 Henley, E. J.; Seader, J. D.; Roper, D. K., Separation process principles. Wiley: 2011.

8 Gani, R.; Brignole, E. A., Molecular Design of Solvents for Liquid Extraction Based on Unifac. Fluid Phase Equilibria 1983, 13, (Oct), 331-340.

9 Weis, D. C.; Visco, D. P., Computer-aided molecular design using the Signature molecular descriptor: Application to solvent selection. Computers & Chemical Engineering 2010, 34, (7), 1018-1029.

10 Zhang, J. A.; Peng, D. L.; Song, Z.; Zhou, T.; Cheng, H. Y.; Chen, L. F.; Qi, Z. W., COSMO-descriptor based computer-aided ionic liquid design for separation processes. Part I: Modified group contribution methodology for predicting surface charge density profile of ionic liquids. Chemical Engineering Science 2017, 162, 355-363.

11 Ferreira, O.; Pinho, S. P., Solubility of Flavonoids in Pure Solvents. Industrial & Engineering Chemistry Research 2012, 51, (18), 6586-6590.

12 Sevillano, D. M.; van der Wielen, L. A. M.; Hooshyar, N.; Ottens, M., MPP-UNIFAC, a predictive activity coefficient model for polyphenols. Fluid Phase Equilibria 2014, 384, 82-88.

13 Klamt, A., Conductor-Like Screening Model for Real Solvents - a New Approach to the Quantitative Calculation of Solvation Phenomena. Journal of Physical Chemistry 1995, 99, (7), 2224-2235.

14 Bouillot, B.; Teychené, S.; Biscans, B., An evaluation of thermodynamic models for the prediction of drug and drug-like molecule solubility in organic solvents. Fluid Phase Equilibria 2011, 309, (1), 36-52.

15 Dimian, A.; Bildea, C.; Kiss, A., Integrated Design and Simulation of Chemical Processes. 2nd Edition ed.; Elsevier Science: 2014.

16 Wu, H. S.; Sandler, S. I., Proximity effects on the predictions of the UNIFAC model: I. Ethers. AIChE Journal 1989, 35, (1), 168-172.

17 Chen, C. C.; Song, Y. H., Solubility modeling with a nonrandom two-liquid segment activity coefficient model. Industrial & Engineering Chemistry Research 2004, 43, (26), 8354-8362.

18 Chen, C.-C.; Crafts, P. A., Correlation and prediction of drug molecule solubility in mixed solvent systems with the nonrandom two-liquid segment activity coefficient (NRTL-SAC) model. Industrial & engineering chemistry research 2006, 45, (13), 4816-4824.

19 Sangster, J., Octanol-Water Partition Coefficients: Fundamentals and Physical Chemistry. 1997.

20 Sun, X. L.; Shao, Y. D.; Yan, W. D., Measurement and Correlation of Solubilities of trans-Resveratrol in Ethanol plus Water and Acetone plus Water Mixed Solvents at Different Temperatures. Journal of Chemical and Engineering Data 2008, 53, (11), 2562-2566.

21 Ji, W.; Meng, Q.; Li, P.; Yang, B.; Wang, F.; Ding, L.; Wang, B., Measurement and Correlation of the Solubility of p-Coumaric Acid in Nine Pure and Water + Ethanol Mixed

Solvents at Temperatures from 293.15 to 333.15 K. Journal of Chemical & Engineering Data 2016, 61, (10), 3457-3465.

22 Zhang, P. P.; Lin, R.; Yang, G. D.; Zhang, J. Y.; Zhou, L.; Liu, T. T., Solubility of Naringenin in Ethanol and Water Mixtures. Journal of Chemical and Engineering Data 2013, 58, (9), 2402-2404.

23 Zhang, L. Q.; Song, L.; Zhang, P. P.; Liu, T. T.; Zhou, L.; Yang, G. D.; Lin, R.; Zhang, J. Y., Solubilities of Naringin and Naringenin in Different Solvents and Dissociation Constants of Naringenin. Journal of Chemical and Engineering Data 2015, 60, (3), 932-940.

24 Zhang, J. Y.; Zhang, P. P.; Liu, T. T.; Zhou, L.; Zhang, L. Q.; Lin, R.; Yang, G. D.; Wang, W. R.; Li, Y. P., Solubility of naringin in ethanol and water mixtures from 283.15 to 318.15 K. Journal of Molecular Liquids 2015, 203, 98-103.

25 Chen, F. X.; Qi, Z. L.; Feng, L.; Miao, J. Y.; Ren, B. Z., Application of the NRTL method to correlate solubility of diosgenin. Journal of Chemical Thermodynamics 2014, 71, 231-235.

26 Sevillano, D. M. n.; van der Wielen, L. A.; Trifunovic, O.; Ottens, M., Model Comparison for the Prediction of the Solubility of Green Tea Catechins in Ethanol/Water Mixtures. Industrial & Engineering Chemistry Research 2013, 52, (17), 6039-6048.

27 John M. Prausnitz; Azevedo, E. G. d., Molecular Thermodynamics of Fluid-Phase Equilibria. 3rd Edition ed.; 1999.

28 Blum, U., Plant-Plant Allelopathic Interactions II. Springer International Publishing: 2014; p 322.

29 Cordenonsi, L. M.; Sponchiado, R. M.; Campanharo, S. C.; Garcia, C. V.; P., R. R.; Schapoval, E. E. S., Study of Flavonoids present in Pomelo (Citrus maxima) by DSC, UV-VIS, IR, 1H AND 13C NMR AND MS. Drug Analytical Research 2017, 1, (1).

30 von Stockar, U.; Luuk AM Van der Wielen, Biothermodynamics: The Role of Thermodynamics in Biochemical Engineering. 2013.

31 Haghtalab, A.; Yousefi Seyf, J., Vapor–Liquid and Solid–Liquid Modeling with a Universal Quasichemical Segment-Based Activity Coefficient Model. Industrial & Engineering Chemistry Research 2015, 54, (34), 8611-8623.

32 Mota, F. L.; Carneiro, A. R.; Queimada, A. J.; Pinho, S. P.; Macedo, E. A., Temperature and solvent effects in the solubility of some pharmaceutical compounds: Measurements and modeling. European Journal of Pharmaceutical Sciences 2009, 37, (3-4), 499-507.

33 Hendrickson, R.; Kesterson, J. W., Purification of naringin. Florida Agricultural Experiment Station Journal 1956.

34 Franklin, S. J.; Younis, U. S.; Myrdal, P. B., Estimating the Aqueous Solubility of Pharmaceutical Hydrates. J Pharm Sci 2016, 105, (6), 1914-1919.

35 Sangster, J., Octanol-Water Partition-Coefficients of Simple Organic-Compounds. Journal of Physical and Chemical Reference Data 1989, 18, (3), 1111-1229.

36 Chen, C. C.; Simoni, L. D.; Brennecke, J. F.; Stadtherr, M. A., Correlation and prediction of phase behavior of organic compounds in ionic liquids using the nonrandom two-liquid segment activity coefficient model. Industrial & Engineering Chemistry Research 2008, 47, (18), 7081-7093.

3

Purification of polyphenols from a fermentation broth using functionalized macroporous resins

Abstract

Adsorption can be an effective way of purifying polyphenols from complex mixtures. However, polyphenols may be present in small concentrations, making it difficult to selectively adsorb them onto standard hydrophobic resins and obtain appreciable adsorption. In this work, non-functionalized hydrophobic resins (Amberlite® XAD-7HP, XAD-16) are compared with functionalized resins with imidazole (Biotage® RENSA PX) and pyridine (RENSA PY) in terms of capacity and selectivity towards *p*-coumaric acid, *trans*-resveratrol and naringenin. The obtained results indicate that, due to hydrogen bonding, the functionalized resins provide more capacity (e.g., 80 mg.g^{-1} vs 11.3 mg.g^{-1} for *trans*-resveratrol) and up to five times more selectivity than standard resins. Despite such strong affinity, at low pH, the isotherm slope can decrease up to four times when compared to the XAD resins for the same ethanol content, making desorption easier. The included isotherm data is enough to model any chromatography dynamic simulation for the studied compounds.

3.1 Introduction

Polyphenols are molecules which have a range of different biotechnological applications (e.g., as food additives, nutraceuticals and food colorants).[1] These molecules are secondary metabolites naturally produced by plants, which can act as radical scavengers due to the high stabilization provided by ring aromaticity.[2] Over the last years, research on their health properties has grown considerably,[3] with authors studying the properties of these molecules in the prevention of diseases such as Alzheimer and several types of cancer.[4] Furthermore, the increasing interest in these compounds has led to the creation of projects such as the BacHBerry project (www.bachberry.eu), funded by the 7th Framework Programme of the European commission. This project aimed to discover new phenolic compounds with interesting properties (e.g., health-promoting, colorants) and develop a sustainable process for their production using bacterial platforms. The downstream process development for the capture and purification of polyphenols produced in such a way, is then crucial for the success of the project.

It is known that most of the state-of-the-art methods for the capture of these polyphenols – although from plant extracts – consist of an adsorption step,[5] where an aqueous stream is contacted with macroporous hydrophobic resins such as the Amberlite® XAD series, which usually consist of a polystyrene-divinylbenzene copolymer matrix with a very large surface area. Even though extensive investigation on the adsorption of polyphenols onto several macroporous hydrophobic resins, such as the above-mentioned, has been published,[6] not much research work has been done - to the knowledge of the author - concerning hydrophobic functionalised resins and their possible advantages in a capture or purification step of polyphenols. Although in a typical capture step one is looking for resin beads with large surface areas, which should correspond to large adsorption capacities, the bottleneck in the case of hydrophobic polyphenols is their usual low concentration in water. As high concentrations in the liquid phase cannot be attained (e.g., solubility of *trans*-resveratrol in water is around 30 mg.L^{-1}),[7] most hydrophobic resins may not get saturated. Consequently, the

associated costs of a typical batch capture step, in bind and elute mode, may rise due to the larger column volume and increased amount of solvent needed. A strategy that might be followed instead, is to use hydrophobic resins that are functionalised with certain chemical groups (e.g., pyridine, imidazole), which can have an increased affinity towards the polyphenols and get more easily saturated at much lower concentrations. An example of such resins are the RENSA® series from Biotage.

This paper presents the obtained adsorption equilibrium isotherms of three model hydrophobic polyphenols – *p*-coumaric acid, *trans*-resveratrol and naringenin (Figure 3.1) - using functionalised (RENSA PX (imidazole) and RENSA PY (pyridine)) and non-functionalised resins (Amberlite® XAD-7HP and XAD-16) and different water-ethanol mixtures, in order to establish a comparison between their adsorption and desorption performance. This will also allow a preliminary calculation of the associated capital and operational costs of a batch capture step, in bind and elute mode, using the two indicated alternatives. Moreover, the dependence of the isotherm slopes with ethanol are also modelled with an exponential function, so that it is possible to model any chromatography unit operation using well-known mechanistic models.[8]

3
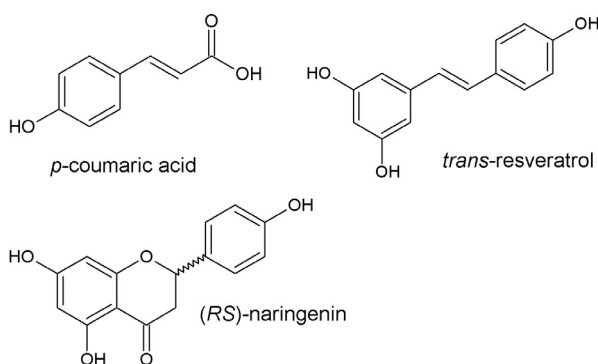
Figure 3.1 — Chemical structure of the model polyphenols used in this work.

In the following section, a description of the used materials and methods is given, including a compilation of the physical

characteristics of the tested resins. The main obtained results and their discussion is presented on section 3.3 and the conclusions are included in section 3.4.

3.2 Experimental

3.2.1 Chemicals

For the preparation of all the solutions, Milli-Q grade water and ethanol absolute for analysis (EMPARTA® ACS, Merck Millipore) were used. The polyphenol *trans*-resveratrol ≥98% was obtained from Evolva. Naringenin (natural (US), 98%) and p-coumaric acid ≥98% were purchased from Sigma-Aldrich. Butyl acetate *purum* ≥98.5% was obtained from Fluka.

3.2.2 Adsorbents

The selected non-functionalized adsorbents were the Amberlite® XAD-16 and XAD-7HP resins from Sigma-Aldrich. The goal was to select resins with different dipole moments (and hence, hydrophobicity) and different surface areas, in order to study their impact on the adsorption of polyphenols. For the functionalized resins, two types of functional groups were selected: phenyl+imidazole (RENSA PX) and phenyl+pyridine (RENSA PY). All these resins possess a styrenic backbone that provides stability for a wide range of pH 1-14. The RENSA resins were obtained from Biotage® AB, Sweden.

The physical properties of the selected resins are indicated in Table S1. Whenever not mentioned, all the values shown were obtained from the suppliers.

In Table B1 (Appendix), the porosity was obtained in mL.g dry^{-1} from the supplier and converted to mL.mL^{-1} using:

$$\varepsilon_p(mL/mL) = \frac{\varepsilon_p(mL/g_{dry})}{\varepsilon_p(mL/g_{dry}) + \frac{1}{\rho_{skel}\ (g/mL)}} \qquad (3.1)$$

The wet/dry mass ratio was obtained considering that the moisture holding capacity of both resins is 65% (data from supplier). The bulk density (ρ_{bulk}) was calculated from the resin wet density (ρ_{wet}) and by considering that the external porosity (ε) is 0.4:[9]

$$\rho_{bulk} = \rho_{wet} \cdot (1 - \varepsilon) \qquad (3.2)$$

The wet density values for the XAD resins were obtained from the supplier. For the functionalized resins, those values were calculated using the following equation:

$$\rho_{wet} = \frac{1}{\dfrac{\phi}{\rho_{wat}} + \dfrac{(1 - \phi)}{\rho_{skel}}} \qquad (3.3)$$

Where ϕ is the water mass fraction of the wet resin (determined from the wet/dry mass ratio), ρ_{wat} is the water density at 20°C (0.998 g.mL^{-1})[10] and ρ_{skel} the skeletal density.

The porosity values (in mL.g dry[-1]) were obtained using eq. 3.4:

$$\varepsilon_p\left(mL/g_{dry}\right) = \frac{1}{\rho_{wat}\ (g/mL)} \cdot \left(\frac{m_{wet}}{m_{dry}} - 1\right) \qquad (3.4)$$

Where m_{wet} and m_{dry} correspond to the resin wet and dry mass, respectively. These values were then converted to mL.mL^{-1} using eq. 3.1.

For preparing the resins for the batch uptake experiments, they were pre-wetted with ethanol and then washed with MilliQ water. Afterwards, they were equilibrated with the appropriate water-ethanol mixture, depending on the considered experimental condition. For the RENSA resins, this procedure was done using filter plates, to which vacuum was applied in order to remove the excess solvent. For the XAD resins, due to their larger size, this process was performed in a plastic syringe with a 0.2 μm tip filter. In the end, the surface excess moisture would be removed using paper tissue.

3

3.2.3 Resin properties determination

3.2.3.1 Resin skeletal density

The skeletal density of the RENSA resins was obtained by liquid pycnometry, as described elsewhere.[11] The solvent used in this process was ethanol, due to its capability of filling the hydrophobic resin pores.

3.2.3.2 Resin wet/dry ratio

For determining the ratio of wet weight/dry weight, a given mass of pre-wet resin was added to a plastic boat. After it was left to dry at 60°C for one day, the difference between the wet and dry weights was calculated.

3.2.4 Equilibrium experiments

For the batch uptake experiments, depending on the concentration region of the isotherm and the ethanol percentage, two different methods were used. For the solutions containing 0% ethanol (pure MilliQ water) to 20% ethanol, three different shake-flasks were prepared for each polyphenol/resin combination. After equilibrium was reached, a given amount of liquid volume present at the end of the experiment would be replaced by fresh stock solution, saturated with the desired polyphenol. These would be repeated for at most three cycles, in order to obtain the isotherm for successive higher concentrations in the liquid phase. For the case where solutions contained at least 35% ethanol, the isotherm would be determined with only one cycle of experiments, where each shake-flask contained different initial concentrations of the polyphenolic solution.

Glass flasks with either 5 mL or 70 mL were used, to vary the liquid/solid phase ratio. The prepared shake-flasks were closed with rubber stops to prevent evaporation. The shaking of the smaller flaks (5 mL liquid volume) was performed in a Heidolph Titramax 1000 incubation platform and shaken at 450 rpm, at room temperature. For the larger flasks (70 mL liquid volume),

shaking was performed in a Sartorius® Certomat BS-1 at 150 rpm and 20°C. In all the experiments, shaking was maintained for at least 3 hours in order to achieve equilibrium (kinetic data not shown). Room temperature was controlled on a daily basis and it remained between 20±2°C.

The amount of polyphenol adsorbed by each resin was obtained by mass balance, w5here the initial and final concentrations were measured by UHPLC (protocol indicated in section 3.2.5):

$$q^* = (C_0 - C_e)\frac{V_L}{m_{res}}$$

(3.5)

In this equation, C_o and C_e represent the initial and final (equilibrium) concentrations, respectively. V_L is the liquid volume and m_{res}, the mass of wet resin used.

The equilibrium data was either modelled according to the Langmuir isotherm (eq. 3.6) or the linear isotherm model (eq. 3.7):

$$q^* = \frac{q_{max}.K_L.C_{eq}}{1 + K_L.C_{eq}}$$

(3.6)

$$q^* = K.C_{eq}$$

(3.7)

The symbol q_{max} represents the maximum capacity, K_L the affinity constant and K the isotherm slope for the linear model.

The Langmuir isotherm model was chosen, given that it provides a good mechanistic description of the adsorption of neutral molecules.[12] The Langmuir model was chosen over the linear model whenever its Akaike information criteria (eq. 3.8) was lower by, at least, one unit:

(3.8)

$$AIC = 2n_p - 2 \cdot SSE$$

3

In the last equation, n_p is the number of parameters used by the model and *SSE* is the sum of squared errors. This is approximately equivalent to saying that the parameter q_{max} would not bring a sufficient improvement in the description of the experimental data.

For modelling the isotherm dependence on the ethanol concentration, the initial isotherm slope dependence on the modifier (ethanol) was described using an exponential model that resembles a previously developed model used to predict protein retention as a function of salt molality:[13]

$$ln\left[\left(\frac{q_i}{C_i}\right)_0 (C_{mod})\right] = \alpha_i + \gamma_i . C_{mod} \qquad (3.9)$$

The term inside square brackets represents the initial isotherm slope (which is a function of ethanol concentration). The factors α_i and γ_i are regression parameters, dependent on the compound and the adsorbent. C_{mod} is the modifier concentration (volumetric percentage), which in this work corresponds to ethanol.

3.2.5 Analytics

The quantification of *p*-coumaric acid, *trans*-resveratrol and naringenin was carried out by UHPLC (Ultimate 3000, Thermo Scientific, USA) in a C18 column (Acquity UPLC HSS column, 1.8μm, 2.1mm x100 mm Waters, Milford, USA). Mobile phase A consisted of 10% formic acid in Milli-Q water and mobile phase B of 10% formic acid in acetonitrile. Every run was performed in isocratic mode, with the mobile phase containing 33.5% of B and 66.5% of A and flowing at 0.30 mL/min. The detection of *p*-coumaric acid was performed at 340 nm, that of *trans*-resveratrol at 304 nm and naringenin at 289 nm.

3

3.2.6 Error analysis

For all the performed batch experiments, the uncertainty associated with the measurements and the regressed parameters was obtained as described elsewhere.[14] The standard deviation of the measurements was calculated according to the theory of error propagation.[15] The standard deviation of the estimated parameters was obtained by taking the parameter covariance matrix as the inverse of the Fisher information matrix:

$$FIM = \sum_{i=1}^{N} J^T \frac{1}{\sigma_i} J \qquad (3.10)$$

Where σ_i is the standard deviation of the ith observation and J is the Jacobian matrix of the least squares regression function.

3.3 Results and discussion

3.3.1 Adsorption equilibrium isotherm determination

In order to be able to compare the adsorption and desorption efficiency of the different resins, the knowledge of the isotherms of the three considered polyphenols is essential. In this section, the adsorption equilibrium isotherms for *p*-coumaric acid, naringenin and *trans*-resveratrol, in different water-ethanol solutions, are presented. The results are compared and discussed taking into account the different chemical properties of each compound and of each resin.

3.3.1.1 *p*-coumaric acid

The adsorption equilibrium isotherms of *p*-coumaric acid onto the Amberlite XAD-16 resin and XAD-7HP are shown in Figure 3.2.

3
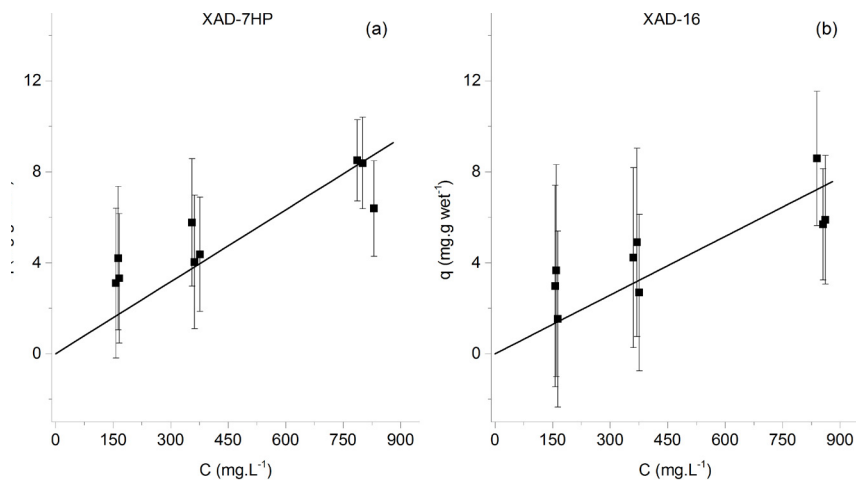
Figure 3.2 — Adsorption equilibrium isotherms of *p*-coumaric acid onto the Amberlite XAD-7HP resin (left) and the Amberlite XAD-16 resin (right). The isotherm data for the adsorption onto the XAD-7HP resin was published elsewhere.[16]

The capacity was expected to be relatively low, as *p*-coumaric acid is in its basic form in a pH 7.0 buffer (pka is 4.01)[17]. As the molecule carries a negative charge, its solubility in water is expected to increase and its hydrophobic interaction with the resin polymer backbone is also expected to decrease. As it is also possible to observe, there is a slightly higher adsorption capacity when using the XAD-7HP than the XAD-16 resin. The proposed explanation is that the XAD-7HP, since is made of an acrylic polymer with a higher dipole moment, can better establish polar interactions than the XAD-16 version, which is composed of a low dipole moment, styrene-divinylbenzene polymer.

The adsorption equilibrium isotherms of *p*-coumaric acid were also determined for the RENSA resins (shown in Figure 3.3) in the same pH 7.0 buffer. The adsorption strength seems to be only slightly stronger when compared to the Amberlite XAD resins. One possible explanation is that, although *p*-coumaric acid is deprotonated at pH 7.0, one of its hydroxyl groups is still able to participate in hydrogen bonding with the nitrogen atoms present

both in imidazole and pyridine functional groups. Both those molecules have a lone pair of electrons localized on a nitrogen atom, which can act as a hydrogen bond donor.
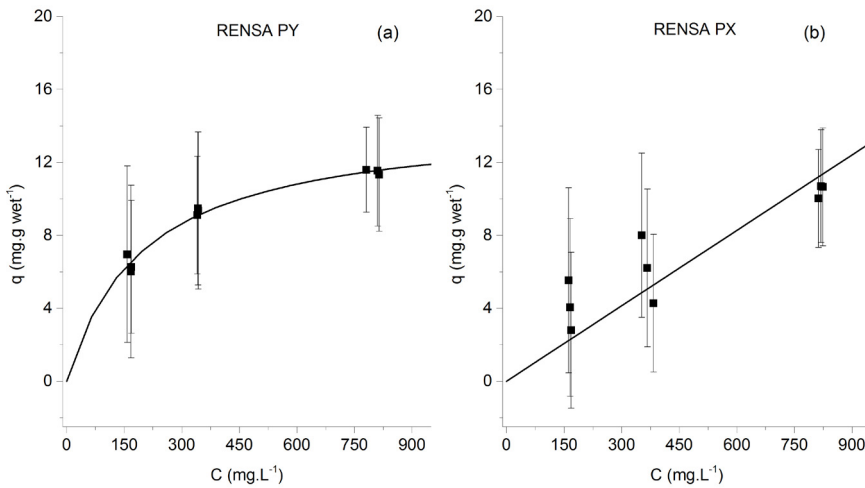
Figure 3.3 — Adsorption equilibrium isotherms of p-coumaric acid onto the RENSA PY resin (left) and the RENSA PX resin (right).

For all the adsorption equilibrium isotherm data obtained for *p*-coumaric acid, the estimated parameters are indicated in Table 3.1.

Table 3.1 – Estimated isotherm parameters for p-coumaric acid onto the XAD and the RENSA resins, using MilliQ water as solvent. When the parameter K is indicated, the linear isotherm was used. Otherwise, the Langmuir model was applied.

	XAD-7HP	XAD-16	PX	PY
Q_{max} (mg.g$_{wet}^{-1}$)	-	-	-	14±3
K_L (L.mg^{-1})	-	-	-	0.005±0.002
K (L.g$_{wet}^{-1}$)	0.011 ± 0.001	0.009±0.001	0.014±0.001	-

3.3.1.2 Naringenin

The fact that important hydrogen bonding can occur between polyphenols and these functionalised resins is what most likely contributes for a much stronger affinity. This effect is much more pronounced for naringenin and *trans*-resveratrol than for *p*-coumaric acid. In Figure 3.4 and Figure 3.5, the adsorption equilibrium isotherms of naringenin onto the Amberlite XAD-16 and XAD-7HP resins are shown. The results are depicted in two different figures for clarity, given the difference in the liquid phase concentration range.

For the aqueous solution, the maximum capacity is in the order of 19 mg.g wet^{-1} for the XAD-16 resin and of 11 mg g wet^{-1} for the XAD-7HP resin (Table 3.2). The affinity constants are 0.77 L.mg^{-1} and 0.53 L.mg^{-1} for the XAD-16 and XAD-7HP resins, respectively (Table 3.2).

3
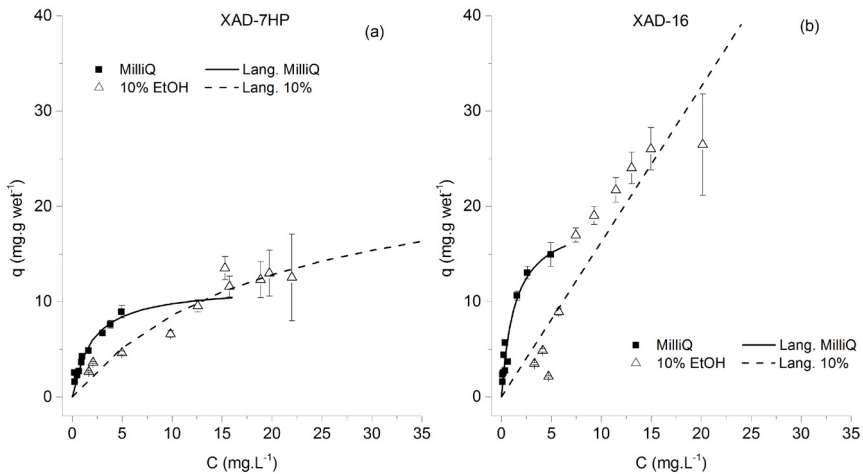
Figure 3.4 — Adsorption equilibrium isotherms of naringenin onto the Amberlite XAD-7HP (a) and XAD-16 (b) resins. Results are shown for MilliQ water and 10% ethanol.

Figure 3.5 — Adsorption equilibrium isotherms of naringenin onto the Amberlite XAD-7HP (c) and XAD-16 (d) resins. Results are shown for 20% and 35% ethanol.

As expected, the affinity of naringenin towards the resins decreased with the percentage of ethanol. This behaviour is probably mainly due to the increased interactions between the hydrophobic molecule and the more hydrophobic liquid phase, as the ethanol content increases. Unlike what was observed for *p*-coumaric acid, the XAD-16 resin seemed now to have a better adsorption performance than the XAD-7HP. The proposed explanation is equivalent to the one proposed for *p*-coumaric acid: since the XAD-16 resin is made of a more hydrophobic polymer, it is expected to participate in stronger interactions with naringenin, when compared to the XAD-7HP.

The isotherm data of naringenin onto the RENSA resins is depicted in Figure 3.6. As it is possible to observe, the isotherms determined with MilliQ water are much steeper than the ones for the XAD resins. For example, the affinity constant for the RENSA PY is of 4.1 L.mg^{-1} (Table 3.2), which is about ten times higher than for the XAD-16. This order-of-magnitude for the affinity constant is also much higher than what was observed for the adsorption of similar polyphenols onto standard hydrophobic resins.[18] This increased

3

affinity is probably due to the hydrogen bonding interactions that can occur between the hydroxyl groups in the polyphenols and the nitrogen atoms present in both RENSA PX and RENSA PY resins. This effect is now much more pronounced than it was for *p*-coumaric acid. Furthermore, the maximum capacity attained for the PY resin is approximately 38 mg.g wet[-1] and for the PX resin it is 31 mg.g wet[-1]. These values are between 1.6 and 3.5 times higher than the ones obtained for XAD resins, which proves that a larger surface area does not necessarily imply a higher capacity.

Table 3.2 — Estimated isotherm parameters for naringenin onto the XAD and the RENSA resins, using different water/ethanol solutions. When the parameter K is indicated, the linear isotherm was used. Otherwise, the Langmuir model was applied.

Ethanol %	0%	10%	20%	35%
XAD-7HP				
Q_{max} (mg.g$_{wet}^{-1}$)	11±1	25±5	-	-
K_L (L.mg^{-1})	0.53±0.07	0.05±0.01	-	-
K (L.g$_{wet}^{-1}$)	-	-	0.53±0.01	0.019±0.003
RENSA PY				
Q_{max} (mg.g$_{wet}^{-1}$)	38±2	-	38±2	38±2
K_L (L.mg^{-1})	4.1±0.4	-	0.104±0.009	0.0085±0.0009

Ethanol %	0%	10%	20%	35%
XAD-16				
Q_{max} (mg.g$_{wet}^{-1}$)	19±2	-	-	-
K_L (L.mg^{-1})	0.77±0.09	-	-	-
K (L.g$_{wet}^{-1}$)	-	1.63±0.02	0.77±0.02	0.017±0.004
RENSA PX				
Q_{max} (mg.g$_{wet}^{-1}$)	19±2	-	-	-
K_L (L.mg^{-1})	1.2±0.1	-	0.052±0.005	0.013±0.002

It should also be stated at this point that for the adsorption parameter estimation with the RENSA resins, a constant q_{max} was assumed (independent of the ethanol percentage). The reason

was twofold: the assumption of a constant saturation capacity for small molecules in reverse-phase adsorption has been observed previously[8] and a Langmuir model with a constant saturation capacity provided a lower Akaike information value than a model with three different capacities (one for each ethanol percentage).
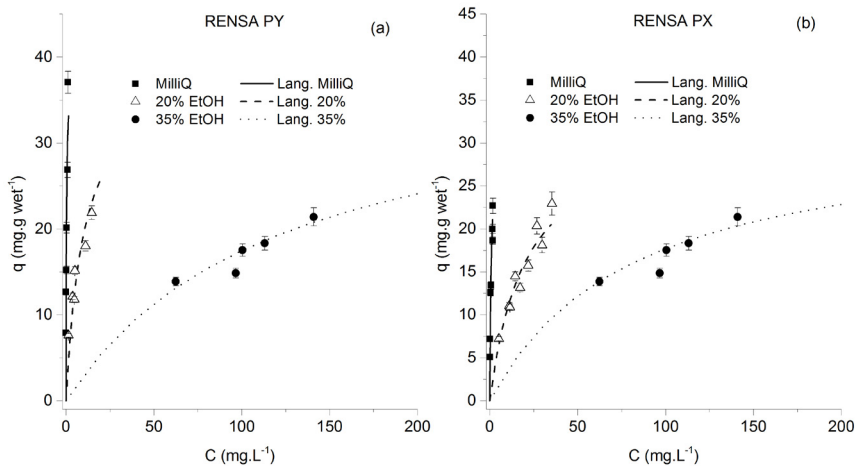
Figure 3.6 — Adsorption equilibrium isotherms of naringenin onto the RENSA PY resin (a) and the RENSA PX resin (b), using different ethanol percentages.

As it was shown in the previous isotherms, the tendency is for the isotherm slope to decrease with increasing concentration of ethanol. The suggested explanation is also the same as given before: the increased hydrophobicity of the mobile phase.

The fact that the maximum capacity for the RENSA resins can be assumed to be constant, independently of the percentage of ethanol does not seem to occur with the XAD resins. The proposed justification is that the orientation in which the polyphenol binds to the non-functionalised hydrophobic resins varies with increasing ethanol percentage. When an aqueous solution is present, probably the molecule tends to completely spread over the surface in order to minimize its content with the water molecules and maximize its hydrophobic interactions with the resin. On the other hand,

3

if ethanol is added, its orientation towards the surface might change in order to balance the interactions with the solvent and the hydrophobic surface. For the case of the functionalized resins, a similar mechanism might exist as in affinity chromatography: a specific molecule positioning ensures that a lower energy state is achieved, which might be solvent invariable (at least in this case using water-ethanol mixtures).

3.3.1.3 *trans*-resveratrol

For the case of *trans*-resveratrol, a much more noticeable difference between the performance of the XAD resins and the RENSA resins occurs. In Figure 3.7 and Figure 3.8, the isotherms for the XAD resins are depicted. The maximum capacity for a *trans*-resveratrol aqueous solution seems to reach 18 mg.g wet^{-1} for the XAD-16 and 11 mg.g wet^{-1} for the XAD-7HP.
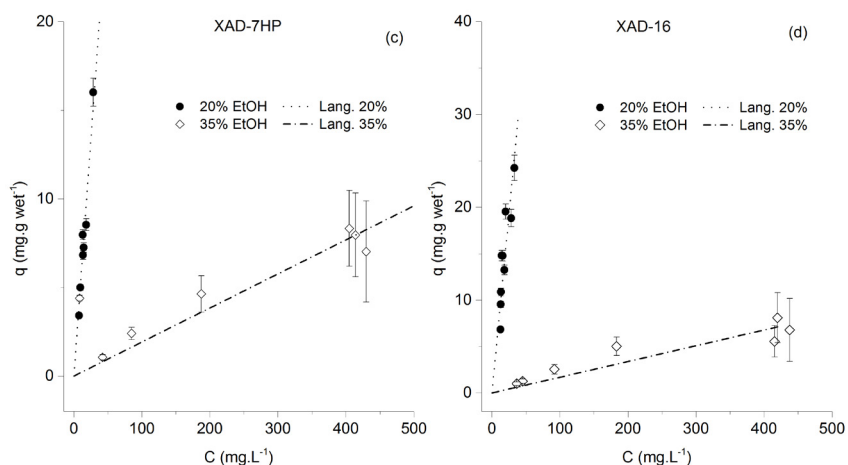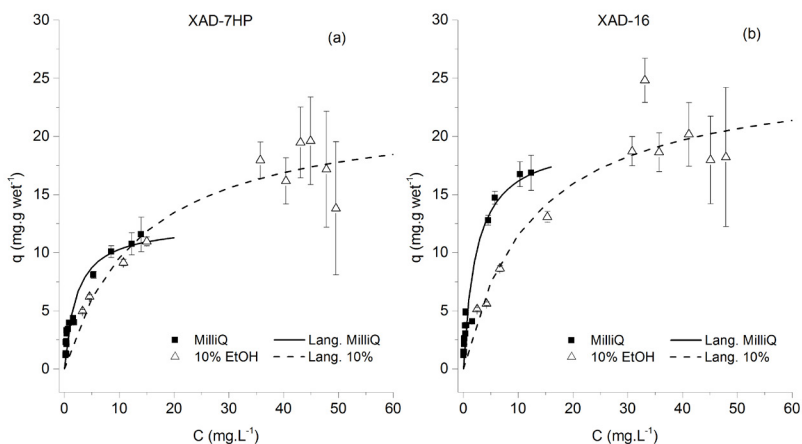

Figure 3.7 — Adsorption equilibrium isotherms of *trans*-resveratrol onto the Amberlite XAD-7HP (a) and XAD-16 (b) resins. Results are shown for MilliQ water and 10% ethanol. The isotherm data for the adsorption onto the XAD-7HP resin, using MilliQ water, was published elsewhere.[16]
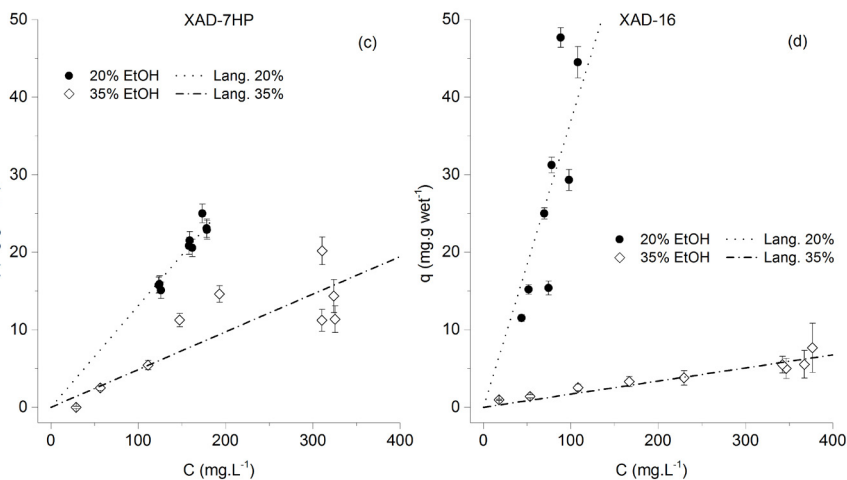
Figure 3.8 — Adsorption equilibrium isotherms of *trans*-resveratrol onto the Amberlite XAD-7HP (c) and XAD-16 (d) resins. Results are shown for 20% and 35% ethanol.

Like in the case of naringenin, the resin maximum capacity, for both XAD resins, seems to depend on the ethanol percentage. In Table 3.3, the regressed isotherm parameters are indicated. As previously mentioned, these isotherms were represented in different plots for improved clarity.

For the functionalized resins, a much better performance was obtained. The maximum capacity for the PX resin was estimated at 80 mg.g wet[-1] and that of PY at 58 mg.g wet resin[-1]. These results in an improvement of at least 3.3 times (when comparing RENSA PY over the XAD-16). The isotherm determined in pure water presents also an higher slope than with the XAD resins, which is again an indication of a possible specific interaction between these resins and the polyphenols (through hydrogen bonding). The improved performance of these functionalized resins is also seen when compared to other hydrophobic macroporous resins not considered in this work, where the adsorption capacities for *trans*-resveratrol are around 25 mg.g^{-1}.[19]
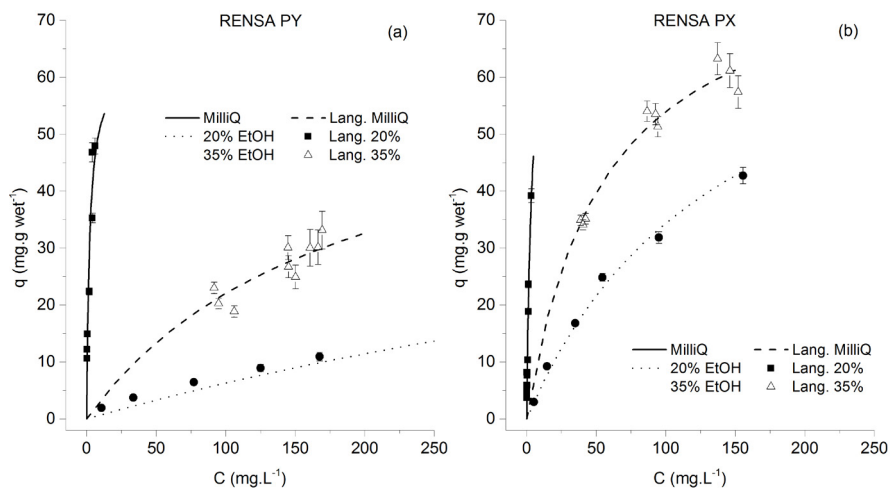
Figure 3.9 – Adsorption equilibrium isotherms of *trans*-resveratrol onto the RENSA PY resin (left) and the RENSA PX resin (right).

The estimated isotherm parameters for *trans*-resveratrol onto the RENSA resins are compiled in Table 3.3. It is worth mentioning that specific strong interactions between polyphenols and molecules containing nitrogen has been already documented. For example, it is known that there is a highly strong interaction between polyphenols and proteins which have a large number of histidine and proline residues.[20] Interestingly, histidine has a side chain imidazole group – included in the PX resins – and proline a pyrrolidine group.

Table 3.3 — Estimated isotherm parameters for naringenin onto the XAD and the RENSA resins, using different water/ethanol solutions. When the parameter K is indicated, the linear isotherm was used. Otherwise, the Langmuir model was applied.

Ethanol %	0%	10%	20%	35%
XAD-7HP				
Q_{max} (mg·g$_{wet}^{-1}$)	11±1	25±5	-	-
K_L (L.mg^{-1})	0.53±0.07	0.05±0.01	-	-

Ethanol %	0%	10%	20%	35%
K (L.g$_{wet}^{-1}$)	-	-	0.53±0.01	0.019±0.003
RENSA PY				
Q_{max} (mg.g$_{wet}^{-1}$)	38±2	-	38±2	38±2
K_L (L.mg^{-1})	4.1±0.4	-	0.104±0.009	0.0085±0.0009

Ethanol %	0%	10%	20%	35%
XAD-16				
Q_{max} (mg.g$_{wet}^{-1}$)	19±2	-	-	-
K_L (L.mg^{-1})	0.77±0.09	-	-	-
K (L.g$_{wet}^{-1}$)	-	1.63±0.02	0.77±0.02	0.017±0.004
RENSA PX				
Q_{max} (mg.g$_{wet}^{-1}$)	19±2	-	-	-
K_L (L.mg^{-1})	1.2±0.1	-	0.052±0.005	0.013±0.002

Despite the high affinity of these hydrophobic polyphenols towards the RENSA resins, one of the possible drawbacks when using these adsorbents is a difficult desorption. To confirm this, when analysing Table 3.3, one can check that the isotherm slope for resveratrol when using the RENSA PX resin is more than ten times higher than when using the XAD-7HP. One of the possibilities to counter-act this effect is to protonate the nitrogen groups present in pyridine or imidazole, in order for them not to act as hydrogen bond donors and thus weaken their interaction (Figure 3.10).
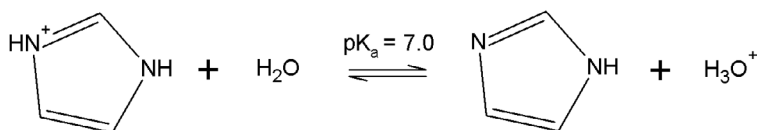
Figure 3.10 – Acid-base reaction involving the molecule of imidazole

To confirm this hypothesis, the adsorption equilibrium isotherms of both *trans*-resveratrol and naringenin onto the RENSA PX were

obtained for 20% ethanol solutions containing 1% v/v of a 37% HCl solution and they are displayed in Figure 3.11.
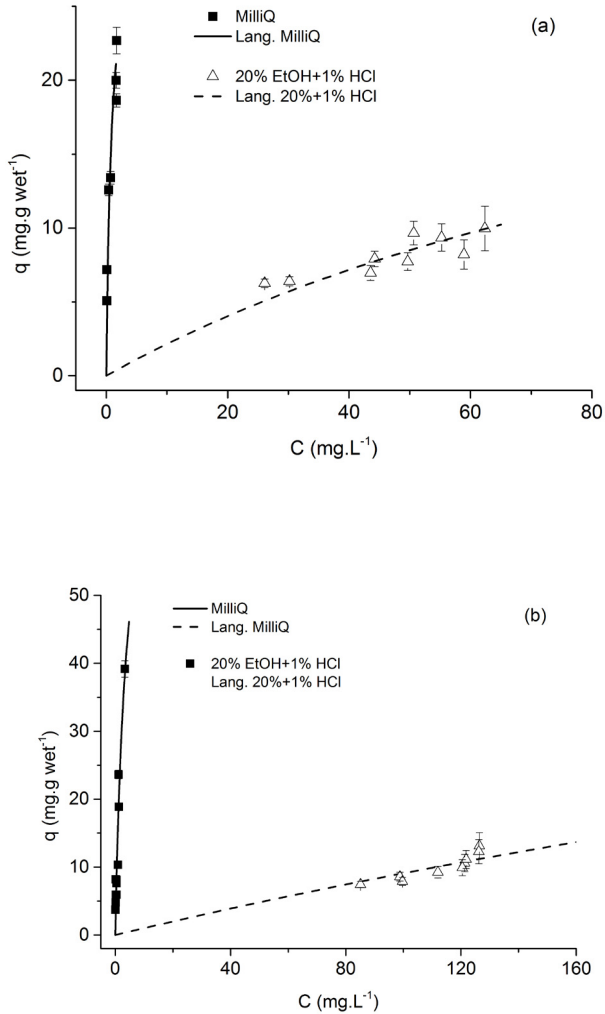
Figure 3.11 — Adsorption equilibrium isotherms of naringenin (left) and *trans*-resveratrol (right) onto the RENSA PX resin, when adding 1% HCl to the ethanolic solutions.

The estimated isotherm parameters, again assuming a constant q_{max}, are indicated in Table 3.4.

Table 3.4 – Comparison of the estimated isotherm parameters for *trans*-resveratrol and naringenin onto the RENSA resins, for 20% ethanol (the parameters for the experiments with MilliQ water are shown as a reference). As it is indicated, the slope reduces approximately by a factor of 10.

	Water	20%	20%+1%HCl
***trans*-resveratrol on RENSA PX**			
Q_{max} (mg.g$_{wet}$$^{-1}$)	80±5	80±5	80±5
K_L (L.mg^{-1})	0.26±0.02	0.019±0.003	0.0013±0.0001

	Water	20%	20%+1%HCl
naringenin on RENSA PX			
Q_{max} (mg.g$_{wet}$$^{-1}$)	31±1	31±1	31±1
K_L (L.mg^{-1})	1.2±0.1	0.052±0.005	0.0074±0.0006

As it was proposed, by adding 1% HCl to the water-ethanol solutions, a much weaker adsorption equilibrium isotherm is obtained. The fact that imidazole is no longer able to participate in hydrogen bonding, not only makes desorption possible, but it also seems to become easier than for the XAD resins. In Table 3.5, the initial slope of the isotherms of *trans*-resveratrol and naringenin is compared for both XAD and RENSA resins.

3

Table 3.5 – Initial isotherm slope of *trans*-resveratrol (left) and naringenin (right) onto the studied XAD resins and the RENSA PX resin at 20% EtOH and 20% EtOH+1% HCl.

	trans-resveratrol		naringenin	
	K 20% EtOH (L.g wet^{-1})	K 20% EtOH + 1% HCl (L.g wet^{-1})	K 20% EtOH (L.g wet^{-1})	K 20% EtOH + 1% HCl (L.g wet^{-1})
XAD-7HP	0.129±0.006	-	0.53±0.01	-
XAD-16	0.369±0.007	-	0.77±0.02	-
PX	1.5±0.3	0.10±0.02	1.6±0.2	0.23±0.03

As indicated in the table, by adding 1% HCl to the ethanolic solution, the isotherm slope becomes even lower than the weakest XAD resin – XAD-7HP. From these results, it is possible to conclude that by acidifying the ethanolic mixture, elution of both naringenin and *trans*-resveratrol should become even easier than with the XAD resins, making them more efficient not only for adsorption but also for desorption.

3.3.2 Isotherm slope as a function of ethanol content

In order to develop a mechanistic model for any chromatographic process, it is necessary to describe the dependence of the isotherm slope with the modifier concentration to be used (ethanol in this case). For this purpose, the previously introduced exponential model was used (eq. 3.9), that relates the isotherm slope with the concentration of modifier. In Figure 3.12, it is depicted the variation of the isotherm slopes with the ethanol concentration for all the systems investigated, together with the fitted exponential model.
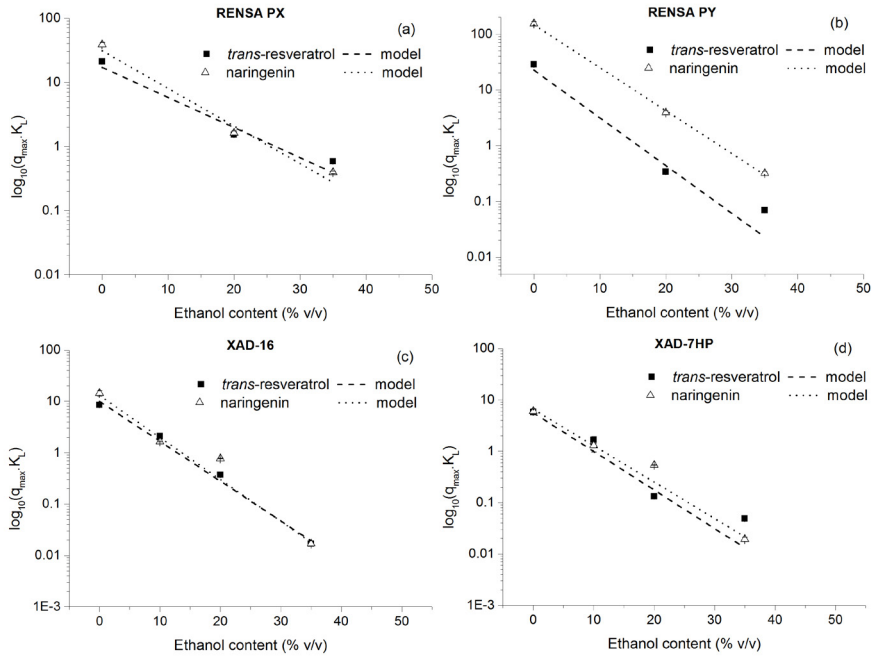
Figure 3.12 – Dependence of the isotherm slope ($q_{max}.K_L$) with the ethanol volumetric percentage in the mobile phase. For all the cases, the exponential model seems to provide a good description of the observed experimental data.

The estimated parameters are indicated in Table 3.6 for both *trans*-resveratrol and naringenin. The obtained results seem to confirm that the lower capacity of the resins at higher ethanol content, is mainly due to the higher partition of these molecules for the liquid phase rather than adsorption competition. This conclusion is based on the previously assumed exponential model, which seems to describe well the trend of the experimental observations, given the obtained R^2 values (Table 3.6).

Table 3.6 – Estimated parameters for the exponential model applied to *trans*-resveratrol and naringenin, describing how the isotherm slope varies with the percentage of modifier (ethanol in this case).

	trans-resveratrol			
	XAD-7HP	XAD-16	PY	PX
	5.59±0.05	9.9±0.1	23±1	17±4
	-0.1728±0.0005	-0.1786±0.0004	-0.197±0.002	-0.108±0.007
R^2	0.978	0.953	0.956	0.956
	naringenin			
	XAD-7HP	XAD-16	PY	PX
	6.6±0.2	13.0±0.2	146±90	31±7
	-0.163±0.001	-0.1882±0.0004	-0.18±0.02	-0.135±0.007
R^2	0.980	0.985	0.998	0.962

3

3.3.3 Resin performance comparison: capacity and selectivity

In order to quantify the different performance of the two groups of resins, two performance parameters were compared: their maximum capacity (Figure 3.13a) and their naringenin/*trans*-resveratrol selectivity (Figure 3.13b). For the calculation of selectivity, the ratio of the initial isotherm slopes determined with MilliQ water was calculated.
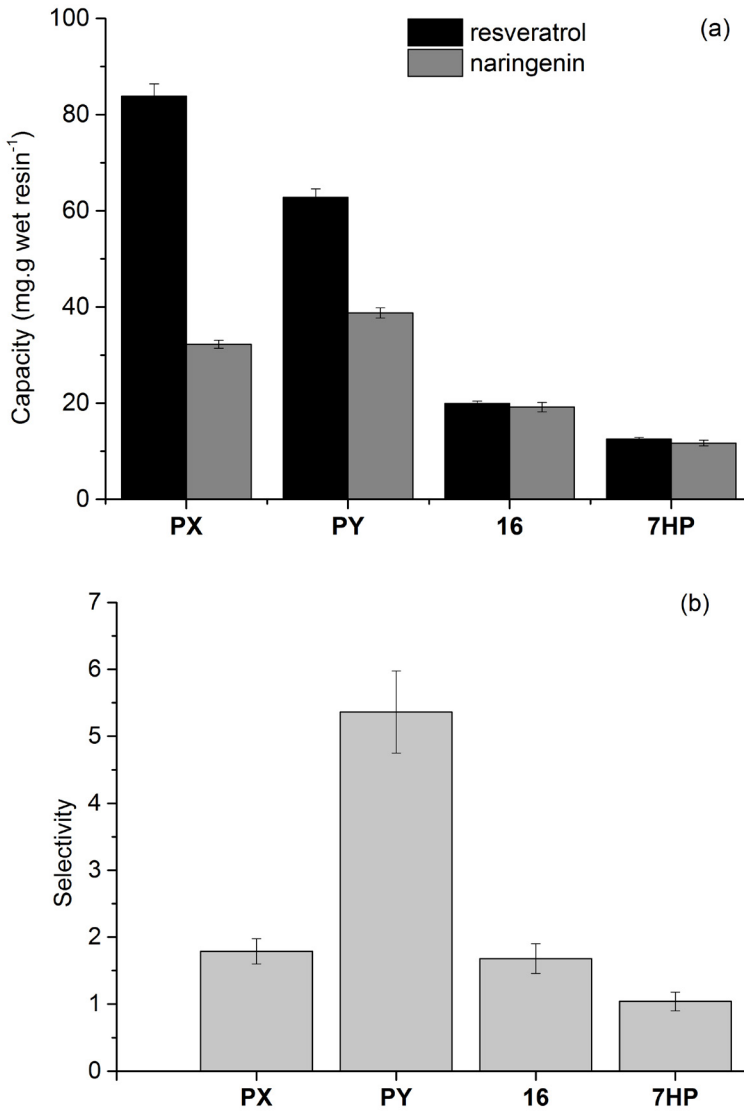
Figure 3.13 – **Comparison of the maximum capacity and selectivity for the three different model polyphenols tested. Capacity (shown on the left) seems to be much higher for the functionalized resins. Regarding selectivity (shown on the right), the RENSA PY clearly outperforms all the other options for a possible _trans_-resveratrol/naringenin separation.**

As one can observe for both cases, the RENSA resins have a better capacity than the XAD series. This indicates that these resins might be a better option when intended for use in an initial capture step. Considering, for example, the adsorption of *trans*-resveratrol onto the PX resin, its capacity is almost ten times the one of XAD-7HP. While the RENSA resins are more expensive than the XAD series, this would mean that almost ten times less resin would be needed, resulting also in a smaller column.

In terms of selectivity, the *trans*-resveratrol/naringenin case was selected, as it is a more challenge purification. From all the studied materials, the RENSA PY clearly stands out. This higher selectivity can be explained from the fact that not only hydrophobicity – like for the XAD resins –, but also hydrogen bonding is also involved during binding. So, in the end, a mixed-mode like behaviour is likely to be present and enhance the specificity of these resins. This did not seem to happen with the PX resin, but other factors might also be involved. It may be possible that, for example, the geometry of the adsorption interaction is similar for both *trans*-resveratrol and naringenin. In that case, despite the higher capacity, not much selectivity is achieved.

Another aspect should also be mentioned at this point and it is related to peak resolution. Given that both RENSA resins have approximately five times less diameter than the XAD resins, even if the selectivity for a given separation is the same (e.g., RENSA PX and XAD-16), peak resolution should be much better due to the improved mass transfer.[21] For this reason, the RENSA resins should also probably be a better option for a purification step than the XAD resins. However, in order to have a more definite conclusion, a more in-depth economic analysis would be needed.

3.4 Conclusion

This work exploited the potential of using hydrophobic resins, functionalized either with imidazole or pyridine, for the adsorption of three polyphenols: *p*-coumaric acid, *trans*-resveratrol and naringenin A comprehensive isotherm determination was performed for a range of different ethanol concentrations in water. A model for

describing the single-component isotherms as function of the modifier concentration (ethanol) was provided and it proved to fit quite well the experimental observations. The regressed parameters are enough for the reader to perform any dynamic chromatography simulations, provided they estimate the needed mass transfer coefficients.

The obtained results indicated that functionalized resins could achieve much higher adsorption capacity, proving that this is not exclusively determined by surface area but probably also by the binding orientation. The suggested explanation is based on the capability of pyridine and imidazole to establish hydrogen bonding, a mechanism that is also present in the strong polyphenol-protein interactions, when histidine and proline residues are present. It thus become possible for polyphenols – rich in hydroxyl groups – not only to establish hydrophobic interactions with the resin backbone (as it happens with the XAD resins), but also to have an increased interaction energy through hydrogen bonding. The same mechanism can probably explain why the RENSA PY resin could achieve a much higher selectivity for the *trans*-resveratrol/ naringenin separation. Unlike the case of the XAD resins, a mixed mode behaviour may be present, based on both hydrophobic and hydrogen bonding interactions. This can add another degree of freedom, which can affect both the geometry and the strength of the adsorption interaction and thus increase selectivity.

These results would have no practical applicability if desorption of the desired compounds would not be possible. Nonetheless this study demonstrated that by acidifying the water/ethanol elution solution, polyphenol desorption became not only possible but even easier than for the XAD resins, for the same ethanol concentration. By protonating the imidazole group in RENSA PX resin, hydrogen bonding could no longer occur, thus weakening the adsorption interaction.

Both in terms of capacity and selectivity, this work proposes that the RENSA resins might be a better option than the standard XAD resins, despite their higher cost. Being able to use less resin would probably result in less inventory and also in a smaller column size and solvent annual cost. However, more detailed economic studies are required to achieve stronger conclusions.

Appendix B

The main physical properties of the resins used in this work are indicated in Table B1.

Table B1 – Summary of the physical characteristics of the selected hydrophobic resins.

Resin	Dipole moment	Diameter (μm)	Surface area (m².g dry⁻¹)	Porosity (mL.mL⁻¹)
XAD-7HP	1.8	500	450	0.59
XAD-16	0.3	500	900	0.66
RENSA PX	n.a.	60	100	0.69
RENSA PY	n.a.	100	500	0.63

These values were obtained by the method explained in section 3.2.3.1

Resin	Wet density (g_{wet}.mL⁻¹)	Wet/dry mass ratio	Skeletal density (g_{dry} . mL⁻¹)	Bulk density (g_{wet} mL⁻¹)
XAD-7HP	1.05	2.9	1.24	630
XAD-16	1.02	2.9	1.08	610
RENSA PX	1.03	2.9	$1.11\pm0.03^{+}$	620
RENSA PY	1.04	2.6	$1.13\pm0.03^{+}$	620

These values were obtained by the method explained in section 3.2.3.2

Acknowledgements

References

1 Transparency Market Research, Polyphenols Market by Product (Grape Seed, Green Tea, Apple and Others), by Application (Functional Beverages, Functional Food, Dietary Supplements and Others): Global Industry Analysis, Size, Share, Growth, Trends and Forecast, 2012 - 2018. **2013**.

2 Alov, P.; Tsakovska, I.; Pajeva, I., Computational Studies of Free Radical-Scavenging Properties of Phenolic Compounds. *Current Topics in Medicinal Chemistry* **2015,** 15, (2), 85-104.

3 Scalbert, A.; Johnson, I. T.; Saltmarsh, M., Polyphenols: antioxidants and beyond. *Am J Clin Nutr* **2005,** 81, (1 Suppl), 215S-217S.

4 Pandey, K. B.; Rizvi, S. I., Plant polyphenols as dietary antioxidants in human health and disease. *Oxidative Medicine and Cellular Longevity* **2009,** 2, (5), 270-278.

5 Kammerer, D. R.; Carle, R.; Stanley, R. A.; Saleh, Z. S., Pilot-scale resin adsorption as a means to recover and fractionate apple polyphenols. *J Agric Food Chem* **2010,** 58, (11), 6787-96.

6 Soto, M. L.; Moure, A.; Domínguez, H.; Parajó, J. C., Recovery, concentration and purification of phenolic compounds by adsorption: a review. *Journal of Food Engineering* **2011,** 105, (1), 1-27.

7 Sun, X. L.; Shao, Y. D.; Yan, W. D., Measurement and Correlation of Solubilities of *trans*-Resveratrol in Ethanol plus Water and Acetone plus Water Mixed Solvents at Different Temperatures. *Journal of Chemical and Engineering Data* **2008,** 53, (11), 2562-2566.

8 Guiochon, G., Attila Felinger, and Dean GG Shirazi, *Fundamentals of Preparative and Nonlinear Chromatography*. Academic Press: 2006.

9 Carta, G.; Jungbauer, A., *Protein Chromatography: process development and scale-up*. 2010.

10 Green, D.; Perry, R., *Perry's Chemical Engineers' Handbook, Eighth Edition*. McGraw-Hill Education: 2007.

11 Dorfner, K., *Ion exchangers*. 1st Edition ed.; Walter de Gruyter: 1991.

12 Monsanto, M.; Mestrom, R.; Zondervan, E.; Bongers, P.; Meuldijk, J., Solvent Swing Adsorption for the Recovery of Polyphenols from Black Tea. *Industrial & Engineering Chemistry Research* **2015,** 54, (1), 434-442.

13 Melander, W. R.; el Rassi, Z.; Horvath, C., Interplay of hydrophobic and electrostatic interactions in biopolymer chromatography. Effect of salts on the retention of proteins. *J Chromatogr* **1989,** 469, 3-27.

14 Sevillano, D. M.; Jankowiak, L.; van Gaalen, T. L. T.; van der Wielen, L. A. M.; Hooshyar, N.; van der Goot, A. J.; Ottens, M., Mechanism of Isoflavone Adsorption from Okara Extracts onto Food-Grade Resins. *Industrial & Engineering Chemistry Research* **2014,** 53, (39), 15245-15252.

15 Skoog, D. A.; F. James Holler; Crouch., S. R., *Principles of instrumental analysis.* 2007.

16 Braga, A.; Silva, M.; Oliveira, J.; Silva, R.; Ferreira, P.; Ottens, M.; Rocha, I.; Faria, N., An adsorptive bioprocess for production and recovery of resveratrol with Corynebacterium glutamicum. *Journal of Chemical Technology & Biotechnology* **2017**.

17 Chemicalize was used for calculating the pKa of p-coumaric acid, January, 2018, https://chemicalize.com/ developed by ChemAxon (http://www.chemaxon.com).

18 Sevillano, D. M.; van der Wielen, L. A.; Hooshyar, N.; Ottens, M., Resin selection for the separation of caffeine from green tea catechins. *Food and Bioproducts Processing* **2014,** 92, (2), 192-198.

19 Xiong, Q.; Zhang, Q.; Zhang, D.; Shi, Y.; Jiang, C.; Shi, X., Preliminary separation and purification of resveratrol from extract of peanut (Arachis hypogaea) sprouts by macroporous adsorption resins. *Food Chem* **2014,** 145, 1-7.

20 Charlton, A. J.; Baxter, N. J.; Khan, M. L.; Moir, A. J.; Haslam, E.; Davies, A. P.; Williamson, M. P., Polyphenol/peptide binding and precipitation. *J Agric Food Chem* **2002,** 50, (6), 1593-601.

21 Felinger, A.; Guiochon, G., Comparison of the kinetic models of linear chromatography. *Chromatographia* **2004,** 60, S175-S180.

4

An adsorptive bioprocess for production and recovery of resveratrol with *Corynebacterium glutamicum DelAro4*

Abstract

The growing interest in polyphenols has led to the design of industrial-scale processes able to produce them by fermentation and recover them in a more sustainable way. The goal of this work is to present two integrated approaches for the recovery of resveratrol, obtained through fermentation. The production of resveratrol using *Corynebacterium glutamicum* and its continuous removal using a hydrophobic resin is described. Batch production is compared with *in-situ* product removal, where Amberlite XAD-7HP is either directly added to the medium (direct adsorption) or is present in an external column (external adsorption).

For both adsorption strategies tested, the amount of extracellular resveratrol increased from 75% to at least 90% of the total amount produced. However, lower total resveratrol concentrations were attained – 3.6 and 2.2 mg L^{-1}, for the external and direct contact strategies, respectively, *versus* 5.3 mg L^{-1} for batch experiments.

The proposed *in-situ* removal strategies demonstrated the potential of increasing the excretion of resveratrol produced intracellularly.. These process configurations may not only lead to a simpler downstream process design, but also to the avoidance of potential problems with the toxicity of polyphenols to the cells, especially when larger titers are obtained.

4.1 INTRODUCTION

Polyphenols are secondary metabolites, naturally produced by plants, which have a wide range of applications, such as colorants and nutraceuticals. The molecule of resveratrol is one of those compounds, which is speculated to help reducing cardiovascular mortality, lung and prostate cancer, with anti-inflammatory, anti-diabetic, antithrombotic, and anti-aging properties.[1]

Although most of the commercially available resveratrol is obtained by extraction from plants, such as *Polygonum cuspidatum*,[2] there can be several advantages associated with the use of fermentation based processes for its production. Some of the most important ones are the less complex purification process (due to the simpler chemical matrix), the possibility of having more productivity by means of strain genetic engineering and the fact that no large crop areas are needed. The concentration of resveratrol that can be obtained from plant cell cultures is at most equal to that reported as naturally occurring in the plant, being the grape cell suspensions (*V. vinifera*) the most promising one, with a resveratrol yield ranging from 2-5 mg L^{-1}.[3,4] The first studies for microbial resveratrol production reported the use of *Saccharomyces cerevisiae* and *Escherichia coli* as cell factories, with a production of around 0.5 g L^{-1}. [2,5-10] More recently, other organisms, such as *C. glutamicum*, which is a workhorse in industrial biotechnology, especially for the production of several aminoacids [11], proved to be a promising host organisms for resveratrol production [12,13]. It is a generally regarded as safe (GRAS status) microorganism able to achieve high cell densities[14], with high resistance to the presence of small aromatic compounds[15], able to grow on *p*-coumaric acid, ferulic acid, caffeic acid and 3-(4-hydroxyphenyl)- propionic acid as sole carbon and energy sources[16]. This bacterium has also already been genetically modified for the synthesis of resveratrol directly from glucose [12,17]. *Corynebacterium glutamicum* DelAro4 pMKEx2_*sts*$_{Ah}$-*4cl*$_{Pc}$ pEKEx3_*aroH*$_{Ec}$_*tal*$_F$ has the shikimate pathway deregulated for overproducing *L*-tyrosine and an heterologous tyrosine ammonia lyase (TAL) for the conversion of *L*-tyrosine to *p*-coumaric acid. Those are key steps for connecting the endogenous amino acid anabolism from glucose to the synthetic polyphenol

pathway[12], avoiding the addition of precursors, which would render the production processes expensive for industrial applications [18,19].

Although effort is being put in the pathway engineering in *C. glutamicum*, the improvement of the resveratrol production as a whole – including the downstream process – is essential. It is known that resveratrol stability is dependent on process conditions such as dissolved oxygen, pH, temperature and light[20]. For example, a temperature higher than 30 °C seemed to affect the production of resveratrol in *E. coli*[21]. Moreover, resveratrol can have a negative effect on cell growth when concentrations are in the 0.5 g L^{-1} range [22]. All these unwanted effects can be avoided to some extent, by using an *in-situ* product removal strategy[23].

The goal of this work is to evaluate and compare the performance (in terms of yield, product excretion and process simplicity) of the batch production of resveratrol using *C. glutamicum* in three scenarios: no product removal, product removal by direct contact with hydrophobic resins (present inside the liquid) and product removal by external adsorption (using an adsorption column).

4.2 Experimental Procedures

4.2.1 Bacterial strain, media and growth conditions

Corynebacterium glutamicum DelAro[4] pMKEx2_sts_{Ah}-$4cl_{Pc}$ pEKEx3_$aroH_{Ec}$_tal_F strain was kindly supplied by the Institute of Bio- and Geosciences (IBG) (Jülich, German) within the scope of the BachBerry project [12]. It was cultivated aerobically at 30 °C in Brain Heart Infusion (BHI) medium (only for precultures) or defined CGXII medium with glucose as sole carbon and energy sources [24]. CGXII medium (pH 7.0) contained (per liter) 20 g of $(NH_4)_2SO_4$, 1 g of KH_2PO_4, 1 g of K_2HPO_4, 0.25 g of $MgSO_4$x$7H_2O$, 10 mg of $CaCl_2$, 10 mg of $FeSO_4$x$7H_2O$, 10 mg of $MnSO_4$xH_2O, 1 mg of $ZnSo_4$x$7H_2O$, 0.2 mg of $CuSO_4$, 0.02 mg of $NiCl_2$x$6H_2O$, 0.2 mg of biotin, 5 g of urea, 42 g of 3-morpholinopropanesulfonic acid (MOPS), 40 g of glucose, and 30 mg of protocatechuic acid. For plasmid

maintenance kanamycin (25 mg L^{-1}) and spectinomycin (100 mg L^{-1}) were added to the medium. In the fermenter experiments, urea and MOPS were omitted as the pH was automatically controlled.

Corynebacterium glutamicum was cultivated for 8-10 hours in a 500 mL baffled Erlenmeyer flask containing 50 mL of BHI medium on a rotary shaker at 200 rpm (first preculture) and was subsequently inoculated into 100 mL CGXII medium in 1 L baffled Erlenmeyer flasks (second preculture). The starting OD_{600} for the second preculture was 1. The second preculture was cultivated for 16-17 hours on a rotary shaker at 200 rpm and used to inoculate the fermenter to an initial OD_{600} of 1. The heterologous gene expression was induced with 1 mM IPTG at a biomass concentration of 2-3 g L^{-1}. The fermentation experiments were performed in a 2-L DASGIP® Parallel Bioreactor System for Microbial Applications with 3 simultaneous bioreactors placed on a temperature controlled BioBlock. The operating volume for the fermentations was 1 L, the temperature set-point was maintained at 30 °C, the pH was automatically controlled at 7 by the addition of NaOH 3 M and HCl 3 M. The dissolved oxygen was kept above 30 % of saturation by feedback control of the stirring speed from 650 rpm until a maximum of 1500 rpm and air-flow rate of 1 vvm. Foam was disrupted by addition of antifoaming agent, Antifoam 204 (Sigma-Aldrich).

In the external adsorption experiments the bioreactor was connected to a microfiltration unit (Microdyn-Nadir Filter Module MD 020 CP 2N) in a closed loop. The fermentation broth was pumped through the microfiltration unit using a peristaltic pump at a flow-rate of 10 L min $^{-1}$. The retentate from the microfiltration unit was led back to the bioreactor and the cell-free permeate was pumped through the adsorption column (bed dimensions 25x400 mm) containing 60 g of Amberlite XAD-7 HP resin and then fed back into the bioreactor (Figure 4.1a). It was determined for the XAD-7 HP resin, that with a resveratrol liquid concentration of 5 mg L^{-1} (value obtained for the batch experiments with no product removal, shown in the Results section), the resin capacity is 5 mg resveratrol g wet^{-1} (shown in the Results section). Assuming that the dynamic binding capacity would be 10 % of the equilibrium

4

binding capacity (adsorption kinetics is not infinitely fast), 10 g of wet resin would be the minimum quantity needed in the column to bind all the produced compound. For that reason and also to account for a possible production increase using this strategy, 60 g of resin were used.

In the direct adsorption experiments, Amberlite XAD-7 HP beads were weighed and placed (10 g L^{-1}) inside the bioreactor before inoculation (Figure 4.1b). This solid phase concentration was also chosen for the above-mentioned reasons.
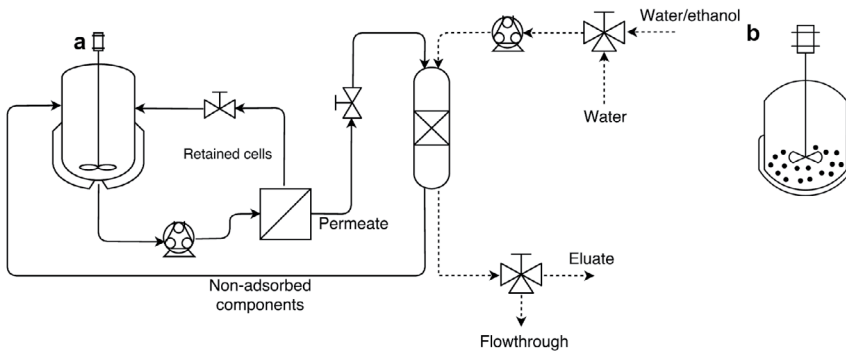
Figure 4.4.1 - Experimental set-up for the "External Adsorption" (a) and "Direct Adsorption" (b) strategies.

4.2.3 Adsorption isotherm determination via batch uptake experiments

The determination of the adsorption isotherms of resveratrol and *p*-coumaric acid was performed by batch uptake experiments, using glass flasks with rubber stops. A stock solution saturated with the compound of interest – either resveratrol or *p*-coumaric acid – was prepared. In the case of resveratrol, the solvent was MilliQ water and for *p*-coumaric acid, the solutions were prepared with 0.1 M sodium phosphate monobasic buffer at pH 7.0, in order to mimic fermentation conditions (where pH is controlled

at 7.0). Before adsorption took place, the XAD-7HP resin was first washed with MilliQ water, then with ethanol and afterwards equilibrated with the desired solvent.

The flasks were shaken at 525 rpm in an orbital shaker Heidolph Titramax 1000 (Heidolph Instruments GmbH & Co. KG, Germany) at room temperature (20 ± 2 °C) for 3 hours, in order to achieve equilibrium (adsorption kinetics data not shown). At the end of the experiment, for the case of *p*-coumaric acid, a sample of 1 µL was injected in the UHPLC. For the case of resveratrol, when the liquid concentration was expected to be too low, the sample was first concentrated by extraction with butyl acetate (concentration factor was 4 or 5). A sample of 1 µL was then taken from the organic phase for UHPLC analysis.

4.2.4 Resin pretreatment

The resin used during the performed fermentation experiments was the Amberlite XAD-7HP from Sigma-Aldrich. The main physical characteristics of the resin are shown in Table 4.1. The resin beads were first soaked in 100 % ethanol for 30 min at room temperature. They were then washed 2 times with MilliQ water in order to remove the salts that come with the shipped product (data from supplier, Sigma-Aldrich), filtered and left to dry.

Table 4.1 — Physical characteristics of the selected resins.

Resin	Dipole moment	Diameter (µm)	Surface area ($m^2\ g_{dry}^{-1}$)	Wet density ($g_{wet}\ mL^{-1}$)	Wet dry mass ratio^{-1}
XAD-7HP	1.8	500	450	1.05	2.9

Skeletal density ($g_{dry}\ mL^{-1}$)	Bulk density ($g_{wet}\ mL^{-1}$)		Porosity (mL mL^{-1})
1.24	630		0.59

In Table 4.1, the porosity was obtained in mL g^{-1} dry from the supplier and converted to mL mL^{-1}. This was achieved by dividing the specific void volume (ε_p) by the total particle volume (void + skeleton volume ($1/\rho_{skel}$)). The term ρ_{skel} corresponds to the resin skeleton density.

$$\varepsilon_p(mL/mL) = \frac{\varepsilon_p(mL/g_{dry})}{\varepsilon_p(mL/g_{dry}) + \dfrac{1}{\rho_{skel}\,(g/mL)}} \qquad (4.1)$$

In Table 4.1, the wet dry^{-1} mass ratio was obtained considering that the moisture holding capacity of the resins is 65% (data from supplier). The bulk density (ρ_{bulk}) was calculated from the resin wet density (ρ_{wet}), obtained from the supplier, and by considering that the external porosity (ε) has a typical value of 0.4 [25]:

$$\rho_{bulk} = \rho_{wet} \cdot (1 - \varepsilon) \qquad (4.2)$$

4.2.4 Sampling and quantification of glucose and biomass

Samples from the bioreactor were taken at regular sampling times for the analysis of biomass and glucose. Biomass concentration was determined by measuring OD_{600}. The OD values were converted to biomass dry weight using a calibration procedure. HPLC analysis was performed in a JASCO system using a refractive index detector (RI- 2031). The supernatants of the samples were analyzed using an Aminex HPX-87H column from Bio-Rad, which was kept at 60 °C and 10 mM H_2SO_4 was used as mobile phase with a flow rate of 0.5 mL min^{-1}. Quantitative analysis of glucose was performed by injecting standards with known concentrations. The calibration curve was calculated using the peak areas of the RI detector for glucose.

4

4.2.5 Extraction of metabolites from the medium

For the quantification of *p*-coumaric acid and resveratrol, metabolite extracts from the cultivation broth were prepared according to Kallscheuer et al. [12] with some modifications. Extracellular and broth (intracellular + extracellular) polyphenols concentrations were measured using the supernatant, after centrifugation, and total broth, respectively. Metabolite extracts were prepared by mixing 1 mL of the samples, acidified at pH 2 with 6 M HCl, with 1 mL ethyl acetate and vigorously shaking for 2 min, in order to permeabilize the cells [26]. The suspension was centrifuged for 5 min at 8000 g and the ethyl acetate layer (600 μL) was transferred to a solvent-resistant micro tube (Eppendorf, Germany). After evaporation of the ethyl acetate overnight, dried extracts were resuspended in 100 μL of acetonitrile and directly used for UHPLC analysis.

4.2.6 Extraction of metabolites from resins

At the end of the fermentation, the resin was separated from the broth by sedimentation and was first washed with a 10% ethanol/water volume equivalent to 5-fold of wet bead weight (direct adsorption) or 5 column volumes (external adsorption). The amount of resveratrol extracted, after this washing step, was quantified and found to be negligible. In the end, the resin was eluted with 70 % ethanol/water (10 column volumes for the external adsorption and 10 times the wet bead weight for direct adsorption). With this ethanol content, no binding of resveratrol is expected to occur (Silva et al. (unpublished)). Although not specifically for this molecule, the same conclusions regarding similar polyphenols were obtained by Monsanto et al. [27] and David Mendez et al. [28] called isoflavones, among other components (i.e., proteins, sugars, fibers, etc.. Both fractions, from the washing and elution steps, were used for UHPLC analysis.

4

4.2.7 Stilbenes determination – fermentation experiments

Stilbenes (resveratrol and *p*-coumaric acid) in extracted samples were quantified by using an UHPLC SHIMADZU system using a diode array detector SPD-M20A. Separation was carried out with a Kinetex 1.7u C18 100 Å pore size column (50 mm by 2.1 mm [internal diameter]; Phenomenex) at 50 °C. For elution, 0.1 % acetic acid (solvent A) and acetonitrile supplemented with 0.1 % acetic acid (solvent B) were applied as the mobile phases at a flow rate of 0.5 mL min^{-1}. A gradient was used, where the amount of solvent B was increased stepwise: minute 0 to 6: 10 % to 30 %, minute 6 to 7: 30 % to 50 %, minute 7 to 8: 50 % to 100 % and minute 8 to 8.5: 100 % to 10 %[12]. Area values were linear up to metabolite concentrations of at least 250 mg L^{-1}. The detection of *p*-coumaric acid was performed at 277 nm and that of resveratrol at 333 nm.

4.2.8 Stilbenes determination – adsorption experiments

For the experiments involving the resin adsorption isotherm determination and adsorption kinetics, a different UHPLC method was used. In this case, the quantification of *p*-coumaric acid and resveratrol was carried out by UHPLC (Ultimate 3000, Thermo Scientific, USA) in a C18 column (Acquity UPLC HSS column, 1.8μm, 2 .1mm x100 mm Waters, Milford, USA). Mobile phase A consisted of 10% formic acid in Milli-Q water and mobile phase B of 10% formic acid in acetonitrile. Every run was performed in isocratic mode, with the mobile phase containing 33.5% of B and 66.5% of A and flowing at 0.30 mL min^{-1}. The detection of *p*-coumaric acid was performed at 340 nm and that of resveratrol at 304 nm.

4.2.9 Error calculation – adsorption experiments

For all the performed batch experiments, the uncertainty associated with the measurements and the regressed parameters was obtained as described in Sevillano et al.[28.]. The standard deviation

of the measurements was calculated according to the theory of error propagation [29]. The standard deviation of the estimated parameters was obtained by taking the parameter covariance matrix as the inverse of the Fisher information matrix:

$$FIM = \sum_{i=1}^{N} J^T \frac{1}{\sigma_i} J \qquad (4.3)$$

Where σ_i is the standard deviation of the ith observation and J is the Jacobian matrix of the least squares regression function.

4.3 Results and Discussion

4.3.1 Batch production of resveratrol by C. glutamicum

During the cultivation of *C. glutamicum* in bioreactor, in batch mode, a maximum biomass concentration of 18 g L^{-1} was obtained after 23 h of growth (Figure 4.2a). Looking at the substrate consumption profile, it was possible to observe that glucose is completely depleted from the medium, suggesting that cell growth starts to decelerate due to the limitation of this substrate. Under these conditions $Y_{X/glu}$ was 0.46 (g cell dry weight per g glucose), which is in agreement with data already published for this bacteria[30].

It was observed that an increase in the resveratrol titer occurred only during the exponential growth and no further increase was achieved during the stationary phase. After 23 h of growth, a total resveratrol concentration of 5.3 mg L^{-1} was detected (Figure 4.2b). In contrast, the level of extracellular resveratrol was 4 mg L^{-1}. In *C. glutamicum*, malonyl-CoA is exclusively used for the production of fatty acids. Typically, malonyl-CoA synthesis strongly decreases in the stationary phase (as fatty acids are only required for biomass production), which explains why the production of resveratrol stops at this stage.

4

Concerning *p*-coumaric acid (Figure 4.2c), the maximum concentration observed in the culture medium was 1.2 mg L^{-1} and around 1 mg L^{-1} in the supernatant. The *p*-coumaric acid accumulation only in the stationary phase is a clear hint that it is the rate-limiting metabolite during production [12].

In fact, the titers of resveratrol produced by *C. glutamicum* are lower in direct comparison to other already published microbial production strains [2,10], but the use of this strain as a platform for polyphenol production is highly appealing for the reasons explained in the Introduction. Further research and development of this strain, aiming at increasing the resveratrol titers, may result in a good platform for industrial resveratrol production. However, the level of measured resveratrol may not be a true reflection of the amount of resveratrol produced, as an indeterminate amount is probably being degraded by oxygen and other factors, such as pH, temperature and light[20,31,32]. It cannot be ignored that resveratrol tends to oxidize in the aerated fermenter and the high oxygen levels needed for cell growth have a strong negative impact on resveratrol production [13]. Therefore, product removal strategies such as direct and external adsorption can be very promising strategies for adsorbing and storing the secreted resveratrol and simultaneously purifying polyphenol compounds from the fermentation stream.

4
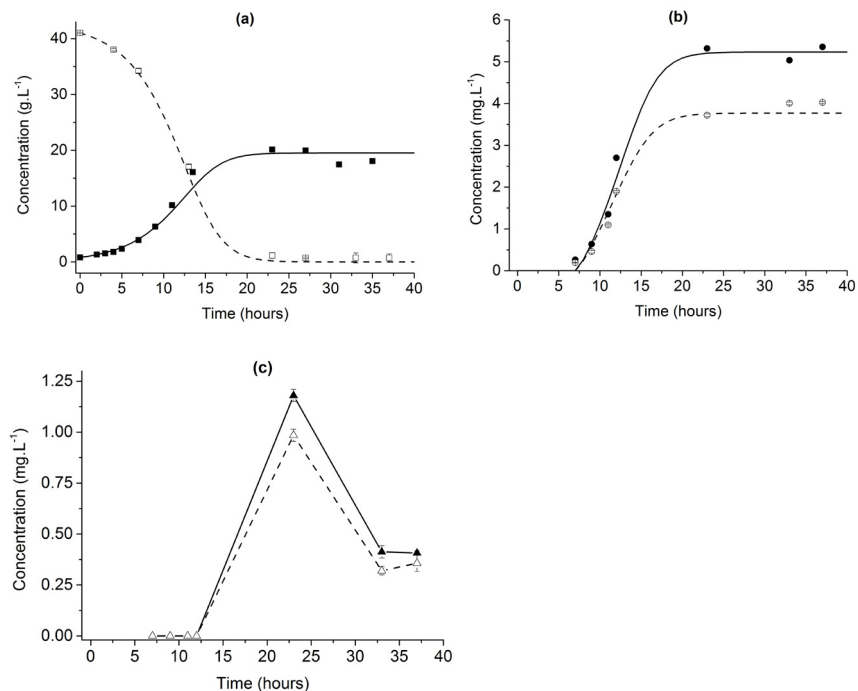
Figure 4.2 — Cultivation profile of *C. glutamicum DelAro4*, including biomass concentration (dwt) (¢) and glucose consumption profile (☐) in batch experiments (a); the broth () and extracellular (○) resveratrol concentrations (b); the broth (▲) and extracellular (△) p-coumaric acid concentrations (△) (c). Data are presented as average and standard deviation of two independent experiments (If no error bars are visible, the standard deviations were too small to be displayed).

4.3.2 Adsorption isotherms of *p*-coumaric acid and resveratrol onto the Amberlite XAD-7HP resin

The choice of using an hydrophobic resin, such as the XAD-7HP, for the continuous removal of resveratrol was twofold. First of all, given that resveratrol is highly hydrophobic (log P of 3.4 (Chemicalize.org)), this resin was expected to strongly adsorb this

polyphenol. Similar results were obtained for many antioxidants like α-tocopherol and α-tocopheryl acetate, which share several common characteristics with resveratrol[33]. More recently, Vuong et al. also described the resveratrol production in *Vitis vinifera* L. cell suspension cultures with *in situ* adsorption, using XAD-7HP as adsorbent[3]. The second reason for the selection of this resin had in consideration that since *p*-coumaric acid is mostly ionized at pH 7.0, its affinity towards the resin is expected to be much lower than for resveratrol. This is of crucial importance, as *p*-coumaric acid is a precursor for the synthesis of resveratrol.

The adsorption isotherm determined for *p*-coumaric acid is indicated in Figure 4.3a, where a linear model was used to fit the experimental data. On Figure 4.3b, the adsorption isotherm of resveratrol is shown. The Langmuir model was used in this case, since the resin started to show some saturation for larger concentrations in the liquid phase. This model was also chosen due to its capacity of describing the physical adsorption of neutral molecules onto adsorption sites [27].
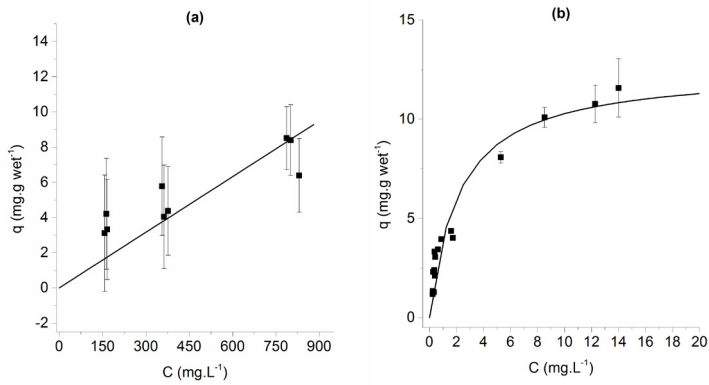
Figure 4.3 — Adsorption isotherms of p-coumaric acid (a) and of resveratrol (b) onto the Amberlite XAD-7HP resin (equilibrium adsorption capacity (mg.g wet^{-1}) is plotted against equilibrium liquid concentration (mg.L^{-1}). Data are presented as average and standard error.

From the analysis of Figure 4.3 it is possible to observe that, as expected, the adsorption of *p*-coumaric acid is much weaker than that of resveratrol. The reasons for this observation lie in the fact that, as previously mentioned, resveratrol is more hydrophobic than *p*-coumaric acid. Moreover, since it is a carboxylic acid, *p*-coumaric acid is negatively charged at pH 7.0, making it even more polar and with higher affinity for the aqueous phase.

In Table 4.2, the regressed parameters for the linear adsorption isotherm of *p*-coumaric acid and the Langmuir adsorption isotherm of resveratrol are indicated.

Table 4.2 — Regressed isotherm parameters for p-coumaric acid and resveratrol onto the Amberlite XAD 7HP resin, using MilliQ water as solvent. The linear isotherm model was fitted to the experimental data of p-coumaric acid and the Langmuir isotherm model was fitted to the experimental data of resveratrol.

	Amberlite XAD-7HP	
	p-coumaric acid	*trans*-resveratrol
Q_{max} (mg g wet^{-1})	-	12.5 ± 0.3
K_L (L mg^{-1})	-	0.46 ± 0.02
K (L g wet^{-1})	0.011 ± 0.001	-

4.3.3 Resveratrol production by *C. glutamicum* with external and direct adsorption

The application of product removal techniques to a biotechnological process may bring benefits such as avoiding or reducing inhibition or toxicity, product stabilization and facilitation of further downstream processing [34]. Advantages of solid resins, in particular, as compared to traditional organic solvents are insolubility in the aqueous phase, no volatilization, high biocompatibility and reduced environmental hazard[35].

Figure 4.4a (filled lines) shows the *C. glutamicum* growth profile and substrate consumption in batch cultures with external adsorption strategy, using XAD-7HP as adsorbent.

Comparing the growth profiles under this condition with batch without adsorption (Figure 4.2a), it was clearly confirmed that the viability of the cells is not affected by the presence of the resins, i.e., neither adsorption of essential nutrients to the resin nor counter-ion release into the medium are problematic for the external adsorption strategy. The results of Figure 4.4a evidence this behavior, since the polymer appeared to have no affinity for glucose, as the substrate consumption profile was not affected. Regarding the production of resveratrol, the results obtained suggest that its kinetic profile is also similar when compared with batch experiments without continuous product removal (Figure 4.4b). Nonetheless, lower amounts were obtained when using the integrated strategies. While for the batch experiments without product removal 5.36 mg L^{-1} of resveratrol were obtained, the value dropped to 2.2 mg L^{-1} for the direct adsorption scenario and to 3.6 mg L^{-1} for the case of external adsorption (Table 4.3).

4
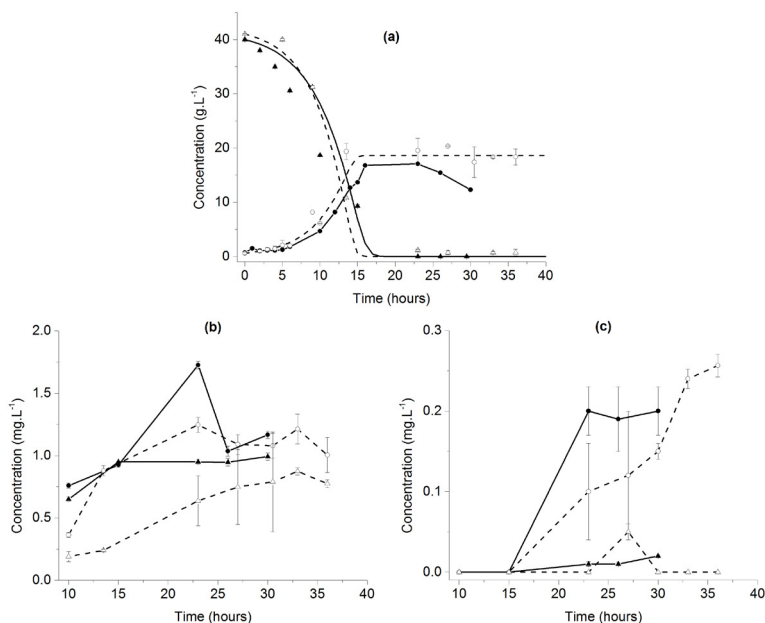
Figure 4.4 — Cultivation profile for C. glutamicum DelAro[4] for the external adsorption (filled lines and symbols) and for the direct adsorption scenarios (dashed lines and empty symbols). In (a), it is shown the biomass concentration (dwt) (circles) and the glucose consumption profiles (triangles); the total produced resveratrol is depicted in (b) (circles), together with the extracellular profiles (triangles); the total produced p-coumaric acid is depicted in (c) (circles), together with the extracellular profiles (triangles). Data are presented as average and standard deviation of two independent experiments (If no error bars are visible, the standard deviations were too small to be displayed).

One of the key points also worth noticing is that the ratio of the extracellular resveratrol (amount in the liquid phase plus the amount adsorbed) compared to the total amount, increased from 70 %, when no product removal was performed, to 90% (direct adsorption) and 95 % (external adsorption), as indicated in Table 4.3. This suggests that the external adsorption strategy might in fact promote product excretion from the cells, as desired. Supposing that only the resveratrol present in the liquid or in the resin could be recovered (no cell breaking step), the scenario without adsorption would provide 4.03 mg L^{-1}, compared to 1.96 mg L^{-1} from the direct adsorption and 3.42 mg L^{-1} from the

external adsorption scenario. When performing this analysis, the "recoverable" resveratrol in the external adsorption scenario is only 15 % lower than in the original batch situation, where no recovery is present.

Table 4.3 — Comparison of the amount of resveratrol produced in the different batch scenarios.

Resveratrol	Batch	Direct adsorption	External adsorption
Extracellular (mg L^{-1})	4.03 ±0.02	0.76 ± 0.03	0.99 ± 0.03
Broth (*extracellular + intracellular*) (mg L^{-1})	5.36 ± 0.01	1.00 ± 0.14	1.17 ± 0.03
Resin (mg L^{-1})	-	1.20 ± 0.02	2.43 ± 0.04
Ratio Extracellular Total^{-1} $\left(\frac{Extracellular+Resin}{Broth+Resin}\right)$	0.75	0.90	0.95

When using a continuous product removal strategy as the ones proposed in this work, two behaviors are expected. First, there might be an increase in production due to the reduction in product toxicity (not studied in this work). Second, by continuously removing resveratrol, the product will tend to accumulate outside the cell, mostly inside the resin beads (Figure 4.5).

4
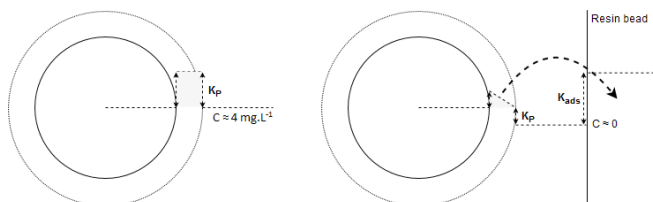
Figure 4.5 — Comparison, at the cellular level, between the concentration profiles of resveratrol in the batch scenario (left) and the in situ product removal scenario (right). When no resin is present, the product concentration inside and outside the cells tend to equalize. Nonetheless, due to the high lipophilicity of resveratrol (expressed by its K_P partition value), a higher concentration is expected in the membrane and, as a result, inside the cells. If adsorbent is put into contact with the cells, while resveratrol is being synthesized inside the cell and diffusing to the liquid (passive diffusion in the membrane is assumed to be the limiting step), it is also being removed from that same liquid phase. This leads to a reduction of this polyphenol concentration inside the cell and its shift to the hydrophobic resin beads, for which it has high affinity.

In figure 4.5 (left), the proposed situation of the *C. glutamicum* cells for the batch experiment scenario is depicted. At the end of the cell growth phase, an equilibrium between the inside cell concentration and the external concentration is obtained. Nonetheless, being highly lipophilic, it is expected that resveratrol is highly partitioned towards the cell membrane. Considering that the intracellular volume is around 2% of the total broth volume and that the intracellular resveratrol concentration is 1.34 mg per L broth, the local concentration inside the cells should be in the range of 60 g L^{-1}, probably mostly in the membrane.

The equivalent situation for the continuous removal strategy is depicted in Figure 4.5 on the right. The figure assumes that a "picture" was taken during the interval when resveratrol is being synthesized and, at the same time, the molecule is being adsorbed onto the XAD-7HP resin (steady-state is also assumed). It is also implied that the limiting step for mass transfer is membrane diffusion. Now, because the extracellular concentration becomes close to zero (adsorption occurs at a fast rate), the intracellular content of resveratrol becomes

much lower than in the batch scenario. That will result in the accumulation of the molecule not inside the cell, but mostly inside the resin beads, from which it can be eluted with a water/ethanol mixture (ethanol rich).

While the provided explanations can explain why the extracellular/intracellular ratio of resveratrol increased for the continuous removal scenarios, it does not explain the decrease in total production. At least two reasons may be given. One of them has to do with the decrease in precursor availability due to the presence of the adsorbent. As shown previously, although the adsorption of p-coumaric acid onto the XAD-7HP is weak (Figure 4.2), it is probably not negligible. As depicted in Figure 4.4c, the level of p-coumaric acid detected in the culture medium when using either the external or the direct product adsorption strategies is roughly 5.9-fold lower than the one detected when no adsorption was applied (Figure 4.2c). The other one is related with the concentration levels attained during the performed experiments. Having such low values (in the range of 0.25 – 5 mg L^{-1}), might make the comparison between the different scenarios more difficult, especially knowing that oxidation and isomerization reactions of resveratrol might occur [13] . Using strains able to achieve higher titers might then lead to a better understanding of the possible improvements given by the continuous product removal strategy.

The key message to be conveyed with this work is that despite having achieved lower titers, the integrated product removal strategy showed potential to be applied in a batch industrial process. Not only the downstream process has the capacity of being integrated with the upstream batch fermentation, possibly leading to energy cost and waste reduction, but it also leads to its own simplification. As this work suggests, not only 70%, but close to 95% of the total produced resveratrol may be present outside the cells, avoiding the need of a cell lysis step and reinforcing the possible energy cost and waste reduction previously mentioned.

4

4.4 Conclusions

This work investigated the possible advantages of continuously extracting resveratrol as it was produced by *C. glutamicum* in a batch fermentation process. In the batch experiments without integrated recovery, a total titer of 5.36 mg resveratrol L^{-1} was obtained. Although it was the largest titer obtained among all the performed experiments, the amount of resveratrol inside the cells was still substantial (25% of the total content). For the continuous removal experiments, titers of 2.2 mg L^{-1} and 3.6 mg L^{-1} were obtained for the direct and external adsorption, respectively. Despite the lower titers obtained in both situations, which might be associated with the adsorption of the precursor of resveratrol, *p*-coumaric acid, the ratio of the extracellular plus adsorbed to the total resveratrol produced, was increased for the scenarios where the XAD-7HP resin was used (90% of the total for the direct adsorption and 95% of the total for the external adsorption). This suggests that, even though lower titers were obtained for the continuous product removal strategies, the desired product could be almost totally recovered outside the cells. For that reason, a possible downstream at a larger scale could potentially avoid using a cell lysis step, which would increase not only costs but also complex the subsequent downstream process steps. The proposed integrated strategies, which might still be improved by manipulating the ratio of solid phase (resin) to liquid ratio, can provide not only a simpler recovery and purification process, but also avoid potential problems with product toxicity to the cells (in case the polyphenol reaches higher concentrations in the medium).

Future work may however unveil a potential increase in productivity. Two strategies should be addressed to try this. One consists of decreasing the amount of *p*-coumaric acid adsorption by the resin. This would certainty lead to a strong increase in the total amount of resveratrol produced per batch volume. The second strategy proposed would consist of forming the batch fermentation into a continuous production process. The *in situ* product removal strategy should allow a continuous or fed-batch fermentation

operation, without falling into toxicity limitations due to an excess of resveratrol in the system and protecting the product from oxidative degradation. These may lead to an increase in the overall production rate per unit time when compared to a batch operation.

Acknowledgements

References

1 Vidavalur R, Otani H, Singal PK, Maulik N. Significance of wine and resveratrol in cardiovascular disease: French paradox revisited. Exp Clin Cardiol 2006;11(3):217–25.

2 Li M, Kildegaard KR, Chen Y, Rodriguez A, Borodina I, Nielsen J. De novo production of resveratrol from glucose or ethanol by engineered Saccharomyces cerevisiae. Metab Eng [Internet] 2015;32:1–11. Available from: http://dx.doi.org/10.1016/j.ymben.2015.08.007

3 Vuong T V., Franco C, Zhang W. Treatment strategies for high resveratrol induction in Vitis vinifera L. cell suspension culture. Biotechnol Reports [Internet] 2014;1–2:15–21. Available from: http://dx.doi.org/10.1016/j.btre.2014.04.002

4 Donnez D, Jeandet P, Clément C, Courot E. Bioproduction of resveratrol and stilbene derivatives by plant cells and microorganisms. Trends Biotechnol 2009;27(12):706–13.

5 Marienhagen J, Bott M. Metabolic engineering of microorganisms for the synthesis of plant natural products. J Biotechnol [Internet] 2013;163(2):166–78. Available from: http://dx.doi.org/10.1016/j.jbiotec.2012.06.001

6 Pandey RP, Parajuli P, Koffas MAG, Sohng JK. Microbial production of natural and non-natural flavonoids: Pathway engineering, directed evolution and systems/synthetic biology. Biotechnol Adv [Internet] 2015;34(5):634–62. Available from: http://dx.doi.org/10.1016/j.biotechadv.2016.02.012

7 van Summeren-Wesenhagen PV, Marienhagen J. Metabolic engineering of Escherichia coli for the synthesis of the plant polyphenol pinosylvin. Appl Environ Microbiol 2015;81(3):840–9.

8 Beekwilder J, Wolswinkel R, Jonker H, Hall R, De Rie Vos CH, Bovy A. Production of resveratrol in recombinant microorganisms. Appl Environ Microbiol 2006;72(8):5670–2.

9 Vos T, de la Torre Cortés P, van Gulik WM, Pronk JT, Daran-Lapujade P. Growth-rate dependency of de novo resveratrol production in chemostat cultures of an engineered Saccharomyces cerevisiae strain. Microb Cell Fact [Internet] 2015;14(1):133. Available from: http://www.microbialcellfactories.com/content/14/1/133

10 Camacho-Zaragoza JM, Hernández-Chávez G, Moreno-Avitia F, Ramírez-Iñiguez R, Martínez A, Bolívar F, et al. Engineering of a microbial coculture of Escherichia coli strains for the biosynthesis of resveratrol. Microb Cell Fact [Internet] 2016;15(1):163. Available from: http://microbialcellfactories.biomedcentral.com/articles/10.1186/s12934-016-0562-z

11 Takors R, Bathe B, Rieping M, Hans S, Kelle R, Huthmacher K. Systems biology for industrial strains and fermentation processes-Example: Amino acids. J Biotechnol 2007;129(2):181–90.

12 Kallscheuer N, Vogt M, Stenzel A, Gätgens J, Bott M, Marienhagen J. Construction of a Corynebacterium glutamicum platform strain for the production of stilbenes and (2S)-flavanones. Metab Eng [Internet] 2016;38:47–55. Available from: http://dx.doi.org/10.1016/j.ymben.2016.06.003

13 Braga A, Oliveira J, Silva R, Ferreira P, Rocha I, Kallscheuer N, et al. Impact of the cultivation strategy on resveratrol production from glucose in engineered Corynebacterium glutamicum. J Biotechnol [Internet] 2017;manuscript in preparation. Available from: http://dx.doi.org/10.1016/j.jbiotec.2017.11.006

14 Eikmanns BJ, Metzger M, Reinscheid D, Kircher M, Sahm H. Amplification of three threonine biosynthesis genes in Corynebacterium glutamicum and its influence on carbon flux in different strains. Appl Microbiol Biotechnol 1991;34:617–22.

15 Liu YB, Long MX, Yin YJ, Si MR, Zhang L, Lu ZQ, et al. Physiological roles of mycothiol in detoxification and tolerance to multiple poisonous chemicals in Corynebacterium glutamicum. Arch Microbiol 2013;195(6):419–29.

16 Kallscheuer N, Vogt M, Kappelmann J, Krumbach K, Noack S, Bott M, et al. Identification of the phd gene cluster responsible for phenylpropanoid utilization in Corynebacterium glutamicum. Appl Microbiol Biotechnol 2016;100(4):1871–81.

17 van Summeren-Wesenhagen P V., Marienhagen J. Putting bugs to the blush: Metabolic engineering for phenylpropanoid-derived products in microorganisms. Bioengineered 2013;4(6).

18 Lim CG, Fowler ZL, Hueller T, Schaffer S, Koffas MAG. High-yield resveratrol production in engineered Escherichia coli. Appl Environ Microbiol 2011;77(10):3451–60.

19 Wu J, Liu P, Fan Y, Bao H, Du G, Zhou J, et al. Multivariate modular metabolic engineering of Escherichia coli to produce resveratrol from l-tyrosine. J Biotechnol [Internet] 2013;167(4):404–11. Available from: *http://dx.doi.org/10.1016/j.jbiotec.2013.07.030*

20 Zupančič Š, Lavrič Z, Kristl J. Stability and solubility of trans-resveratrol are strongly influenced by pH and temperature. Eur J Pharm Biopharm 2015;93:196–204.

21 Afonso MS, Ferreira S, Domingues FC, Silva F. Resveratrol production in bioreactor: Assessment of cell physiological states and plasmid segregational stability. Biotechnol Reports [Internet] 2015;5(1):7–13. Available from: *http://dx.doi.org/10.1016/j.btre.2014.10.008*

22 Hwang D, Lim Y-H. Resveratrol antibacterial activity against Escherichia coli is mediated by Z-ring formation inhibition via suppression of FtsZ expression. Sci Rep [Internet] 2015;5(10029):1–10. Available from: *http://www.nature.com/doifinder/10.1038/srep10029*

23 Woodley J, Bisschops M, Straathof A, Ottens M. Perspective Future directions for in-situ product removal (ISPR). J Chem Technol Biotechnol 2008;83(May):121–3.

24 Keilhauer C, Eggeling L, Sahm H. Isoleucine synthesis in Corynebacterium glutamicum: Molecular analysis of the ilvB-ilvN-ilvC operon. J Bacteriol 1993;175(17):5595–603.

25 Giorgio C, Jungbauer A. Protein Chromatography: Process Development and Scale-Up. Wiley-VCH Verlag GmbH & Co. KGaA; 2010.

26 Kumar A, Awasthi A. Bioseparation engineering : a comprehensive DSP volumen. 2009;209.

27 Monsanto M, Mestrom R, Zondervan E, Bongers P, Meuldijk J. Solvent swing adsorption for the recovery of polyphenols from black tea. Ind Eng Chem Res 2015;54(1):434–42.

28 Sevillano DM, Jankowiak L, Van Gaalen TLT, Van der Wielen LAM, Hooshyar N, Van der Goot A, et al. Mechanism of Iso fl avone Adsorption from Okara Extracts onto Food- Grade Resins. Ind Eng Chem Res 2014;53:15245–52.

29 Skoog D, Holler F, Crouch S. Skoog, Douglas A., F. James Holler, and Stanley R. Crouch. Principles of instrumental analysis. , 2017. Cengage le. Cengage learning; 2017.

30 Buchholz J, Schwentner A, Brunnenkan B, Gabris C, Grimm S, Gerstmeir R, et al. Platform engineering of corynebacterium glutamicum with reduced pyruvate dehydrogenase complex activity for improved production of l-lysine, l-valine, and 2-ketoisovalerate. Appl Environ Microbiol 2013;79(18):5566–75.

31 Trošt K, Golc-Wondra A, Prošek M. Degradation of polyphenolic antioxidants in blueberry nectar aseptically filled in PET. Acta Chim Slov 2009;56(2):494–502.

32 Lucas-Abellán C, Fortea I, López-Nicolás JM, Núñez-Delicado E. Cyclodextrins as resveratrol carrier system. Food Chem 2007;104(1):39–44.

33 Ballesteros E, Gallego M, Valca M. Continuous- ⁻ow determination of natural and synthetic antioxidants in foods by gas chromatography. 1998;359:47–55.

34 Hua D, Ma C, Song L, Lin S, Zhang Z, Deng Z, et al. Enhanced vanillin production from ferulic acid using adsorbent resin. Appl Microbiol Biotechnol 2007;74(4):783–90.

35 Guo JL, Mu XQ, Xu Y. Integration of newly isolated biocatalyst and resin-based in situ product removal technique for the asymmetric synthesis of (R)-methyl mandelate. Bioprocess Biosyst Eng 2010;33(7):797–804.

5

Preferential crystallization for the purification of similar hydrophobic polyphenols

Abstract

Preferential crystallization is a common technique used in the purification of enantiomers, proving that crystallization may also be applied to the purification of very similar molecules by seeding the solution with the desired compound. Nonetheless, its application to other organic molecules is less documented in literature. Knowing that chemically related polyphenols are generally co-produced by fermentation and their purification can be too expensive for their market value, this technique may contribute to developing a downstream process with less expensive steps. The goal of this work is to show the applicability of the preferential crystallization concept to the purification of similar polyphenols - naringenin and *trans*-resveratrol - with either single or coupled crystallizers.

After developing the needed crystallization kinetic models, an experiment using two coupled vessels was devised, where a 63% yield of naringenin and 44% yield of *trans*-resveratrol was obtained, with ≥98% purity in both cases. When the vessels were working independently, 81% of pure *trans*-resveratrol (started 60% pure) and 70% of pure naringenin (started 68% pure) were recovered.

The performed experiments show the possibility of separately purifying two similar molecules (from 60% to roughly 100%) with promising yields, despite their similar solubility. This method, which can be largely improved, might provide an economically attractive way for the production of low added value products.

5.1 INTRODUCTION

Polyphenols are molecules which have a range of different biotechnological applications (e.g., as food additives, nutraceuticals and food colorants[1]). Most of these molecules are secondary metabolites produced naturally by plants and they are composed of multiple phenol structural units. Over the last years, research on their health properties has grown considerably,[2] with authors studying the properties of these molecules in the prevention of diseases such as Alzheimer's and several types of cancer.[3] Furthermore, the increasing interest in these compounds has led to the creation of projects such as the BacHBerry project,[4] funded by the 7th Framework Programme of the European Commission. This project aimed to discover new phenolic compounds with interesting properties (e.g., health-promoting, colorants) and develop a sustainable process for their production using bacterial platforms. The downstream process development for the capture and purification of polyphenols produced in such a way is then crucial for the success of the project.

The production of these molecules, either by fermentation or by extraction from diverse plant material, is likely to result in the release of similar polyphenols in solution. These structurally close molecules might pose a considerable challenge for the downstream process design, since more selective operations should be needed. Since food additives tend to have a low market price and polyphenol fermentation processes normally have low yields,[5] the design and optimization of alternative purification strategies is of paramount importance.

Preferential crystallization is a purification technique first used in 1853 by Pasteur[6] for the resolution of sodium ammonium tartrate tetrahydrate enantiomers and since then, it has been used for similar purposes.[6-8] The basic underlying idea of this technique is that crystallization can achieve purification not only because of a difference between the thermodynamic driving forces (i.e., different solubility curves), but also due to differences in the compounds' crystallization kinetics. By seeding a crystallizer containing a liquid solution with the desired compound, conditions are applied which promote the growth of crystals of the desired molecule and its consumption from the

5

liquid phase, while the impurity only starts nucleating when its supersaturation level is sufficiently high to start nucleation.[6] Despite its logical application to conglomerate forming enantiomers, the applicability of preferential crystallization can be extended to other organic molecules.[9] In this work, preferential crystallization using two coupled vessels is investigated as a method to purify structurally similar, hydrophobic polyphenols, with overlapping solubility curves – naringenin and *trans*-resveratrol – after an hypothetical preliminary purification step using reverse-phase adsorption. It will be assumed that *trans*-resveratrol leaves the adsorption step with a purity of 60% in a 39% w/w ethanol solution and that naringenin is collected in a fraction with 60% purity as well, but in 46% w/w ethanol. This different ethanol contents aim to mimic what would happen in a typical gradient elution profile in chromatography. In order to optimize the applied crystallization controls (temperature in each vessel and flow rates), the kinetics of crystallization was modelled by describing secondary nucleation, crystal growth and crystal dissolution. For estimating the needed kinetic parameters, a set of different batch experiments was performed, where different quantities of seed crystals were used and different temperature profiles were applied, which also included varying the heating and cooling rates. The developed models were then used to optimize the preferential crystallization conditions in the coupled vessel experiment.

5
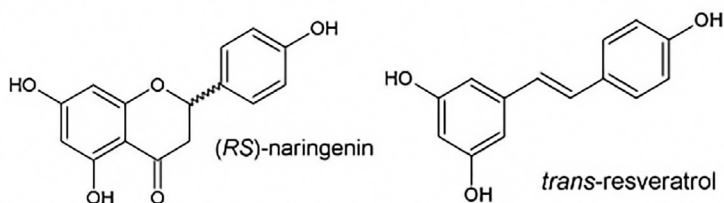
Figure 5.1 — Chemical structure of naringenin and *trans*-resveratrol.

In the following section, a short description of the used crystallization models is given, while the representation of the used set-ups is shown in section 5.2. The obtained results and their discussion is presented in section 5.3 and the conclusions of this work are presented in section 5.4.

5.2 Material and methods

5.2.1 Theoretical background

The major goal of this work was to set-up a coupled vessel preferential crystallization experiment for the purification of naringenin and *trans*-resveratrol. In order to optimize the obtained yields, temperature in each vessel was continuously controlled as well as the flow rates being pumped from each crystallizer to the other. By applying filters in both vessels, only liquid phase was assumed to be pumped from one vessel to another. In order to determine those optimal controls, the approach taken in this work was to model the crystallization kinetics by performing batch experiments. The obtained models were then transferred to the coupled vessel situation, where the predicted yields of both polyphenols were maximized, while constraining their purity to be at least 95%.

In this section, the crystallization kinetic models used for both batch and coupled vessel experiments are introduced. The component mass balances are also described for each case.

5.2.1.1 Crystallization kinetics

For modelling crystallization kinetics, phenomena like nucleation, crystal growth and crystal dissolution have to be described mathematically. The overall goal was to obtain a model that would describe the experimental observations as well as possible, but preserving simplicity. For that reason, primary nucleation was disregarded, since experiments were run at relatively low supersaturation levels and seed crystals were always present. Moreover, crystal aggregation was not considered as well, because the expected improvement in modelling prediction would not compensate for the added complexity.

For modelling secondary nucleation, an empirical power law was used, considering that the most important variables involved in

5

this process are supersaturation, temperature, solid content and rotational speed of the propeller:[10]

$$G_i = k_{G,i}^0 e^{\left(-\frac{E_{G,i}}{RT}\right)} (\Delta c^p)_i \tag{5.1}$$

Since the agitation speed was kept constant throughout all the experiments, its impact in the secondary nucleation rate was not included explicitly, but included in the kinetic constant .

Concerning the description of crystal growth, it was assumed that no dependence on the crystal characteristic size, *L*, occurred. Thus, a structurally similar empirical expression to the one provided for secondary nucleation was used:[10-11]

$$D_i = k_{D,i}^0 e^{\left(-\frac{E_{D,i}}{RT}\right)} \left(\Delta c_{us}^q\right)_i \tag{5.2}$$

This equation incorporates, in the *p* exponent, the combined effect of diffusion and surface integration into the growth kinetics.[10]

By analogy with the growth rate kinetics, the rate of dissolution was described by the same model, but with the undersaturation level replacing supersaturation:[11]

$$\frac{d\left(\hat{\mu}_{0,i} \cdot V^k\right)}{dt} = B_{2,i} \cdot V^k \tag{5.3}$$

5.2.1.2 Mass balances for the liquid and solid phases

In order to describe the concentration of each polyphenol in both liquid and solid phases, the method of moments was applied.[12][13] Taking into account that the liquid volume might vary with time - in the case of the coupled vessel experiments -, the equations for the 0th and higher moments are given by:[12]

$$D_i = k_{D,i}^0 e^{\left(-\frac{E_{D,i}}{RT}\right)} \left(\Delta c_{us}^q\right)_i \tag{5.4}$$

5

$$\frac{d(\hat{\mu}_{m,i} \cdot V^k)}{dt} = mG_i(\hat{\mu}_{m-1,i} \cdot V^k) \tag{5.5}$$

In these equations, k stands for the vessel number ($k = 1, 2$), as for the coupled vessel experiment the liquid volume in each vessel may be different.

At time zero, seed crystals with known particle size distribution are added to the crystallizer. Because the determined particle size distribution was obtained using the relative frequency ($\bar{n}_i$), it is necessary to multiply by the total number of crystals in suspension, in order to obtain the mth moment of the absolute particle distribution (volume specific):

$$\hat{\mu}_{m,i}(t = 0) = \frac{N_i}{V^k} \int_0^\infty (L_i^m \cdot \bar{n}_i)\, dL \tag{5.6}$$

Once the crystal size distribution is known at time zero and the differential equations for the evolution of its moments along time are known (equations (4) and (5)), the mass balance for the liquid phase can be described by equations (7) and (8). Their usage depends on whether the solution is supersaturated or undersaturated:

$$\frac{d(C_{l,i} \cdot V^k)}{dt} = -3 \cdot \rho_{c,i} \cdot \bar{k}_{v,i} \cdot G_i \cdot (\hat{\mu}_{2,i} \cdot V^k) \tag{5.7}$$

$$\frac{d(C_{l,i} \cdot V^k)}{dt} = 3 \cdot \rho_{c,i} \cdot \bar{k}_{v,i} \cdot D_i \cdot (\hat{\mu}_{2,i} \cdot V^k) \tag{5.8}$$

These equations basically state that an eventual increase or decrease of dissolved compound mass is consumed in either the crystal growth or dissolution process. In both of them, the average volume shape factor of the crystals, $\bar{k}_{v,i}$, is introduced. The inconvenience with this formulation is that the volume shape factor will depend on the crystal characteristic length (shown

5

in the following section). Since the method of moments was preferred due to its simplicity, avoiding solving partial differential equations, a consistent way of defining the average volume shape factor was devised: it was taken as the one of the seed crystals used in each experiment. The underlying assumption was that the number of crystals in suspension were in sufficient number so that crystal growth would led to a negligible impact on crystal size (a small growth in a large crystal population consumes as much supersaturation as a large growth in a small population). How this average was calculated and used to take into account the fact that the aspect ratio of the crystals depends on their characteristic size *L*, is shown in the next section.

Similarly to how the previously mass balances were written, the mass balance for the solid phase is symmetric:

$$\frac{d\left(C_{l,i} \cdot V^k\right)}{dt} = 3 \cdot \rho_{c,i} \cdot \bar{k}_{v,i} \cdot D_i \cdot \left(\hat{\mu}_{2,i} \cdot V^k\right) \tag{5.9}$$

$$\frac{d\left(C_{s,i} \cdot V^k\right)}{dt} = -3 \cdot \rho_{c,i} \cdot \bar{k}_{v,i} \cdot D_i \cdot \left(\hat{\mu}_{2,i} \cdot V^k\right) \tag{5.10}$$

When both crystallizers are connected, an inlet filter of 10 μm is put on each tubing inlet and an inline filter of 0.2 μm is put on the discharge side of each peristaltic pump, so that it is assumed that only liquid phase is exchanged between them. Due to the liquid flow between each vessel, the liquid volume is expected to vary according to the following differential equation:

$$\frac{dV^k}{dt} = F_{nk} - F_{kn} \tag{5.11}$$

In this equation, F_{nk} stands for the flow rate coming from vessel *n* to vessel *k*.

5

Because the used tubing had a significant dead volume (approximately 9 mL, compared to a 100 mL liquid volume inside each crystallizer), it could have an effect on the crystallization model predictions, if not taken into account. Thus, the flow inside the tubing interconnecting both crystallizers was modelled as a plug flow:

$$\frac{\partial(C_{l,i,nk}^{tub})}{\partial t} = -\frac{F_{nk}}{A_{tub}}\frac{\partial(C_{l,i,nk}^{tub})}{\partial x} \tag{5.12}$$

In this equation, x is the coordinate axis pointing in the direction of the liquid flow. The tubing internal area, A_{tub}, was calculated from the tubing internal diameter of 3.1 mm provided by the supplier (data from Masterflex).

The fact that liquid can be pumped across the two different reactors has two implications. First of all, when the experiments are run, both crystallizers start with different ethanol in water concentrations. Because of that, as liquid is transported from one vessel to the other, that ethanol concentration changes with time. Second, as it was assumed that no solid material is able to pass through the filters, the major difference between eq. 5.13 and eq. 5.7, is that the mass of dissolved product not only can change due to crystal growth/dissolution, but also by being transported from each vessel to another. Thus, for the liquid phase:

$$\frac{\partial(C_{l,i}^{k} \cdot V^{k})}{\partial t} = F_{nk}\, C_{l,i,nk}^{tub} - F_{kn}\, C_{l,i}^{k} - 3 \cdot \rho_{c,i} \cdot \bar{k}_{v,i} \cdot G_{i} \cdot \left(\hat{\mu}_{2,i} \cdot V^{k}\right) \tag{5.13}$$

For the solid phase, because no solid material is assumed to be transferred, the balance remains unchanged:

$$\frac{\partial(C_{s,i}^{k} \cdot V^{k})}{\partial t} = 3 \cdot \rho_{c,i} \cdot \bar{k}_{v,i} \cdot G_{i} \cdot \left(\hat{\mu}_{2,i} \cdot V^{k}\right) \tag{5.14}$$

As indicated in all the equations presented before, describing the kinetics of crystallization requires knowing both supersaturation

and undersaturation levels at each time point. Because both temperature and ethanol concentration might! vary with time, the knowledge of the solubility curves of both polyphenols as a function of those two variables is essential. Using experimental data already available in the literature,[13, 14] the Jouyban-Acree model[15] was used in order to have an explicit solubility function:

$$T \cdot ln(x_i) = A_0 + A_1 T + A_2 T x_{EtOH} \\ + A_3 x_{EtOH} + A_4 x_{EtOH}^2 + A_5 x_{EtOH}^3 + A_6 x_{EtOH}^4 \qquad (5.15)$$

In this equation, x_i is the molar fraction of polyphenol i, x_{EtOH} is the ethanol molar fraction in solution and A_o to A_6 are regressed parameters.

5.2.1.3 Temperature control

When solving the optimal control problem, it is considered that the user defines a temperature set-point at defined time intervals. However, because the thermostat does not reach the desired set-point instantaneously, but rather takes some time to reach it, two types of equations were used to describe the time taken by the thermostat to warm or cool the liquid solution to the desired level.

For heating, a linear model was sufficient to describe the observations:

$$T_t = a + b \cdot t \qquad (5.16)$$

For cooling, a quadratic model provided a better fit to the obtained data (data not shown):

$$T_t = c + d \cdot t + e \cdot t^2 \qquad (5.17)$$

In both equations shown, T_t represents the actual temperature of the thermostatic bath. The parameters a, b, c, d and e were estimated by performing heating and cooling rate experiments with the used thermostats. In each of the performed experiments,

5

it was determined how much time each thermostat would take to reach a certain set-point, after it was defined.

5.2.2 Chemicals

Milli-Q ultrapure water was available through an ultrapure water system provided from Merck Millipore. The ethanol used was EMSURE Ethanol absolute for analysis. The polyphenol *trans*-resveratrol was provided from Evolva SA, a part of Olon S.P.A. (Italy), with a purity ≥ 98%. Naringenin, natural (US) with a purity of 98% was provided from Sigma-Aldrich.

5.2.3 Seed crystal preparation

To prepare seed crystals of *trans*-resveratrol, the polyphenol was first dissolved in a solution of 39% (w/w) ethanol/water. Once dissolved, the solution was filtered and deposited in a wide Petri dish. The filtered solution was then transferred to the oven at 60°C. After approximately 2.5 hours, the solution containing crystals was taken out of the oven and stored in a flask for further use, letting the temperature equilibrate with room temperature. To prepare seed crystals of naringenin, the compound was first dissolved in a solution of 46% (w/w) ethanol/water at 60°C and put in a crystallization vessel. The temperature was then decreased to -5°C at a rate of -10°C.h^{-1}. After crystal formation, the suspension would be filtered and the crystals resuspended in an aqueous solution saturated with naringenin. At the end of the process, the slurry was stored in a flask for further use. The only exception was for the coupled vessel experiment, where instead of filtering, the slurry was re-heated to 20°C in order to achieve room temperature and stored afterwards.

The crystals of naringenin were prepared by 5cooling, instead of evaporation, in order to prevent agglomeration as much as possible. However, for the crystal density determination, the crystals were prepared as it was mentioned for *trans*-resveratrol.

In both the cases above-mentioned, the solid content was measured by mass balance most of the times (knowing the initial and

5

final volumes and liquid phase concentrations). For the coupled preferential crystallization experiment, the solid content was measured by vacuum filtering a known volume of seed crystal solution and determining the solid weight.

5.2.4 Particle size distribution measurement

The particle size distributions were measured using a Leica DM5500B microscope (Leica Microsystems GmbH, Germany) combined with an automated image analysis software (LEICA Qwin). In order to analyze particle sizes offline, samples were taken using a pipette with a cut tip to prevent clogging and in order to have a representative size distribution of the sample. The samples were then observed under the microscope and several pictures were taken. The developed script using the LEICA Qwin software removed the background noise and counted only the single crystals. Since agglomerates were observed to be composed of multiple individual needle crystals together (figure in supplementary material), it was considered that their size distribution was the same as the one determined when considering only single crystals.

5.2.5 Crystal density measurement

The crystal density was measured by using a 50 mL volumetric flask and then measuring the volume displaced by a given mass of crystals. This method, based on volume displacement, is described elsewhere.[16] The solution used for filling the flask was a saturated aqueous solution of the respective polyphenol, at room temperature, in order to avoid any dissolution. The obtained densities were of (1.37±0.07) g.mL^{-1} for naringenin and (1.4±0.1) g.mL^{-1} for *trans*-resveratrol.

5.2.6 Experimental set-up

For the estimation of the crystallization kinetic parameters, batch experiments were performed in a single vessel with double wall glass (product code 6.1418.250) from Metrohm Applikon (Netherlands). The liquid temperature was controlled using a

5

cooling thermostat (RE 307 Ecoline star edition from LAUDA).

The agitation, fixed at 250 rpm, was provided by a Hei-TORQUE 100 overhead stirrer from Heidolph Instruments GmbH & Co. KG (Germany) and a mini-propeller from Bohlender GmbH (Germany).

For the preferential crystallization experiment with two coupled vessels, there were two similar double wall batch crystallizers as described above. Moreover, there were 10 μm inlet filters and 0.2 μm inline filters at the pump discharge side, to avoid pumping crystals that might have gone through the tubing. The flow rate was controlled by a NI USB-6001 DAQ device from National Instruments, connected to two Masterflex® pumps, model 77521-57. The tubing used was Chem-Durance Bio Pump Tubing, L/S 16, from Masterflex®.
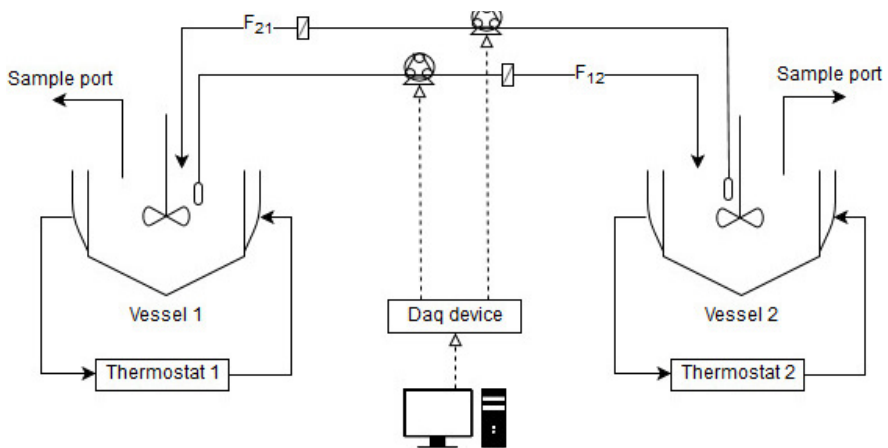
Figure 5.2 — Scheme of the coupled crystallizer set-up for the preferential crystallization experiments.

5.2.7 Sampling and polyphenol quantification

Samples were taken with cellulose acetate 0.2 μm filter in order to prevent crystal suction and then measured by UHPLC (Ultimate 3000, Thermo Scientific, USA) in a C18 column (Acquity UPLC HSS column, 1.8μm, 2.1mm x100 mm Waters, Milford, USA). Mobile phase A (10% formic acid in Milli-Q water) and mobile phase B (10% formic acid in acetonitrile) were run through the column at a constant flowrate of 0.4 mL.min^{-1}. Every run was performed in isocratic mode, containing 33.5% of mobile phase B and 66.5% of mobile phase A. The detection of *trans*-resveratrol was performed at 304 nm and that of naringenin at 289 nm.

5.3 RESULTS AND DISCUSSION

5.3.1 Solution density

Since the temperature during the experiments varied from -5°C to 50°C, the density of both ethanol and water had to be modelled as a function of temperature. For that, the DIPPR105 equation in the DDBST GmbH database was used:[17]

$$\rho = \frac{A}{B^{1+\left(1-\frac{T}{C}\right)^{D}}} \qquad (5.18)$$

The *A*, *B*, *C* and *D* parameters in this equation do not have any relation with the crystallization parameters previously defined. They correspond to the parameters provided in the DDBST GmbH database, for describing the densities of both water and ethanol (Table 5.1). The density of water/ethanol mixtures was considered to be the density of the pure components, weighted by their mass fraction.

Table 5.1 — Parameters for the DIPPR105 equation describing how the solvent density changes with temperature.

Solvent	A	B	C	D
Ethanol	99.374	0.310729	513.18	0.305143
Water	0.14395	0.0112	649.727	0.05107

5.3.2 Solubility data fitting

The solubility data of both naringenin and *trans*-resveratrol as a function of ethanol concentration and temperature is available from the literature.[13, 14] This data was then used in order to regress the needed parameters for the Jouyban-Acree model, as described in subsection 5.2.1.2. This equation describes the solubility as a function of temperature and the co-solvent molar fraction (ethanol in this case). For the case of naringenin, the experimental data between 0.1 ethanol molar fraction up to 0.4 was used (the range of interest). For *trans*-resveratrol, the solubility data up to 0.4 molar fraction was considered (also within the range of interest). The parameters obtained for the Jouyban-Acree model were obtained by minimized the sum of squared relative errors, as it was observed that the uncertainty of the experimental data increased with the solubility absolute value. The regressed parameters are indicated in Table 5.2.

Table 5.2 — Jouyban-Acree parameters for modelling the solubility of *trans*-resveratrol and naringenin as a function of the ethanol content and temperature.

Parameter	*trans*-resveratrol	naringenin
A_0	$(-6.0\pm0.4) \times 10^3$	$(-6.0\pm0.2) \times 10^3$
A_1	7 ± 1	6.2 ± 0.7
A_2	-15 ± 4	-6 ± 3
A_3	$(2.0\pm0.2) \times 10^4$	$(1.42\pm0.08) \times 10^4$
A_4	$(-3.7\pm0.6) \times 10^4$	$(-2.73\pm0.02) \times 10^4$
A_5	$(4.3\pm0.5) \times 10^3$	$(3.68\pm0.01) \times 10^3$
A_6	$(-1.8\pm0.7) \times 10^3$	$(-2.289\pm0.006) \times 10^3$
RMSE	2.3×10^{-4}	9.3×10^{-5}

The comparison between the experimental data and the model predictions are indicated in Figure 5.3. As it is possible to observe, the predictions match quite well the literature data, as it is also implied by the low RMSE values of the model.

5
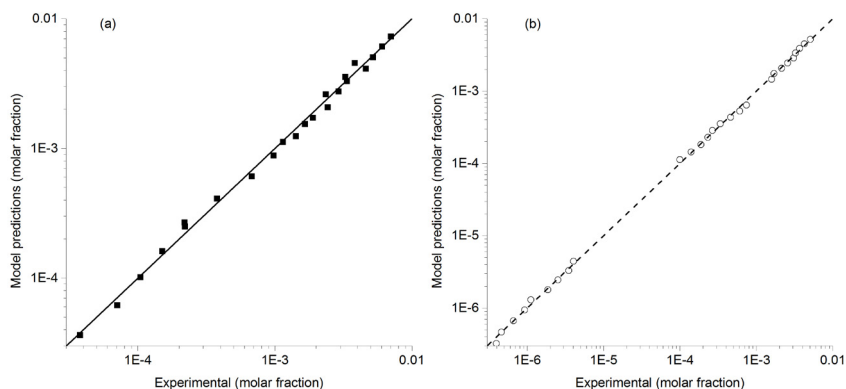
Figure 5.3 — Comparison between the experimental solubility data and the Jouyban-Acree model predictions.

5.3.3 Single vessel preferential crystallization and determination of maximum supersaturation levels

For the preferential crystallization to be successful, a maximum supersaturation level has to be defined in order to prevent the crystallization of the unwanted polyphenol. For setting those limits in the coupled vessel experiment, preferential crystallization experiments in a single vessel were performed, where either *trans*-resveratrol or naringenin were initially present with a 60% purity (the 40% impurity consisted of the other polyphenol). After dissolving both compounds and allowing the temperature to decrease, in order to achieve some supersaturation, seed crystals of the desired polyphenol were added. Temperature was then allowed to decrease at a rate of -10°C.h^{-1} and the liquid concentration of both polyphenols monitored along time. The results are shown in Figure 5.4.

5
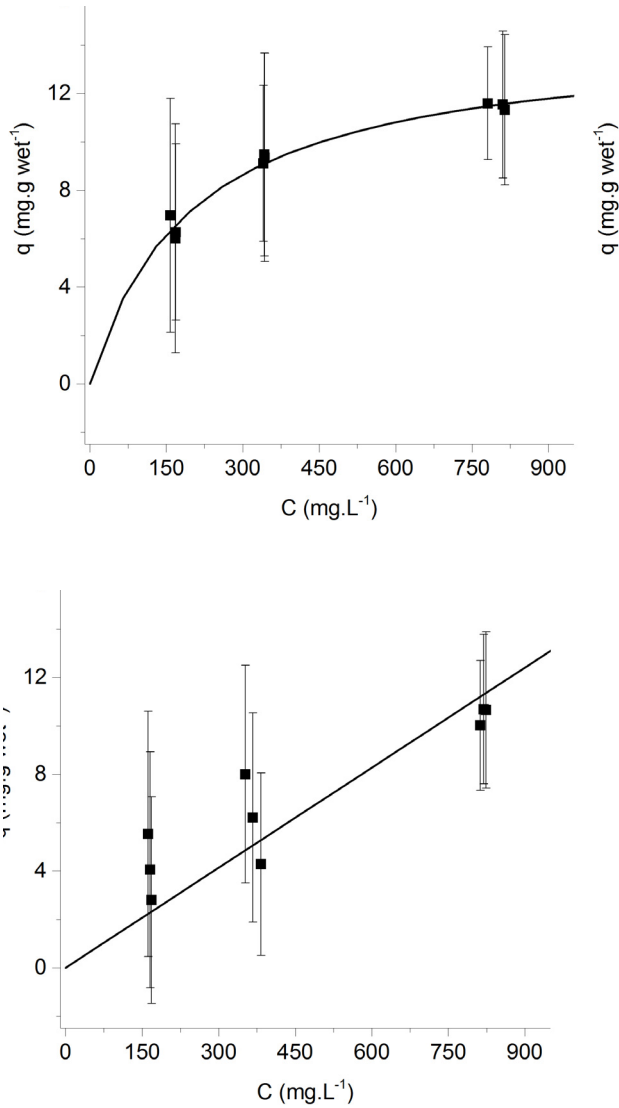
Figure 5.4 — **Progress of the preferential crystallization experiment performed in a single vessel. On the left, it is depicted the experiment performed with a 39% w/w solution of ethanol, where *trans*-resveratrol starts with a purity of 60%. On the right, an analogous experiment was performed, starting with naringenin 60% pure in a solution of 46% w/w ethanol. The error bars indicate the standard deviation in the UHPLC concentration measurements.**

For the case of *trans*-resveratrol, one can observe that naringenin (in this case, the impurity) only starts nucleating and growing at approximately 20°C, where the supersaturation ratio is around 4.5. For the analogous experiment with naringenin, *trans*-resveratrol appeared to have not reached enough supersaturation in order to start nucleating. Nonetheless a maximum level of supersaturation ratio was set at 2.6.

At this point is also worth mentioning that these experiments provided a proof-of-concept for the use of preferential crystallization. Although there was still no coupling between both vessels, it was observed that even above the solubility curve of the undesired polyphenol, nucleation only occurred considerably after the crystals of the desired molecule started growing. For the case represented in Figure 5.4 (on the left), *trans*-resveratrol started with 61% purity and, when temperature reached 25°C, the solid phase attained 81% yield at a purity of around 100% (no naringenin crystallizing). In Figure 5.4 (on the right), naringenin started 68% pure and, when at 0°C, the solid phase had reached 70% yield naringenin with approximately 100% purity (still no *trans*-resveratrol crystallizing).

5.3.4 Crystal volume shape factor determination

In order to account for the non-cubic shape of the crystals, their volumetric shape factor had to be calculated. In both cases, it was observed that both crystals were needle-like shaped (although naringenin crystals tended to aggregate). For that reason, their shape was approximated as a rectangular parallelepiped.

It was experimentally determined that the preferential growth direction of the crystals was along the parallelepiped length (L). Thus, that length L was chosen as the characteristic length of the crystal. Due to the fact that growth not only occurred in length but also in width (W), the shape factor, k_v, was expected to vary with L according to the following expression:

$$k_{v,i}(L) = \left(\frac{W}{L}\right)^2 \qquad (5.19)$$

In order to model the dependence of the shape factor on the characteristic length, a power model seemed to properly describe the experimental data:

$$k_{v,i}(L) = k_{v,i0} \cdot L^x \qquad (5.20)$$

The regressed parameters ($k_{v,i0}$ and x) for both polyphenols are indicated in Table 5.3.

Table 5.3 — Regressed parameters for the eq. 5.19, which relates the crystal volumetric shape factor as a function of the crystal characteristic length.

Polyphenol	$k_{v,0}$	v
naringenin	1.4±0.1	-1.62±0.02
trans-resveratrol	23±2	-2.09±0.02

The model fit to the experimental data is depicted in Figure 5.5:
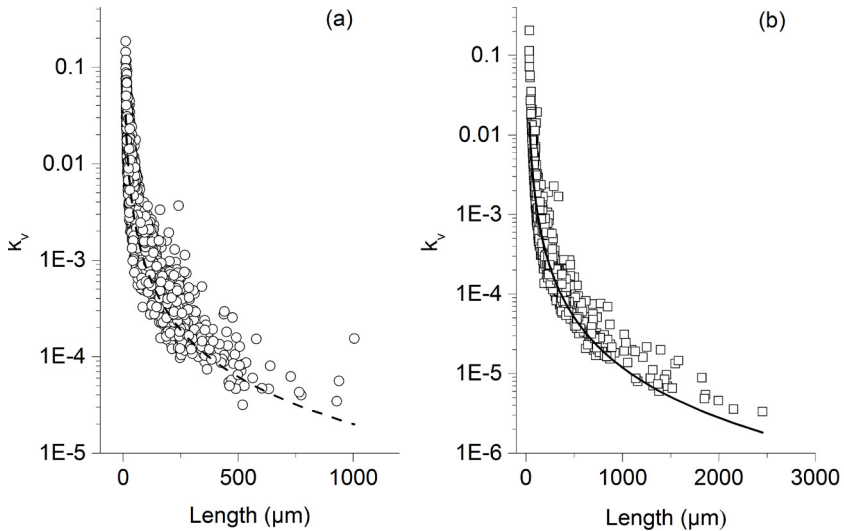
Figure 5.5 — Volumetric shape factor of *trans*-resveratrol (a) and naringenin (b), as a function of their characteristic length.

For using the volume shape factor in the method of moments, the value should be a constant and not have a dependence on the characteristic length. As previously explained, due to the fact that the calculation of $\bar{k}_v$ could not be coupled with the characteristic length (it would be necessary to solve partial differential equations), an approximation had to be made. In this work, the average crystal shape factor was calculated from the particle size distribution of the seed crystals:

$$\bar{k}_{v,i} = \int_{L_0}^{L_f} \bar{n} \cdot k_{v,i} \; dL \qquad (5.21)$$

5.3.5 Crystallization kinetic parameters estimation

For modelling the time evolution of polyphenol concentration in the crystallizer, the kinetic parameters associated with secondary nucleation, growth and dissolution still had to be determined. In order to do so, four experiments in a single batch crystallizer were devised for each polyphenol. For each of them, different temperature profiles were applied and different mass of seed crystals were used (values are indicated in each graph). The range of temperature covered was the range of interest for the preferential crystallization experiment using coupled vessels. Thus, for both *trans*-resveratrol and naringenin, temperature was varied between -5°C and 50°C.

5

For the case of *trans*-resveratrol, the following temperature profiles were applied:
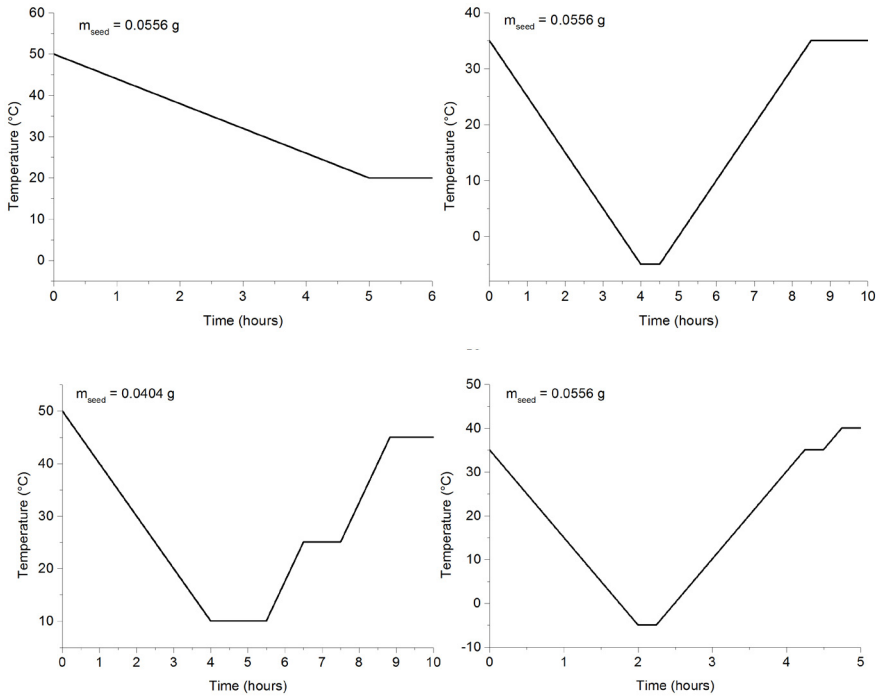
Figure 5.6 — Temperature profiles used for the single batch experiments using *trans*-resveratrol. It is also indicated in each graphic, the introduced mass of seed crystals, so that crystal growth was promoted.

The goal of these experiments was to cool and heat the solution at different rates, in order to achieve different supersaturation and undersaturation levels throughout time. The reasoning behind this, is that in terms of optimal experimental design, the higher those levels, the more "information" is obtained for the determination of the kinetic parameters. That can be derived from the mathematical description of secondary nucleation, growth and dissolution, which consists of a power function of either supersaturation or undersaturation.

After regressing the ten kinetic parameters associated with the performed batch crystallization experiments (Table 5.4), the comparison between the liquid concentration profiles obtained experimentally and the ones provided by the model are shown in Figure 5.7.
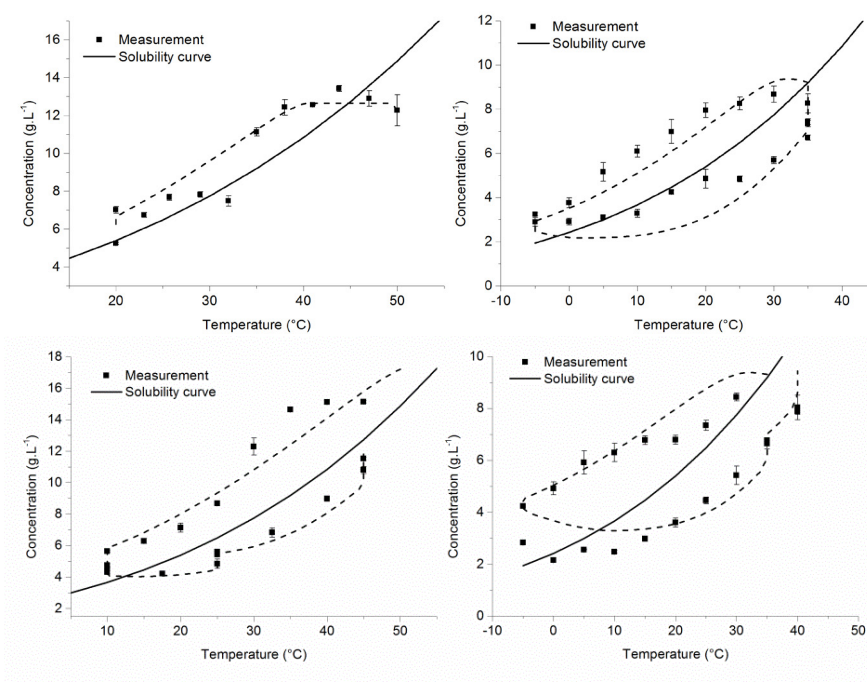
Figure 5.7 — Progress of the liquid phase concentration of *trans*-resveratrol, during each of the four batch crystallization experiments previously indicated. Model predictions are shown in dashed lines and the solubility curve in 46% w/w ethanol solution is shown in full line. The error bars indicate the standard deviation in the UHPLC concentration measurements.

As it is possible to observe, the used kinetic models seem to be able to follow quite well the liquid concentration profile of the polyphenol. Nonetheless, the confidence intervals on the secondary nucleation parameters of *trans*-resveratrol were larger than their average value (Table 5.4). This result suggests that, during the performed experiments, secondary nucleation might not have had a significant impact for the supersaturation levels

applied. To confirm that was the case, the same model was run, but assuming no secondary nucleation would take place (all the remaining parameters were kept unchanged). The obtained model was undistinguishable from the first one (data not shown). A possible explanation for this has to do with the supersaturation level attained in the reactor. Unlike most of the cooling crystallization processes at industrial scale, where most compounds have solubility between 100-300 g.L^{-1}, [18] solubility of the polyphenols used in this work is at most around 15 g.L^{-1}. Because of that, provided the cooling rate is low enough, the supersaturation in the system should be consumed mostly for crystal growth and not for secondary nucleation (higher supersaturation levels are usually needed for secondary nucleation to significantly occur).

Table 5.4 — Regressed kinetic parameters for *trans*-resveratrol.

Parameter	Regressed value
k_{N2}^0	2.09 x 10^8*
E_{N2}	5.00 x 10^6*
b	4.05*
j	3.05*
k_G^0	(6.6$\pm$0.3) x 10^6
E_G	(3.00$\pm$0.01) x 10^4
p	(5.819$\pm$0.002) x 10^{-1}
k_D^0	(5.84$\pm$0.01) x 10^8
E_D	(3.5113$\pm$0.0009) x 10^4
q	1.1521$\pm$0.0002

For the case of naringenin, the applied temperature profiles are shown in Figure 5.8. The goal when designing these experiments was the same as in the case before. However, because naringenin required higher supersaturation levels to start growing, the applied cooling profiles were quite similar in all the experiments. In order to circumvent that limitation and to try achieving different

5

supersaturation/undersaturation levels during each experiment, different mass of seed crystals were added at the beginning of experiment.
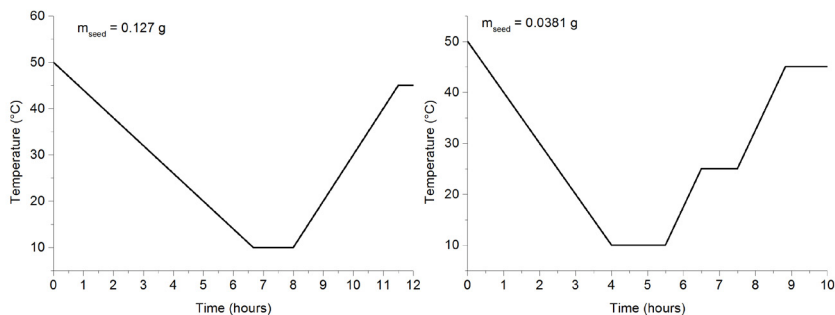
Figure 5.8 — Temperature profiles used for the single batch experiments using naringenin. It is also indicated in each graphic, the introduced mass of seed crystals, so that crystal growth was promoted.

The same comparison between the experimental values and the model predictions, as the one performed for *trans*-resveratrol, is indicated in Figure 5.9.

5
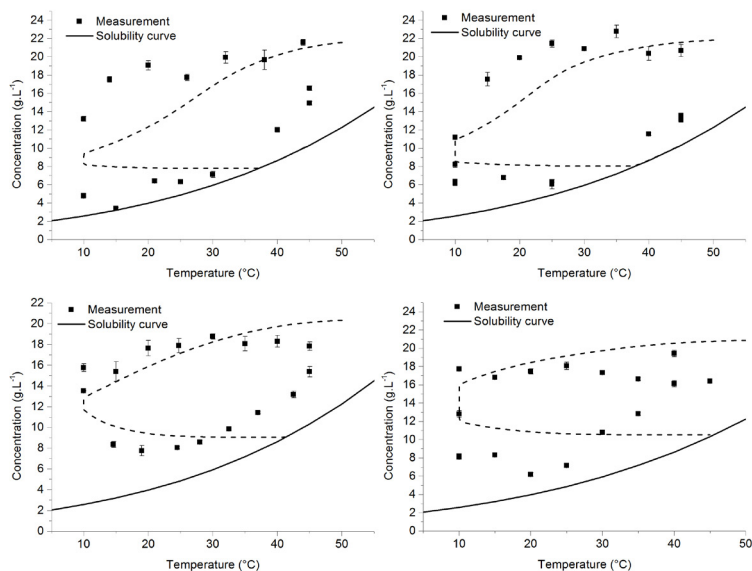
Figure 5.9 — Progress of the liquid phase concentration of naringenin, during each of the four batch crystallization experiments previously indicated. Model predictions are shown in dashed lines and the solubility curve in 46% w/w ethanol solution is shown in full line. The error bars indicate the standard deviation in the UHPLC concentration measurements.

5

When comparing to *trans*-resveratrol, significant differences could be detected in the behavior of naringenin. First of all, it was observed that agglomeration was occurring with time, which was not accounted for in the simpler kinetic model used. On the other hand, the level of supersaturation needed for growth to occur was significantly higher than the one for *trans*-resveratrol, despite seed crystals being added at the beginning of the experiment. By looking at Table 5.5, which contains the regressed parameters for naringenin, it is possible to check that the growth exponent, *p*, is 4.19, much higher than the value of 0.58 for *trans*-resveratrol. This difference might encounter an explanation in a set of reasons. First of all, there is some uncertainty associated with the solubility curve determination, which was interpolated using the Jouyban-Acree model. Second, a polynuclear growth mechanism might be present, which is associated with a larger growth rate exponent.[19] The last explanation proposed is related to the occurrence of

agglomeration itself, observed in the performed experiments and that was not accounted for. Since the used models had the goal of being able to predict the liquid concentration profile along time while keeping simplicity, they may not be fully able, as in this case of naringenin, to fully describe the physical and chemical aspects of the crystallization process. Because of that, the regressed parameters in Table 5.5 had a too small confidence region, but to which no statistical meaning was given.

Table 5.5 — Regressed kinetic parameters for naringenin. The confidence intervals are not provided, since they do not provide a reasonalbe statistical interpretation of their degree of uncertainty.

Parameter	Regressed value
k_{N2}^0	9.33 x 10^{30}
E_{N2}	3.87 x 10^3
b	5.76
j	3.13
k_G^0	2.59 x 10^9
E_G	2.39 x 10^3
p	4.31
k_D^0	1.75 x 10^{11}
E_D	1.70 x 10^4
q	1.36

Figure 5.10 shows the comparison between model predictions and experimental data. In this picture, it is possible to check that the systems containing only trans-resveratrol are better described than the ones containing naringenin, possibly due to the reasons detailed before.

5
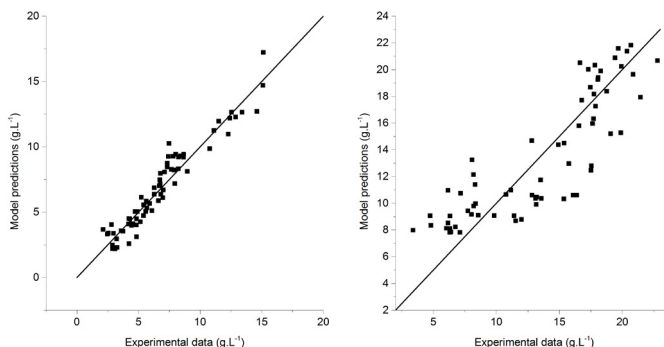
Figure 5.10 — **Comparison between the experimental liquid concentration data and the crystallization kinetic model for *trans*-resveratrol (left) and naringenin (right).**

5.3.6 Preferential crystallization experiment using coupled vessels

As it was shown before, the concept of preferential crystallization was validated by performing two independent batch experiments, where both polyphenols were initially present, but only the seeded compound was able to grow until a certain level of supersaturation of the impurity. In order to improve the yield of both compounds in their respective vessel, a strategy using two coupled vessels was executed[8]. In this experiment lasting for 6 hours, both the temperatures in each vessel as well as the flow rates, were controlled every 20 minutes. In order to approach the optimal process conditions, an optimal control problem was formulated:

$$\max_{T_1(t),\ T_2(t),F_{12}(t),\ F_{21}(t)} \min \left(Y_{naringenin}, Y_{t-resveratrol}\right) \qquad (5.22)$$

In this expression, $Y_{naringenin}$ and $Y_{t-resveratrol}$ correspond to the yields of the respective polyphenol. In each reactor, the temperature controls could not be set below 0°C or above 50°C.

$$0 \leq T(°C) \leq 50 \qquad (5.23)$$

The flow rates being delivered by the pumps were also subject to constraints. The minimum was set as the minimum flow rate the pump could deliver (1 mL.min⁻¹). The maximum was set at 5 mL.min⁻¹, to avoid that a small offset between the set-point and the flow rate actually delivered would not cause an overfilling of the vessels:

$$1 \leq F_{ij}(mL \cdot min^{-1}) \leq 5 \qquad (5.24)$$

Additional constraints were set as indicated in eq. 25. The liquid volume in each vessel should not be lower than 60 mL or higher than 150 mL. This is to avoid overfilling the vessel or having a too low volume to be stirred. The imposed boundaries on the supersaturation ratios were obtained from the previous preferential crystallization experiments using single vessels (2.6 for *trans*-resveratrol and 4.5 for naringenin). The liquid temperature was also required to be always equal or larger to the temperature at the time when the seed crystals are added, in order to avoid their dissolution. The solid content was also limited to a maximum of 20 g.L⁻¹, because with too high concentration, the inlet filter started being covered with solid mass and the pump cavitating and not delivering the desired flow.

$$\begin{bmatrix} T(t \geq t_{seed}) \leq T(t_{seed}) \\[2ex] 60 \leq V(mL) \leq 150 \\[2ex] SSR_{resv,1} \leq 2.6 \\[2ex] SSR_{nar,2} \leq 4.5 \\[2ex] C_s(g \cdot L^{-1}) \leq 20 \end{bmatrix} \qquad (5.25)$$

In eq. 5.25, $SSR_{resv,1}$ is the supersaturation ratio of *trans*-resveratrol in vessel 1 and $SSR_{nar,2}$ the supersaturation ratio in vessel 2. The formulated optimal control problem was solved using Matlab and the NOMAD algorithm.[20-23]

The optimal temperature controls obtained after performing the optimization are indicated in Figure 5.11.
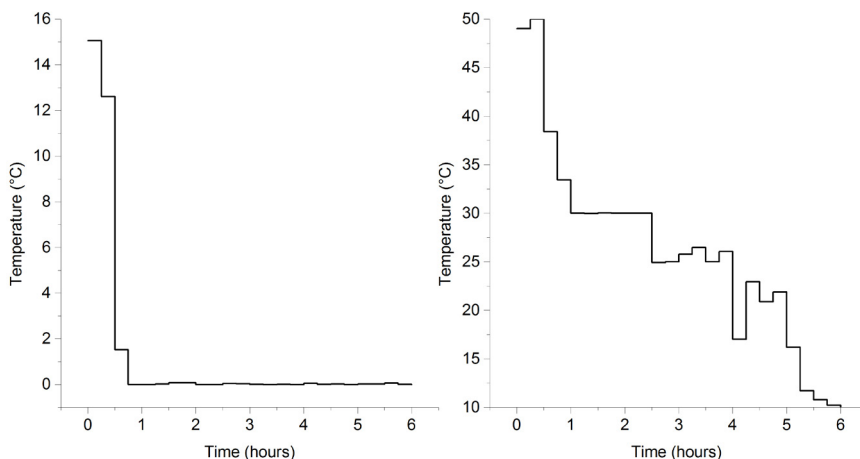
Figure 5.11 — Optimal temperature set-points for crystallizer 1, where naringenin is preferentially crystallized (left) and crystallizer 2 (right), where *trans*-resveratrol is preferentially crystallized. The unexpected jumps in the temperature level, might be due to an existence of several local minima.

Due to the high nonlinearity of this problem, It is expected that multiple minima can exist. For the temperature control in crystallizer 1 (Figure 5.11, on the left), the obtained solution starts, almost from the beginning, asking for a temperature close to 0°C. This is because naringenin requires a high supersaturation level to start growing and also because at that temperature, *trans*-resveratrol is still below a supersaturation ratio of 2.6 (the set constraint in order to avoid primary nucleation). On the other hand, in vessel 2, the temperature starts by slowly decreasing until 25°C. At this point, the model assumes that *trans*-resveratrol is able to grow, while keeping naringenin below a supersaturation ratio of 4.8. After approximately 3.5 hours, when the crystallizers are exchanging fluid, because the concentration of naringenin is supposed to lower (more dilute naringenin solution comes from vessel 1 and more concentrated solution leaves vessel 2), the temperature is further dropped to 10°C. The goal being to increase yield and keep a high purity.

5

The optimal controls obtained for the flow rates exchange by each vessel are indicated in Figure 5.12.
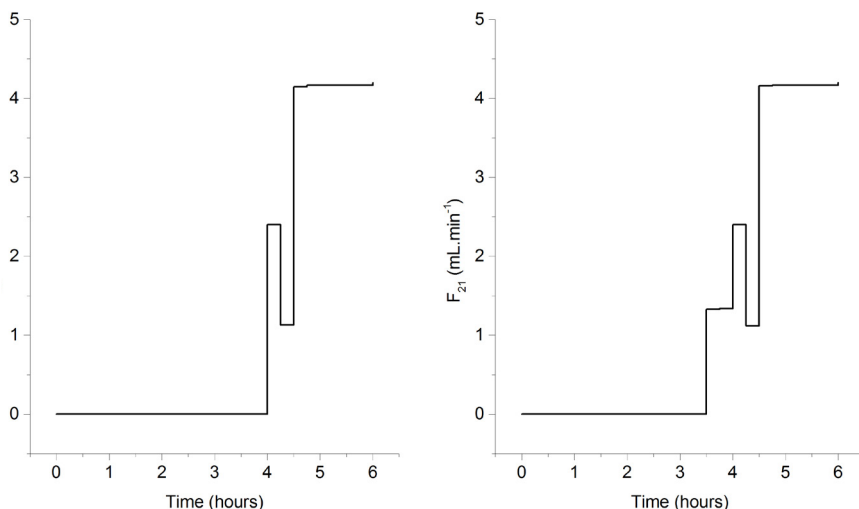
Figure 5.12 — Optimal flowrate set-points for crystallizer 1, where naringenin is preferentially crystallized (left) and crystallizer 2 (right), where *trans*-resveratrol is preferentially crystallized.

As it possible to observe, the pumps were only started after approximately 3.5 hours of experiment. This is because it only makes sense to start pumping when the solution becomes richer in the impurity. Vessel 2 ends up with a volume of 60 mL and vessel 1 with 140 mL. This is because the model assumes that the most difficult polyphenol to crystallize, given the constraints, is naringenin (the supersaturation ratio of *trans*-resveratrol has to be below 2.6). Because the minimum yield is being maximized and increasing the yield of *trans*-resveratrol is "easier", the obtained mathematical solution asks for more volume in vessel 1 in order to crystallize more naringenin (the limiting polyphenol). Based on the determined controls, the developed Matlab script predicted a 78% yield of *trans*-resveratrol and a 68% yield of naringenin, both reaching a final purity of 100%.

5

The experiment was performed using the coupled crystallizer scheme and the results are plotted in Figure 5.13.
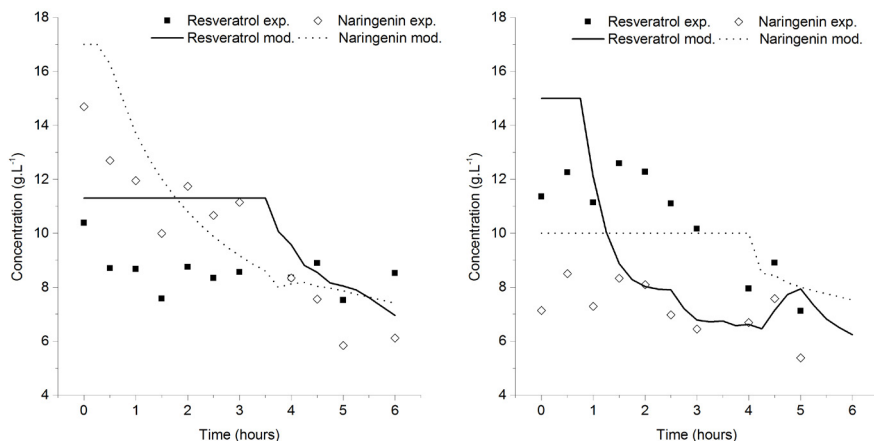
Figure 5.13 — Liquid concentration of both naringenin and *trans*-resveratrol along time, for crystallizer 1 (left) and crystallizer 2 (right). The model predictions are indicated in full and dashed lines in order to provide a comparison with the obtained experimental data.

Two analyses are done in this section to the results depicted in Figure 5.13. First of all, regarding the vertical offset between the model predictions and the experimentally obtained values, the difference can be explained by the impact of the cellulose acetate filter on the sampling process. For instance, the initial concentration of naringenin in vessel 1 was determined to be 17.7 g.L⁻¹ without using the filter and 14.7 g.L⁻¹ when using the filter. The same happened with *trans*-resveratrol and in both solutions. Although the sampling process may have a certain impact on the absolute concentration determination, the same protocol was followed in all experiments and thus, all the model predictions should be consistent. Moreover, the error in the concentration determination should be considerably lower than the model uncertainty, which does not take into account aspects like agglomeration or the effect of the impurities on the growth rates. Considering now how the model predicts the liquid concentration progress in time for both polyphenols, it can be observed that naringenin in vessel 1 is quite well described, while resveratrol seems to

5

remain essentially constant, although the model predicts that some dilution should occur after the 3.5 hours (fluid is coming from vessel 2). Since almost no *trans*-resveratrol crystallized in vessel 1 (naringenin purity is close to 100%), the suggested explanation is that the *trans*-resveratrol coming from vessel 2 is more concentrated than predicted by the model, as possible to check in Figure 5.13, on the right. In vessel 2, the description of *trans*-resveratrol seems to have an horizontal offset, before there is any fluid exchange between the vessels (after 3.5 hours). The proposed explanation is that naringenin might be acting as a growth inhibitor impurity, thus increasing the needed supersaturation for *trans*-resveratrol to start growing. The concentration profile of naringenin is qualitatively well predicted, the only difference being more towards the end, where it seems to be more diluted than expected. The reason for that, since no naringenin crystallized in vessel 2 (see Table 5.6), is that naringenin being transported from vessel 1 is also more dilute than predicted by the model.

The final yield of each compound was calculated using eq. 5.26, where the final solid mass was obtained by vacuum filtration.

$$Yield_i^k = \frac{final\ mass\ of\ polyphenol\ in\ vessel\ i - m_{seed}}{C_{0,l,i}^k V_0} \tag{5.26}$$

The term $Yield_i^k$ corresponds to the yield of polyphenol i in the vessel k.

Alternatively, the yield was calculated by mass balance. For the generic case of a polyphenol i in vessel 1, the expression used is indicated in eq. (5.27):

$$
\begin{aligned}
&Yield_i^1 \\
&= \frac{(C_{0,l,i}^1 + C_{0,l,i}^2)V_0 - (C_{f,l,i}^1 V_{f,1} + C_{f,l,i}^1 V_{f,2}) - C_{f,s,i}^2 V_{f,2} - m_{seed}}{m_{0,i}^1}
\end{aligned}
\tag{5.27}
$$

The purity of the solids in both vessels was determined by UHPLC and using eq. (5.28). In this equation, the desired polyphenol corresponds to compound i and the impurity is represented by j.

5

$$Purity_i^k = \frac{C_{f,s,i}^k}{C_{f,s,i}^k + C_{f,s,j}^k}$$

(5.28)

The obtained results are compiled in Table 5.6.

Table 5.6 — Yield and purity of each polyphenol in both vessels 1 and 2, at the end of the preferential crystallization experiment. The value higher than 1 obtained for the yield of naringenin is a consequence of the definition of yield provided in this work and indicated in eq. 5.25.

Vessel	Yield*	Yield†	Predicted yield	Purity
1 (naringenin)	24%	63%	64%	98%
2 (*trans*-resveratrol)	6%	44%	78%	100%

* Yield obtained using filtration

† Yield obtained using mass balance

As it is possible to observe, there is a significant discrepancy between the yields calculated either by mass balance and when measuring the solids after filtering the slurry.

First of all, the difference between the yield obtained by mass balance and the one predicted by the model, is assumed to be mainly due to the uncertainty associated with the regressed parameters and to the fact that those parameters were estimated from single component crystallization experiments. Regarding the difference between the yield calculated by mass balance or by weighting the total final solid mass, the reason might be associated with crystal loss inside the tubing and on the inline filter. Due to their shape, despite the fact that needle crystals may be larger than 10 µm in their characteristic length, their width and depth might be low enough, so that they can enter the inlet filter through different angles. Moreover, knowing that liquid velocity inside the tubing is relatively low (in the range of 2×10^{-3} m.s^{-1}) and especially as the crystals grow, they might become more difficult to transport with the pumped fluid. Because they probably get blocked at the inline filter (0.2 µm pore size), they may tend to either get accumulated at the filter or attach to the

5

tubing walls (tubing has a dead volume of around 9 mL). Since this mass of crystals was not taken into account, it might explain the difference between the two different ways of calculating the yield. One aspect that supports this reason, is that the liquid concentration of *trans*-resveratrol in vessel 2 effectively decreased, as shown in Figure 5.16 (figure on the right). However, by the time both vessels were exchanging liquid at the same rate, the concentration of this molecule on both vessels was similar, so no dilution effect should be present.

In the end, the goal of the coupled vessel experiment was to prove that it was possible to perform an offline process optimization using previously developed crystallization kinetics models and, within a certain error margin, to predict the time evolution of the liquid concentration of both polyphenols. Another aim was to suggest that, given some process changes (e.g., different filter pore sizes, preventing filter clogging, using online process control), this strategy should give a yield at least as large as the one obtained by using two uncoupled vessels. One possible way of overcoming these hurdles observed at the lab scale, would be to use a continuous filtration unit between the two vessels. This would not only avoid passing solid material to the other vessel, but also keep the solids concentration within the desired level.

5.4 Conclusions

In this work the applicability of preferential crystallization towards the recovery and purification of two similar polyphenols, naringenin and *trans*-resveratrol, was tested. First of all, it was assumed that a preliminary purification, based on reverse-phase adsorption, had been executed after a fermentation step. This purification step would have provided two fractions, each with a 60% purity of both naringenin and *trans*-resveratrol. The preferential crystallization would then be a possible further purification unit, where the purity of each polyphenol would increase to at least 95% and the minimum yield would be maximized.

The strategy followed in this work had three steps: first, performing the necessary batch experiments with the pure compounds in order to estimate their crystallization kinetic parameters (secondary nucleation, growth and dissolution); second, the optimal control problem was formulated in Matlab and solved in order to maximize the minimum polyphenol yield, while obeying to certain constraints such as purity; last, the preferential crystallization experiment using two coupled vessels was executed and the results compared with the model predictions. One of the main conclusions obtained from this work is that preferential crystallization proved to be a feasible method of purifying two similar compounds, up until the point that the supersaturation level of the impurity leads to its nucleation. This was observed with the performed batch experiments, where either naringenin or *trans*-resveratrol started with a 60% purity level. The goal here was to evaluate the maximum supersaturation level that would make the undesired polyphenol to start nucleating. In fact, these experiments were no different from a coupled vessel preferential experiment with no fluid being exchanged between the two vessels. The second conclusion is related with the crystallization kinetic models developed. It was shown that for the case of *trans*-resveratrol the model is able to predict quite well the liquid phase concentrations. Nonetheless, for naringenin, the model predictions were not as good, probably due to the fact that the underlying assumptions, such as no aggregation or no crystal growth dependence on the characteristic size, were not correct. However, the obtained model still had the capability of providing reasonable good predictions of the naringenin concentration in the liquid phase and, in the end, to prove its applicability to solve the final optimal control problem. The last point is related with the actual coupled preferential crystallization experiment. The obtained results showed a relative success of this set-up, by increasing the purity of both polyphenols to approximately 100%, despite of the relatively low yields (44% for *trans*-resveratrol and 63% for naringenin, when calculated by mass balance). Although some discrepancy between the model predictions and the experimental concentration values was observed, the developed models had relative success in predicting the qualitative behavior of the crystallization progress. However, in order to explore the full potential of this technique, using a continuous filtration unit in between the two crystallizers could be more efficient. In that way,

5

not only crystals could not pass to the other crystallizer, but also the solids concentration would be kept at the desired level in each vessel. In the end, the major goal of this study was to reinforce the idea that preferential crystallization can be applied for cases other than the resolution of racemic compounds and that this method can also be an economical way of purifying polyphenols, in case they are closely related to each other, making it a better alternative to a possible more expensive chromatography step.

Nomenclature

Variable	Name	Units
$B_{2,i}$	Secondary nucleation rate of polyphenol i	#.cm^{-3}.min^{-1}
$k^0_{N2,i}$	Secondary nucleation parameter	#.cm^{-3}.min^{-1}
$E_{N2,i}$	Activation energy for secondary nucleation	J.mol^{-1}
R	Universal gas constant	J.K^{-1}.mol^{-1}
b	Secondary nucleation parameter	-
M_T	Total mass of crystals in suspension	kg.L^{-1}
j	Secondary nucleation parameter	-
m	Momentum order of the crystal size distribution	-
Δc	Supersaturation level	kg.kg^{-1} suspension
Δc_{us}	Undersaturation level	kg.kg^{-1} suspension
G_i	Growth rate of polyphenol i	µm.min^{-1}
k^0_G	Growth parameter	µm.min^{-1}
E_G	Activation energy for crystal growth	J.mol^{-1}
p	Growth parameter	-
D_i	Dissolution rate of polyphenol i	µm.min^{-1}
k^0_D	Dissolution parameter	µm.min^{-1}
E_D	Activation energy for crystal dissolution	J.mol^{-1}
q	Dissolution parameter	-
$\hat{\mu}_{m,i}$	m^{th} distribution moment of polyphenol i	#.µm^m.L^{-1}
$\bar{n}_i$	Relative number of crystals of polyphenol i in suspension	µm^{-1}
N_i	Total number of crystals of polyphenol i in suspension	#
$\rho_{c,i}$	Crystal density	kg.m^{-3}
$k_{v,i}$	Crystal volume shape factor	-
$\bar{k}_{v,i}$	Average volume shape factor	-
$k_{v,i0}$	Parameter for describing $k_{v,i}$	µm^{-x}

t_{seed}	Time point at which seed crystals are added to the vessel	h
$C_{l,i}^{k}$	Liquid concentration of polyphenol i in vessel k	g.L^{-1}
$C_{s,i}^{k}$	Solid concentration of polyphenol i in vessel k	g.L^{-1}
$C_{l,i,nk}^{tub}$	Liquid concentration of polyphenol i inside tubing coming from vessel n to vessel k	g.L^{-1}
$C_{0,l,i}^{k}$	Initial liquid concentration of polyphenol i in vessel k	g.L^{-1}
$C_{0,s,i}^{k}$	Initial solid concentration of polyphenol i in vessel k	g.L^{-1}
$C_{f,l,i}^{k}$	Final liquid concentration of polyphenol i in vessel k	g.L^{-1}
$C_{f,s,i}^{k}$	Final solid concentration of polyphenol i in vessel k	g.L^{-1}
m_{seed}	Mass of seed crystals of a given polyphenol	g
$m_{0,i}^{k}$	Initial mass of polyphenol i in vessel k	g
F_{nk}	Flow rate from crystallizer n to crystallizer k	L.h^{-1}
V^{k}	Liquid volume in vessel k	L
T	Liquid temperature	C°
T_{t}	Actual temperature in the thermostat, after applying a given set-point	C°
x	Exponent for describing	-

Acknowledgements

References

1 Transparency Market Research, Polyphenols Market by Product (Grape Seed, Green Tea, Apple and Others), by Application (Functional Beverages, Functional Food, Dietary Supplements and Others): Global Industry Analysis, Size, Share, Growth, Trends and Forecast, 2012 - 2018. (2013).

2 Scalbert A, Johnson IT and Saltmarsh M, Polyphenols: antioxidants and beyond. *Am J Clin Nutr* **81**: 215S-217S (2005).

3 Pandey KB and Rizvi SI, Plant polyphenols as dietary antioxidants in human health and disease. *Oxid Med Cell Longev* **2**: 270-278 (2009).

4 BacHBerry consortium, BacHBerry (2015).

5 Hara KY, Araki M, Okai N, Wakai S, Hasunuma T and Kondo A, Development of bio-based fine chemical production through synthetic bioengineering. *Microb Cell Fact* **13** (2014).

6 Rougeot C and Hein JE, Application of Continuous Preferential Crystallization to Efficiently Access Enantiopure Chemicals. *Org Process Res Dev* **19**: 1809-1819 (2015).

7 Chaaban JH, Dam-Johansen K, Skovby T and Kiil S, Separation of Enantiomers by Preferential Crystallization: Mathematical Modeling of a Coupled Crystallizer Configuration. *Org Process Res Dev* **18**: 601-612 (2014).

8 Elsner MP, Ziomek G and Seidel-Morgenstern A, Simultaneous preferential crystallization in a coupled, batch operation mode—Part I: Theoretical analysis and optimization. *Chemical Engineering Science* **62**: 4760-4769 (2007).

9 Levilain G and Coquerel G, Pitfalls and rewards of preferential crystallization. *Crystengcomm* **12**: 1983-1992 (2010).

10 Myerson A, Handbook of Industrial Crystallization (2002).

11 Eisenschmidt H, Voigt A and Sundmacher K, Face-Specific Growth and Dissolution Kinetics of Potassium Dihydrogen Phosphate Crystals from Batch Crystallization Experiments. *Cryst Growth Des* **15**: 219-227 (2015).

12 Chung SH, Ma DL and Braatz RD, Optimal model-based experimental design in batch crystallization. *Chemometr Intell Lab* **50**: 83-90 (2000).

13 Zhang PP, Lin R, Yang GD, Zhang JY, Zhou L and Liu TT, Solubility of Naringenin in Ethanol and Water Mixtures. *J Chem Eng Data* **58**: 2402-2404 (2013).

14 Sun XL, Shao YD and Yan WD, Measurement and Correlation of Solubilities of trans-Resveratrol in Ethanol plus Water and Acetone plus Water Mixed Solvents at Different Temperatures. *J Chem Eng Data* **53**: 2562-2566 (2008).

15 Jouyban A, Shayanfar A, Panahi-Azar V, Soleymani J, Yousefi BH, Acree WE, Jr. and York P, Solubility prediction of drugs in mixed solvents using partial solubility parameters. *Journal of pharmaceutical sciences* (2011).

16 Dorfner K, Ion exchangers. De Gruyter (1991).

17 Dortmund Data Bank, Dortmund Data Bank (2017).

18 Lewis A, Seckler M, Kramer H and van Rosmalen G, Industrial Crystallization: Fundamentals and Applications. Cambridge University Press (2015).

19 Wedlock DJ, Controlled particle, droplet and bubble formation. Butterworth-Heinemann (2012).

20 Tribes CAaSLDaC, NOMAD user guide. Les cahiers du GERAD (2009).

21 M.A. Abramson and C. Audet and G. Couture and J.E. Dennis JaSLDaCT, The NOMAD project, Software available at https://www.gerad.ca/nomad/.

22 Le Digabel S, Algorithm 909: NOMAD: Nonlinear Optimization with the MADS Algorithm. *Acm T Math Software* **37** (2011).

23 Audet C and Dennis JE, Mesh Adaptive Direct Search Algorithms for Constrained Optimization. *SIAM Journal on Optimization* **17**: 188-217 (2006).

6

Downstream process synthesis for the recovery and purification of polyphenols from a fermentation broth

Abstract

The growing market for polyphenols has motivated the development of fermentation based processes for their production. This new paradigm requires different approaches for the downstream process (DSP) and a techno-economical study of different alternatives.

In this work, different scenarios for the purification of polyphenols present in a fermentation broth were compared, targeting a production rate of 3 ton.y^{-1}. Two different cases were addressed: the recovery of *trans*-resveratrol from a broth containing hydrophilic molecules as impurities (S1) and and purification of both *trans*-resveratrol and naringenin from a similar matrix (S2). In S1, liquid-liquid extraction (LLE) and reverse-phase adsorption (RPA) were compared. In S2, LLE was compared with RPA and with preferential crystallization (PC).

For S1, RPA proved to be less expensive (110 $.kg^{-1} vs 140 $.kg^{-1}), while using a less toxic solvent. For S2, LLE was the least expensive approach despite adding two solvents to the DSP (73 $.kg^{-1}). RPA presented a larger operational expenditures (OPEX) than either LLE or PC due to the costs associated with the RENSA PY resin.

The results shown in this work assist in a more rational process design for the recovery and purification of polyphenols produced by fermentation.

6.1 Introduction

Polyphenols are secondary metabolites produced by plants which find applications in the biotechnological industry as colorants and health promoting agents. For example, research has shown that bioactivity is associated with protection against several cardiovascular[1] and neurological diseases.[2] Moreover, anthocyanins are known for their properties as colorants which are of interest for the food industry as alternatives to synthetic dyes.[3]

This growing interest in these phytochemicals has led to a market growth which is expected to arrive at 850 million USD by 2018.[3] To meet this expected increase in demand, not only more efficient processes are needed, but also greener alternatives to the current plant extraction methods. One of the possibilities is to produce these valuable compounds by fermentation.

The fact that the paradigm might shift from a situation where the desired product is in a solid matrix to a scenario where it is present in a complex aqueous matrix containing fermentation by-products, demands for different downstream process strategies as well. Two main concerns arise: not only the separation and purification train should be economically feasible, given that these products have a relatively small market price, but also environmental friendly. The latter is because not only regulatory agency criteria has to be met, but also because the whole process goal when producing these compounds by fermentation, is to have an overall low environmental impact.

Previous work has been devoted to the investigation of different methodologies for the recovery and purification of polyphenols from a typical fermentation broth of *C. glutamicum*, under aerobic conditions.[4, 5] Liquid-liquid extraction can be a simple and flexible approach to the recovery of these compounds, but has the downside of having to deal with complex solvent recovery. Adsorption has the advantage of only using water/ethanol mixtures in the entire downstream process, but might not be selective enough if two related polyphenols are co-produced during fermentation. Preferential

crystallization might appear as a possible strategy for that complex purification scenario. Nonetheless, the compounds of interest have to be able to form crystalline structures and have sufficiently different crystallization kinetics, in order to achieve sufficient purification.

Although these different downstream process strategies were studied before, their discussion was mainly done in the scientific and technical feasibility plane, without giving a cost estimation of their industrial implementation. The goal of this chapter is to establish and economically evaluate different relevant case-scenarios involving the separation and purification of hydrophobic polyphenols, either when only one compound is present among other hydrophilic molecules (e.g., sugars, proteins, organic acids) or when two similar polyphenols are present in a similar aqueous matrix.

This study starts by setting the process constraints associated with the production of these phytochemicals. Parameters such as yield, annual production, temperature and pH windows are defined in the beginning of this work and serve as a guide for the suggestion of the different downstream process scenarios. The different, continuous processes, are then implemented in Aspen Plus® version 8.8 (https://www.aspentech.com) to solve the associated mass and energy balances. However, whenever adsorption is used and due to its inherently batch character, its simulation has to be performed independently using Aspen Chromatography® version 8.8 (https://www.aspentech.com).

In order to solve the simulations, thermodynamic models are needed whenever Aspen Plus does not have the adequate parameters in its database. In this study, results obtained previously were used not only to model the liquid-liquid partition of polyphenols, but also the needed adsorption equilibrium isotherms onto the XAD and RENSA resins using different water/ethanol mobile phases. The needed values for solubility were directly taken from available literature.

The performed simulations using the Aspen software package enabled the determination of the needed capital investment for the necessary equipment (CAPEX) and also the cost associated with raw materials and utilities, which take part on the operational

expenditures (OPEX). In order to have a fair comparison between all the process alternatives, the E-factor for all the scenarios was fixed below 1 kg solvent.kg product[-1], meaning that most of the solvents used in the processes were almost completely recovered and recycled back to the process.

The results obtained in this study allow now for a broader overview of the different possible downstream strategies that can be used in the purification of polyphenols from a fermentation broth. While previous work describes the scientific and technical feasibility aspects of the different scenarios proposed here, this work not only performs their economical comparison, but also serves as a guide to which downstream process to select depending on the purification problem encountered.

In section 6.2 of this chapter, the strategy used for the downstream process optimization is discussed, along with the thermodynamic models used for the process design. In section 6.3, the proposed downstream process scenarios are introduced for each case-study and the main results obtained from the economic analysis are indicated and discussed, leading to the selection of the optimal designs. The conclusions from this chapter are presented in section 6.4.

6.2 Materials and methods

6.2.1 Process assumptions

For the downstream process design, the fermentation medium needs to be well characterized. For the *C. glutamicum* fermentations, the CGXII medium was used in previous experiments.[4] Using data from the project partners, the following table displays the initial components in the medium and the expected composition at the end of the fermentation.

Table 6.1 – Detailed medium composition of a typical aerobic fermentation of *C. glutamicum*, when using defined medium. Both the initial compound concentration and their expected final concentration are indicated.

Initial medium	C_0 (mass per liter)	C_f (mass per liter)
Mineral basis		
$(NH_4)_2SO_4$ (N-source)	20 g	≈0
KH_2PO_4	1 g	1 g
K_2HPO_4	1 g	1 g
$MgSO_4 x7H_2o$	0.25 g	0.25 g
$CaCl_2$	10 mg	10 mg
Trace elements		
$FeSO_4 x7H_2o$	10 mg	10 mg
$MnSO_4 xH_2o$	10 mg	10 mg
$ZnSo_4 x7H_2o$	1 mg	1 mg
$CuSO_4$	0.2 mg	0.2 mg
$NiCl_2 x6H_2o$	0.02 mg	0.02 mg
Vitamin		
Biotin	0.2 mg	≈0
Carbon source		
Glucose	40 g	≈0
Growth inductor		
Protocatechuic acid	30 mg	30 mg
Heterologous gene expression inductor		
IPTG	238 mg	238 mg
Antibiotics		
kanamycin	25 mg	25 mg
spectinomycin	100 mg	100 mg
Antifoam		
Antifoam 204	As needed	1% v/v
Product		
trans-resveratrol	-	100 mg
Intermediates/by-products		

6

Initial medium	C_0 (mass per liter)	C_f (mass per liter)
p-coumaric acid	-	25 mg (*)
Lactic acid	-	25 mg
Fatty acids	-	1 mg
Proteins	-	n.s. (extracellular rec.)
DNA	-	n.s. (extracellular rec.)

From the analysis of Table 6.1, it is possible to conclude that the most similar molecules to *trans*-resveratrol (or naringenin), in terms of hydrophobicity, are fatty acids and biotin (weak acids, as *p*-coumaric acid and protocatechuic acid, can be made more hydrophilic at neutral pH). In a first analysis, those molecules are expected to be in significantly lower concentrations than *trans*-resveratrol. Moreover, they are food-grade molecules and their potential presence in the final product is not seen as a problem. Nonetheless, the final polyphenol product is to be recovered in a solid form in all the downstream strategies presented in this chapter. Thus, being crystallization a very selective process,[6] it is assumed that, despite potentially being present in the stream although not harmful, those impurities will be not be present in the final product.

All the remaining molecules will be assumed to be removed either during a liquid-liquid extraction or a reverse-phase adsorption process.

The downstream process design options considered in the following section include liquid-liquid extraction (two variants), reverse-phase adsorption and reverse-phase adsorption coupled with preferential crystallization. These techniques are the ones that, according to previous research, present the best techno-economical potential. Crystallization after fermentation (either external or *in-situ*) was not considered, since the expected product concentrations (100 mg.L^{-1}) would require the evaporation/cooling of a large aqueous stream. Moreover, the presence of a large quantity of impurities in the medium would be expected to

6

interfere with the crystallization process and the product yield and purity.

All the downstream process strategies presented in this chapter are planned to work in continuous. The reason being that it reduces equipment costs and ensures product batch-to-batch quality. For that to occur, it assumed that the fermentation section is run with staggered reactors, filling a holding tank which is able to deliver a continuous stream to the downstream section. Being an inherently batch process, whenever an adsorption step is utilized, at least two columns are used, so that one of them is always in the loading stage.

6.2.2 Process definition and constraints

For defining the process in terms of equipment size, raw materials and utilities, a production target has to be set. Based on previous work,[7] the desired production of either *trans*-resveratrol or naringenin will be set at 3 ton.y^{-1}. Given that each year is assumed to have 7920 of working hours, the target product flow-rate is of 0.38 kg.h^{-1}.

For the process design the following constraints were set:

- Product stability requires pH $\leq$ 7 and T $\leq$ 45°C

- Desired yield: > 80%. Desired purity: > 95%

- Liquid-liquid extraction: limited to organic solvents present in NRTL-SAC database

- For solvent recovery only distillation is considered

- Only water or ethanol could be involved as solvents in the adsorption process

6

- Preferential crystallization is assumed only possible for the purification of a mixture of resveratrol/naringenin and after adsorption is performed

6.2.3 Process selection and evaluation strategy

In this study, two case-studies will be considered: the recovery of *trans*-resveratrol from a typical *C. glutamicum* fermentation broth and the recovery and purification of both *trans*-resveratrol and naringenin from the same broth. In both cases, the same strategy was followed for the selection and comparison of the different downstream process strategies. First, the processes are selected based on previous knowledge[7, 8] and rules-of-thumb. The flowsheets are then implemented in Aspen Plus, where the mass and energy balances are solved. When distillation was used for solvent recovery, the reflux ratio and the distillate rate would be optimized in order to minimize solvent consumption. The number of stages, in all the situations, was fixed at 20 stages.

Based on the obtained mass and energy balances, the needed equipment can be sized and the costs with raw materials and utilities can be computed. Those variables are then used to calculate three parameters: capital expenditures (CAPEX), operational expenditures (OPEX) and the environmental factor (E-factor).

6
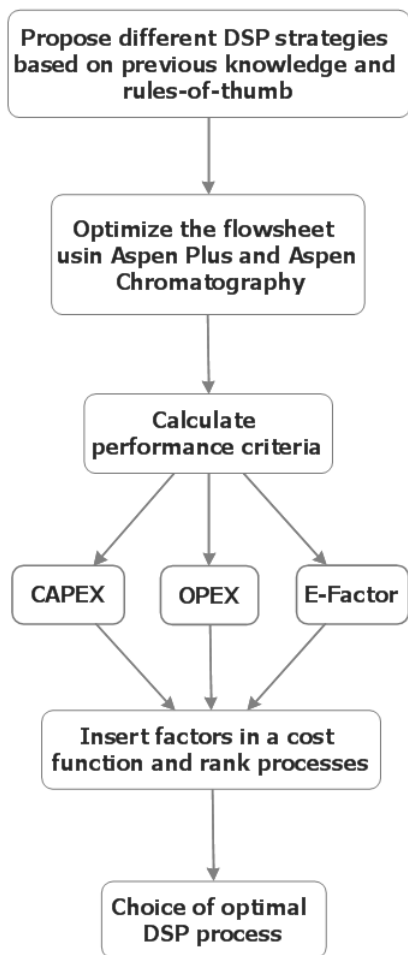
Figure 6.1 – Approach used for the selection and evaluation of the different downstream process strategies for the recovery and purification of polyphenols. After deciding on the processes and optimizing the different flowsheets using Aspen Plus, performance criteria are computed and introduced in a cost function which is used to rank them.

Based on those three parameters, the following cost function is used to rank the different DSP strategies:

$$F_{cost} = CAPEX + 10 \cdot OPEX \; ; \quad E - factor < 1 \; kg.kg^{-1} \; product \tag{6.1}$$

6.2.4 Thermodynamic models

For solving the required mass and energy balances using Aspen Plus, the knowledge of the equilibrium data of the desired polyphenols (e.g., liquid-liquid equilibrium, adsorption isotherms) is essential. In this sub-section, it is described how the equilibrium properties were calculated for the reverse-phase adsorption and liquid-liquid extraction unit operations. The solubility data needed for dealing with the crystallization unit was obtained from the literature. Whenever not mentioned, thermodynamic properties, such as vapor-liquid equilibrium (VLE), were calculated using the NRTL-SAC model available in Aspen Plus to describe the liquid non-ideality. The vapor phase was described as an ideal gas.

6.2.4.1 Reverse-phase adsorption

In order to model the adsorption columns, the Aspen Chromatography software package was used. The following differential mass balance is used, when solving a dynamic simulation:[9]

$$\frac{\partial C_i}{\partial t} + \phi . \frac{\partial q_i}{\partial t} + u \frac{\partial C_i}{\partial z} = D_L \frac{\partial^2 C_i}{\partial z^2} \tag{6.2}$$

C_i is the liquid phase concentration of component i, q_i the respective solid phase concentration, its axial dispersion coefficient and the phase ratio, which is calculated using the knowledge of the column total porosity (ε_T):

$$\phi = \frac{1 - \varepsilon_T}{\varepsilon_T} \tag{6.3}$$

The axial dispersion coefficient is estimate by Aspen Chromatography using the model of Chun and Wen.[10, 11]

During adsorption, mass transfer is assumed not to be instantaneous, and the solid linear driving force model was used to describe its kinetics:

$$\frac{\partial q_i}{\partial t} = k_m(q_i^* - q_i) \tag{6.4}$$

In this expression, q_i^* is the concentration in the solid phase in equilibrium with a given liquid phase concentration. The constant k_m is the mass transfer coefficient, which is estimated by Aspen Chromatography using the solid linear driving force model.[12]

The polyphenol solid phase concentration in equilibrium with its liquid concentration and of the other impurities, is calculated using the multicomponent Langmuir model:

$$q_i = \frac{q_{max,i} K_{L,i} C_i}{1 + \sum_{j=1}^{N} K_{L,j} C_j} \tag{6.5}$$

Where $K_{L,i}$ is the affinity coefficient and $q_{max,i}$ the maximum capacity of component *i*. Because ethanol will be used during adsorption as an eluent, the knowledge of how both Langmuir parameters (K_L and q_{max}) vary with its concentration is crucial. For that reason, the following logarithmic model was used to model the variation of the isotherm slope, $\left(\frac{q_i}{c_i}\right)_0$, with the percentage of ethanol:

$$ln\left[\frac{q_i}{C_i}_0 (C_{mod})\right] = \alpha_i + \gamma_i . C_{mod} \tag{6.6}$$

From previous work, it is known that the saturation capacity of polyphenol onto XAD resins may vary with the ethanol content as well. In that case, an empirical expression was used, which is described in Appendix C.

6

6.2.4.2 Liquid-liquid partition coefficient and solubility

For modelling the liquid-liquid partition coefficients of the desired polyphenols, the following equation was used:

$$log\ P = log\left(\frac{C_i^{org.}}{C_i^{aq.}}\right) = log\left(\frac{\gamma_i^{aq.}}{\gamma_i^{org.}}\right) \tag{6.7}$$

Its derivation is included elsewhere.[13]

For the weak acids, the log D (equivalent to the log P, but pH dependent) was calculated according to the following relation.

$$log\ D = log\ P - log(1 + 10^{pH-pKa}) \tag{6.8}$$

For the calculation of the solubility, the following equation was used:[13]

$$ln(\gamma_i \cdot x_i) = \frac{\Delta H_m}{RT_m}\left(\frac{T_m}{T} - 1\right) \tag{6.9}$$

In the last equation, is the solubility (molar fraction), R is the universal gas constant and and are the melting enthalpy and melting temperature of the specific molecule. Those values were obtained from chapter 2 of this thesis.

6.2.5 General equipment sizing details

In this section, the different proposed downstream process flowsheets are described and evaluated. In each subsection, and depending on the considered scenario (*trans*-resveratrol purification or *trans*-resveratrol + naringenin purification), each unit operation is sized as well as the needed raw materials and utilities. However, common to all proposed scenarios is the presence of tray dryers,

6

rotary vacuum filters, disk stack centrifuges, holding tanks and heat exchangers. For that reason, the description on how these particular units were sized is described here.

Heat exchangers

For the heat exchangers, it was considered that cooling water was available at 10°C and low pressure steam at 100°C and 1 atm. For the calculation of the needed heating/cooling area, the following overall heat transfer coefficients were considered:[14]

Table 6.2 – Overall heat transfer coefficients when different hot and cold fluids are contacted in a heat exchanger.[14]

Hot fluid	Cold fluid	U $(W.m^{-2}.K^{-1})$
Light organics	Water	500
Steam	Light organics	750

In all the calculations, the minimum approach temperature was taken as 10°C.[7] The cost of a heat exchanger as a function of its area was taken from Matches.[15]

Disc-stack centrifuge

For the sizing of the centrifuge, a mass balance on the water and solids is performed. It is assumed that the feed (the fermentation broth) contains 0.1 $kg.kg^{-1}$ of dry cells and that the cake formed in the centrifuge carries 20% moisture.

The mass balances then become:

$$F_{in} \cdot 0.1 = F_c \cdot (1 - 0.2) \tag{6.10}$$

$$F_{in} \cdot (1 - 0.1) = F_c \cdot 0.2 + F_v \tag{6.11}$$

In the last equation, F_{in} is the incoming flow-rate, F_c the cake flow-rate and F_v the filtrate flow-rate, which is assumed not to have any solid content.

Table 6.3 – Water and solid mass balances for the disk-stack centrifuge used in each of the downstream process strategies.

	Feed	Filtrate	Cake
Water (ton.h⁻¹)	3909	3800	109
Solid (ton.h⁻¹)	434	0	434

For this operation, an Alfa-Laval VO 10 centrifuge is chosen, which can operate at a flow rate of 10 m³.h⁻¹. The power consumption is of 18.5 kW (data from vendor) and its cost is considered to be 150 k\$. This value was taken from the literature, assuming that the power consumption would be 30 kW (the minimum value available).[14]

Holding tanks

Assuming that the holding tank receives an incoming flow-rate, F_{in}, for a given amount of time, t_{in}. Moreover, the time it spends without receiving the inlet stream is t_{hold}. The outlet continuous flow-rate is then given by:

$$F_{out} = \frac{F_{in} \cdot t_{in}}{t_{hold}} \qquad (6.12)$$

After reaching its maximum liquid volume (assumed to be 80% of its total volume), the minimum volume (assumed to be 20% of the total volume) is attained while its content is discharged and no inlet feed is present:

$$V_{max} - F_{out} \cdot t_{hold} = V_{min} \qquad (6.13)$$

6

$$0.8\,V - F_{out} \cdot t_{hold} = 0.2\,V \Leftrightarrow V = \frac{F_{out} \cdot t_{hold}}{0.6} \qquad (6.14)$$

Using eq. 6.12 and eq. 6.14, the holding tanks can be sized for each situation.

Evaporative crystallizer

For sizing the evaporative crystallizers, a simple approach was taken. Knowing the slurry flow-rate coming out of the vessel, its volume was calculated by assuming a 8 hour residence time. Moreover, a 20% over-design factor was applied. Thus:

$$V = F_{slurry} \cdot 8\,h \cdot 1.2 \qquad (6.15)$$

Rotary vacuum filter

For the rotary vacuum filter, a similar mass balance to the water and solids is also needed. However, in the following equation, the amount of filtrate or solids per unit time is described in terms of design parameters related with the vacuum filter (e.g., pressure difference or number of rpm).[14]

For all the calculations, a typical specific cake resistance of 10^{10} m.kg^{-1} was defined.[16]

The volume of filtrate per unit time (m^3.s^{-1}) is given by:[14]

$$v_R N_r = A_D \left(\frac{2\Psi_f N_r \Delta p}{\alpha \omega \mu} \right)^{1/2} \qquad (6.16)$$

Where the filtration area fraction is taken as 0.3.

6

The mass of dry cake per time (kg.s^{-1}) is given by:[14]

$$v_R N_r \omega = A_D \left(\frac{2 \Psi_f N_r \omega \Delta p}{\alpha \mu} \right)^{1/2} \qquad (6.17)$$

The volume of air that has to be removed per unit time is given by:[14]

$$\frac{Volume\ of\ air\ per\ unit\ time}{Weight\ of\ dry\ cake\ per\ unit\ time} = \left(\frac{\Psi_a}{\Psi_f} \right) \left(\frac{\mu}{\mu_a} \right) \left(\frac{\alpha}{2\beta' \omega} \right) \qquad (6.18)$$

Where the air suction area fraction is considered to be 0.2.

The power consumed by the vacuum pump is calculated by assuming an isentropic compression:[14]

$$Power = \frac{RT}{(k-1)/k} = \left[\left(\frac{P_2}{P_1} \right)^{(k-1)/k} - 1 \right] \qquad (6.19)$$

Where P_1 is the outlet pressure (atmospheric pressure) and, P_2 is the inlet presure.

It was assumed that the cake coming out of the filtration unit, and going to the drying section, contained 20% moisture.

Tray dryer

6

For the tray drier, it is assumed that the solids are dried from 20% humidity (w.w[-1]) to 1% humidity (w.w[-1]). In the following calculation, it is assumed that the moisture needed to be removed is free-water and that the drying process will proceed at a constant rate with the solid temperature equal to the wet bulb temperature of the air stream at all times.

For a cross-circulation unit, the following equation gives the time needed to complete drying in the constant-phase:[17]

$$t_c = \frac{m_v \Delta H_w^{vap}}{h(T_d - T_w)A} \qquad (6.20)$$

Air is assumed to enter at 80°C and 10% relative humidity. This corresponds to a wet bulb temperature of 40°C. Water vaporization enthalpy is of 2413 kJ.kg^{-1} and the air velocity on each tray is taken as 4 m.s^{-1}.[17] Moist air specific volume is 1.051 m^3.kg^{-1}.

The air flow-rate needed per unit area is then given by:

$$G = \frac{4}{1.051} = 3.81 \; kg.m^{-2}.s^{-1} = 13700 \; kg.m^{-2}.h^{-1} \qquad (6.21)$$

The convective heat transfer coefficient was obtained from a correlation:[17]

$$h = 0.0204(13700)^{0.8} = 43 \; Wm^{-2}.K^{-1} \qquad (6.22)$$

Because the needed total air flow-rate will depend on the number of trays, that specific value will be computed in each of the following scenarios. Nonetheless, those calculations will take into account the results obtained here.

6.3 Results and Discussion

In this section, the different approaches for the recovery and purification of *trans*-resveratrol and naringenin are discussed. The goal is to obtain order-of-magnitude estimates of both capital and operational expenditures for the different scenarios, so that their economical potential can be evaluated and compared.

Section 6.3.1 presents two proposed scenarios for the recovery of *trans*-resveratrol from a *C. glutamicum* fermentation broth. In the first scenario (1-1), liquid-liquid extraction is used while in scenario (1-2), reverse-phase chromatography is preferred.

6

Section 6.3.2 presents and discusses three scenarios for the recovery and purification of both *trans*-resveratrol and naringenin: scenario (2-1) uses two liquid-liquid extraction columns in series, scenario (2-2) uses reverse-phase chromatography with a functionalized resin (RENSA PY) and scenario (2-3) couples the usage of reverse-phase chromatography (using the XAD-16 resin) with preferential crystallization.

6.3.1 Hydrophobic polyphenol: *trans*-resveratrol (1)

This section deals with the recovery of *trans*-resveratrol from a typical fermentation broth of *C. glutamicum*. Two scenarios are proposed: liquid-liquid extraction using an organic solvent such as ethyl acetate and reverse-phase adsorption using the Amberlite XAD-16 resin.

6.3.1.1 Scenario 1-1

In the first proposed scenario, liquid-liquid extraction is used for the recovery and purification of *trans*-resveratrol. The fermentation broth is first centrifuged to separate the cells from the clarified broth. Afterwards, the clarified stream is contacted with ethyl acetate, which is able to extract *trans*-resveratrol from the broth, while leaving *p*-coumaric acid and other hydrophilic components behind (e.g., glucose, proteins).

6
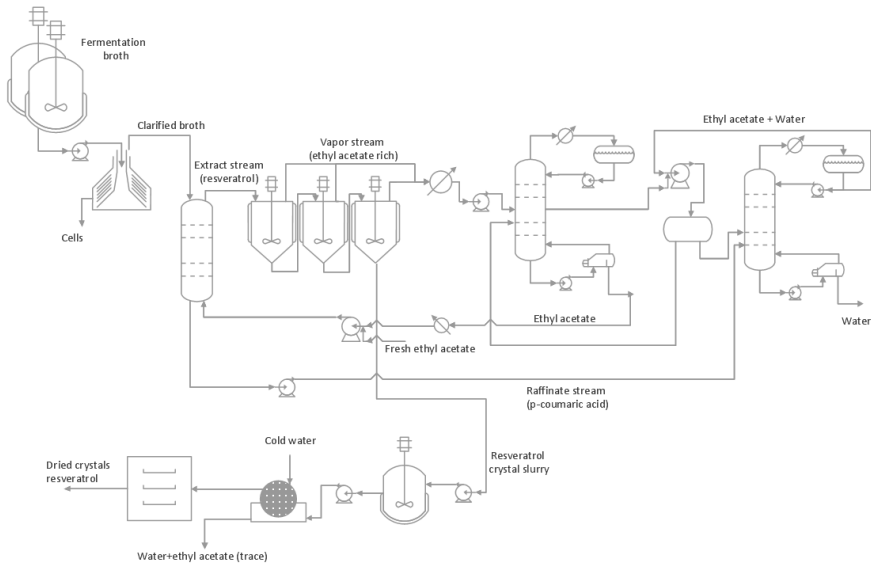
Figure 6.2 - Conceptual downstream process train for the recovery of *trans*-resveratrol, a hydrophobic polyphenol, from a fermentation broth containing hydrophilic impurities. The clarified stream goes through a LLE step, where the polyphenol is preferentially extracted. Afterwards, the desired compound is crystallized, filtered, washed and dried to obtain the final formulation. The solvent used for the extraction, ethyl acetate, is distilled and recycled to the extraction column.

The extract stream, containing the compound of interest, goes to a multi-effect evaporator where it is concentrated to the solubility limit and the desired polyphenol is then crystallized. The crystals are then filtered in a rotary vacuum filter and dried afterwards in a tray drier. The detailed calculations of these sequence of downstream process stages are indicated in the Appendix D1.

The ethyl acetate which is used in the liquid-liquid extraction stage is recovered by an azeotropic distillation step and then combined with a make-up stream of fresh ethyl acetate. Since most of the ethyl acetate ends up being recovered, the needed make-up stream is almost negligible as one can observe in Table 6.4.

6

Table 6.4 – Quantity and cost of the different raw materials used in scenario 1-1.

Raw material	Quantity (ton.y⁻¹)	Price (k$.ton⁻¹)	Total cost (k$.y⁻¹)
Ethyl acetate	0.08	1.18[†]	n.s.
Water	15	-	n.s.

* n.s. means not significant

[†] The price was obtained from the ICIS public database of chemical prices.[18] Whenever the chemical had a price range, the average price was considered.

The E-factor for this process is of 0.03 kg waste.kg product⁻¹, obeying the criteria defined in eq. 6.1.

Knowing all the stream temperatures throughout the process and the needed heat of evaporation for the crystallizers, the utility costs could be obtained. Those details are included in Appendix E1. In Figure 6.3, the components contributing to the total cost with utilities are discriminated.

Dry air
4.95%

Total utility cost = 192 k$.year⁻¹

Electricity
21.35%

LP Steam
70.73%

Cooling water
2.97%
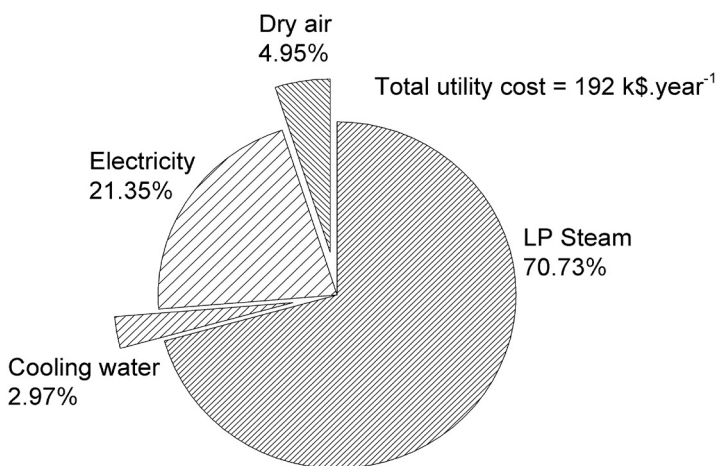
Figure 6.3 – Detailed utility costs used in scenario 1-1. All the costs specified are given as a percentage of the total value (192 k$.year⁻¹).

The cost of equipment capital investment is detailed in Table 6.5.

For the centrifugal pumps, a cost of 4.9 k$/unit was assumed. This corresponds to 1-stage centrifugal pump with a 2 inch discharge pipe diameter.[15] The cost of the liquid-liquid extraction column was obtained from correlations available in the literature.[16]

For the vacuum pumps associated with multi-effect evaporators and with the rotary filter, a cost of 12.9 k$/unit was considered. This corresponds to 1-stage liquid seal vacuum pump with a 500 cfm flow-rate.[15] The vacuum crystallizer cost was obtained from the following correlation:[19]

$$Cost = 8.16 \cdot V^{0.47} \tag{6.23}$$

Where *V* is the crystallizer volume in cubic foot.

Table 6.5 – Detailed costs for each equipment piece used in scenario 1-1.

Utility	Unitary cost (k$/unit)	# units	Total cost (k$)
Extraction column	27.4	1	27.4
Disk stack centrifuge	150	1	150
Distillation column 1	110.6	1	110.6
Distillation column 2	128.5	1	128.5
Condensers*	2.6	1	2.6
Holding tanks**	10	4	40
Rotary vacuum filter	116.5	1	116.5
Evaporative crystallizer	25	1	25
Tray dryer	23.8	1	23.8
Centrifugal pumps	4.9	11	54
Vacuum pump	12.9	3	38.7
Total cost			717
Fixed capital investment (Lang factor 4.8)			3440

* The contribution of each condenser to the total cost is given in Appendix D

** The cost per holding tank was taken as the cost of a 1 m³ vessel with agitation

6.3.1.2 Scenario 1-2

In the second proposed scenario, the *trans*-resveratrol present in the fermentation broth is continuously extracted using a reverse-phase column packed with XAD-16 resin. Two columns are used in order to render the downstream process continuous. While the clarified broth is being loaded into one column, the remaining column is performing the remaining cycle steps (washing, elution, regeneration and equilibration).
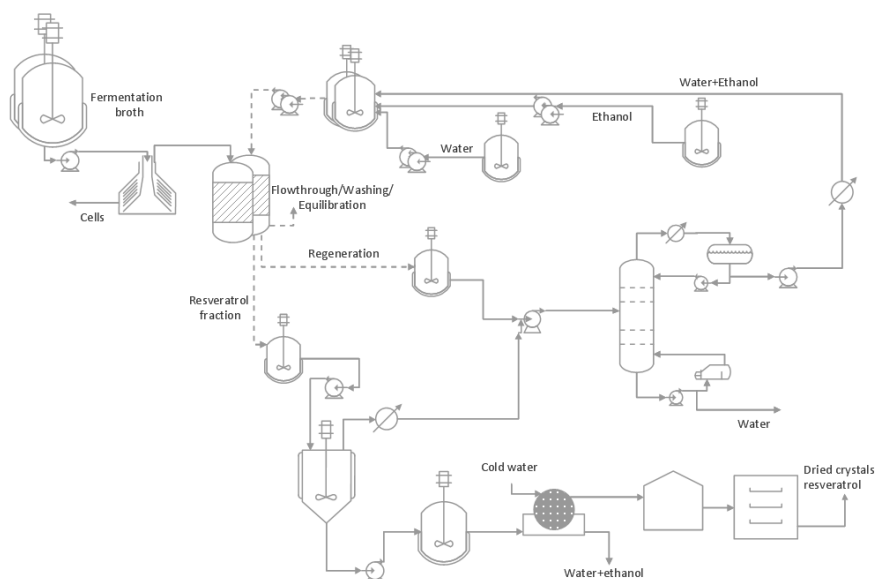
Figure 6.4 - Conceptual downstream process train for the recovery of *trans*-resveratrol from a typical *C. glutamicum* fermentation broth containing hydrophilic impurities. In these scenario, two adsorption columns loaded with XAD-16 resin are used to capture the desired polyphenol (which render the process continuously). After obtaining the product fraction which is then sent to a holding tank, the desired compound is crystallized, filtered, washed and dried to obtain the final formulation. The solvent used for the elution and regeneration steps (ethanol) is recovered by distillation and then recycled to the process.

As in scenario 1-1, the solvents used during the process (water and ethanol in this case) are recovered by distillation. However, as in this case ethanol and water do not form an azeotrope (at least in the concentration range of interest), only one distillation column is needed.

Having this taken into account, the required mass balances were performed using the detailed calculations indicated in Appendix D2 together with the flowsheet simulation package Aspen Plus.

The calculated needed raw materials are indicated in Table 6.6. For calculating the cost associated with the resin XAD-16, its unitary price was taken from published literature.[20] Its cost as a function of the quantity ordered was then obtained by the six-tenths rule.[14]

Table 6.6 - Quantity and cost of the different raw materials used in scenario 1-2.

Raw material	Quantity (ton.y^{-1})	Price (k\$.ton^{-1})	Total cost (k\$.y^{-1})
Water	750	-	n.s.
Ethanol	n.s.	1.14 [†]	n.s.
XAD-16 resin	0.54	1.9	1.0

* n.s. means not significant

[†] The price was obtained from the ICIS public database of chemical prices.[18] Whenever the chemical had a price range, the average price was considered.

This scenario has an E-Factor of approximately zero, when only taking ethanol into account. Thus, the criteria of E-factor lower than 1 kg.kg^{-1} product is met.

Again, the utility costs were calculated taking into account not only the previous calculations shown in this section, but the energy balances obtained from Aspen Plus (Appendix D). The discriminated utilities are shown in Figure 6.6.

6
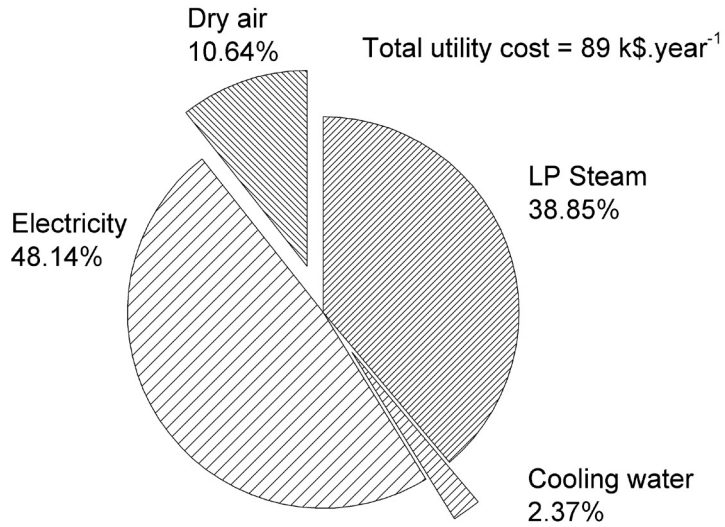
Figure 6.6 - Detailed utility costs used in scenario 1-2. All the costs specified are given as a percentage of the total value (89 k\$.year⁻¹).

The cost of the equipment is indicated in Table 6.7. Given that almost the same pieces of equipment are present here as in the previous scenario, the sources for the obtained values are not indicated.

6

Table 6.7 - Detailed costs for each equipment piece used in scenario 1-2.

Utility	Unitary cost (k$.unit⁻¹)	# units	Total cost (k$)
Adsorption column	49	2	100
Distillation column	111	1	111
Holding tanks**	10	6	60
Silo †	7	1	7
Condensers*	2.3	1	2.3
Disk stack centrifuge	150	1	150
Rotary vacuum filter	116.5	1	116.5
Evaporative crystallizer	35	1	35
Tray dryer	23.8	1	23.8
Centrifugal pumps	4.9	12	58.8
Vacuum pump	12.9	1	12.9
Total cost			677
Fixed capital investment (Lang factor 4.8)			3750

* The contribution of each condenser to the total cost is given in Appendix D

** The cost per holding tank was taken as the cost of a 1 m^3 vessel with agitation

† The cost per silo was taken as the cost of a 1 m^3 vessel without agitation

6.3.1.3 Scenario comparison for case-study

Having obtained all the associated costs with each downstream process strategy, both in terms of equipment cost and utilities, the different options can now be compared. As mentioned in the beginning of this study, the cost function used will sum the contribution of the CAPEX with 10 times the contribution of the OPEX, assuming the process to run for a period of 10 years. The E-factor is not directly took into account. However, since for every scenario its value is below 1 kg.kg product⁻¹ (the target set in the beginning), it will be assumed that its influence in the process cost will be absorbed in the CAPEX and OPEX.

To take into account the fact that each downstream process obtained a slightly different yield, it will be assumed that the CAPEX will be approximately the same, but that the OPEX depends linearly with the plant capacity. For that reason, the lower the yield, the higher the total OPEX. In the following equation, OPEX' is the "corrected" OPEX:

$$OPEX' = \frac{OPEX}{yield} \tag{6.24}$$

Thus, the formula present in eq. 6.1 becomes:

$$F_{cost} = CAPEX + 10 \cdot OPEX', \tag{6.25}$$
$$E - factor < 1 \; kg.kg^{-1} \; product$$

The scenario with a lower F_{cost} value is the one presenting a better option in terms of cost.

$$\tag{6.26}$$
$$Specific \; cost \; (\$/kg) = \frac{0.1 \; CAPEX + OPEX'}{n \cdot 3.8}$$

Where n is the number of produced polyphenols (1 for scenario 1 and 2 for scenario 2).

For the first case-scenario – the recovery of *trans*-resveratrol from the fermentation broth – two strategies were compared: liquid-liquid extraction using an organic solvent (ethyl acetate) and reverse-phase adsorption. In Figure 6.6, the CAPEX, OPEX and the E-factor are compared for the two proposed strategies.

6
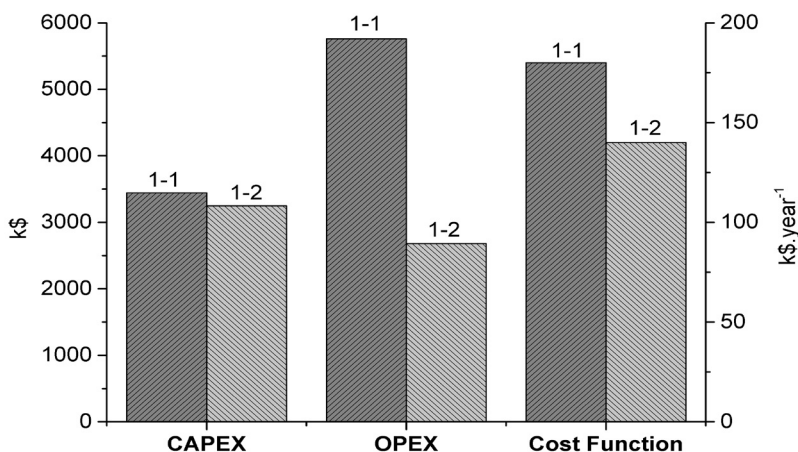
Figure 6.6 – Cost comparison between the different downstream process strategies studied for scenario 1. The OPEX should be read on the right axis and the CAPEX and Cost Function on the left axis.

For the recovery of *trans*-resveratrol, adsorption proved to be a better solution than liquid extraction. Regarding the fixed costs, one less distillation column is needed as no azeotrope has to be broken in the case of water/ethanol separation (at least, in the concentration range of interest). Concerning the cost with utilities, one of the biggest advantages of scenario 1-2 is that after adsorption, the polyphenolic stream (the eluate) is concentrated 11 times. The water that was removed in that step does not suffer further treatment by distillation. In the case LLE is used, the entire raffinate stream goes through a distillation column in order to recover the dissolved ethyl acetate.

Table 6.8 – Compilation of the OPEX and CAPEX values in each scenario addressing the first case-scenario. The cost function value is calculated according to eq.6. 41 and eq. 6.42.

Scenario	OPEX (k\$.y^{-1})	CAPEX (k\$)	Cost function value (k\$)	Specific cost (\$.kg product^{-1})
1-1	192	3440	5400	140
1-2	89	3250	4200	110

The scenario using adsorption also presents further advantages when compared to LLE. First of all, no toxic solvents are employed. Second, if the process is intended to be food-grade, ethanol and the XAD-16 resin already comply with FDA regulations. In the case of LLE, solvent selection is much more limited.

6.3.2 Hydrophobic polyphenol: *trans*-resveratrol and naringenin (2)

This section deals with recovery and purification of both *trans*-resveratrol and naringenin from a typical *C. glutamicum* fermentation broth. Three different strategies are tackled: liquid-liquid extraction using two coupled columns; reverse-phase adsorption using a functionalized resin (RENSA PY); preferential crystallization after a reverse-adsorption unit using the XAD-16 resin.

6.3.2.1 Scenario 2-1

In the first scenario, a similar strategy presented in the previous scenario 1-1 is used. However, in this case, given the significant hydrophobicity of both *trans*-resveratrol and naringenin a different approach has to be used. In this case, two coupled liquid-liquid extraction columns are used. In the first one, the more hydrophobic mixture of 0.2 molar ethyl acetate + heptane is used. This will make it possible to recover naringenin from the broth, while leaving *trans*-resveratrol and the remaining impurities in the

6

raffinate stream. This raffinate stream is then extracted with a more polar mixture of 0.6 molar ethyl acetate + heptane, which is now able to recover *trans*-resveratrol while leaving the undesired impurities behind.

Figure 6.7 - Conceptual downstream process train for the recovery and purification of two similar polyphenols (e.g., *trans*-resveratrol and naringenin) from a fermentation broth. The clarified stream goes through a first LLE step, where naringenin is preferentially extracted by a relatively hydrophobic stream (0.2 molar fraction ethyl acetate in heptane). Connected to it, there is another LLE step where *trans*-resveratrol, present in the "raffinate 1" stream is recovered by using a more polar solvent mixture (0.6 molar fraction ethyl acetate in heptane). After liquid extraction is complete, both compounds are crystallized, filtered, washed and dried to obtain the final formulation. The organic solvents are recovered by using distillation and then recycled to the different extraction columns.

6

After performing liquid-liquid extraction, both polyphenols are recovered in the solid form by evaporative crystallization. In this case, due to the preferential evaporation of ethyl acetate in comparison to heptane, supersaturation is created not only due to solvent volume reduction but also by the relative increasing amount of anti-solvent (heptane in this case).

The calculations involved in the mass balances are indicated in the Appendix D3. Those calculations, together with the flowsheet implementation in Aspen Plus, were used to obtain the process needed raw materials (Table 6.9).

Table 6.9 - Quantity and cost of the different raw materials used in scenario 2-1.

Raw material	Quantity (ton.y⁻¹)	Price (k$.ton⁻¹)	Total cost (k$.y⁻¹)
Heptane	0.038	0.55[†]	n.s.
Ethyl acetate	0.13	1.18[†]	n.s.

* n.s. means not significant

[†] The price was obtained from the ICIS public database of chemical prices.[18] Whenever the chemical had a price range, the average price was considered.

The E-factor for this process is of 0.03 kg waste.kg product⁻¹, meeting the criteria of E-factor $\leq$ 1 kg waste.kg product⁻¹.

The detailed costs of the utilities used in this process are indicated in Figure 6.8. The performed calculations are included in Appendix E3.

6

Figure 6.8 - Detailed utility costs used in scenario 2-1. All the costs specified are given as a percentage of the total value (154 k\$.year⁻¹).

The detailed costs involved in the equipment capital investment are indicated in Table 6.10. As previously, the cost of the liquid-liquid extraction columns was obtained from correlations available in the literature.[16]

6

Table 6.10 - Detailed costs for each equipment piece used in scenario 2-1.

Utility	Unitary cost (k$.unit⁻¹)	# units	Total cost (k$)
Extraction column	27.4	2	54.8
Distillation column 1	133	1	133
Distillation column 2	90	1	90
Holding tanks**	10	4	40
Silo†	7	2	14
Condensers*	2.9	1	2.9
Disk stack centrifuge	150	1	150
Rotary vacuum filter	116.5	1	116.5
Evaporative crystallizer 1	49	1	49
Evaporative crystallizer 2	81	1	81
Tray dryer	23.8	1	23.8
Centrifugal pumps	4.9	12	58.8
Vacuum pump	12.9	2	25.8
Total cost			840
Fixed capital investment (Lang factor 4.8)			4000

* The contribution of each condenser to the total cost is given in Appendix C

** The cost per holding tank was taken as the cost of a 1 m³ vessel with agitation

† The cost per silo was taken as the cost of a 1 m³ vessel without agitation

6.3.2.2 Scenario 2-2

In the second scenario, *trans*-resveratrol and naringenin are separated using a chromatography column containing a RENSA resin. As defined for scenario 1-2, two columns are used in order to provide a continuous loading step. Four holding tanks are used. One for collecting the 10% ethanol washing stream, the second for the 80% regeneration stream and the two others for receiving both the *trans*-resveratrol and the naringenin fractions coming

from the column. Those holding tanks allow that a continuous stream is sent to two different evaporative crystallizers (one for each polyphenol).
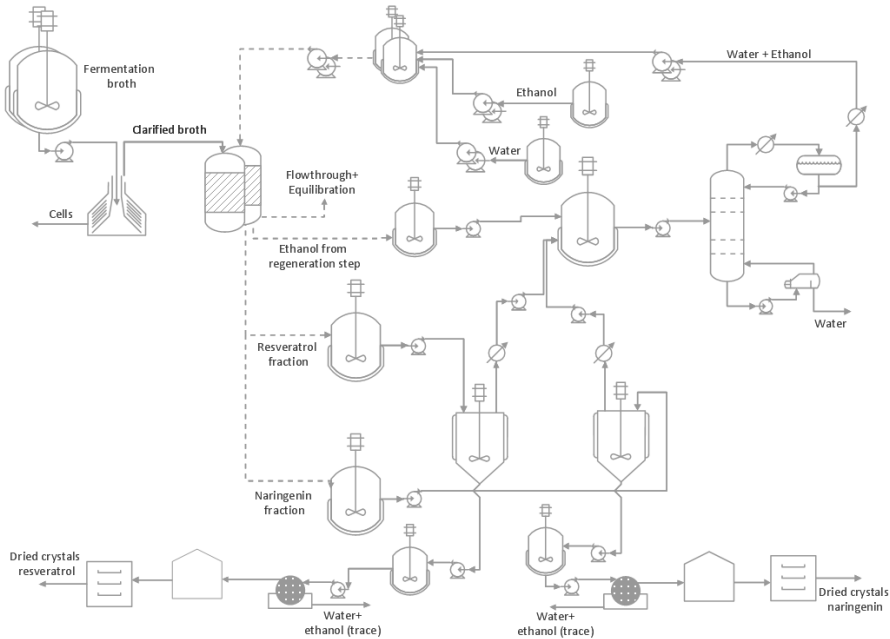
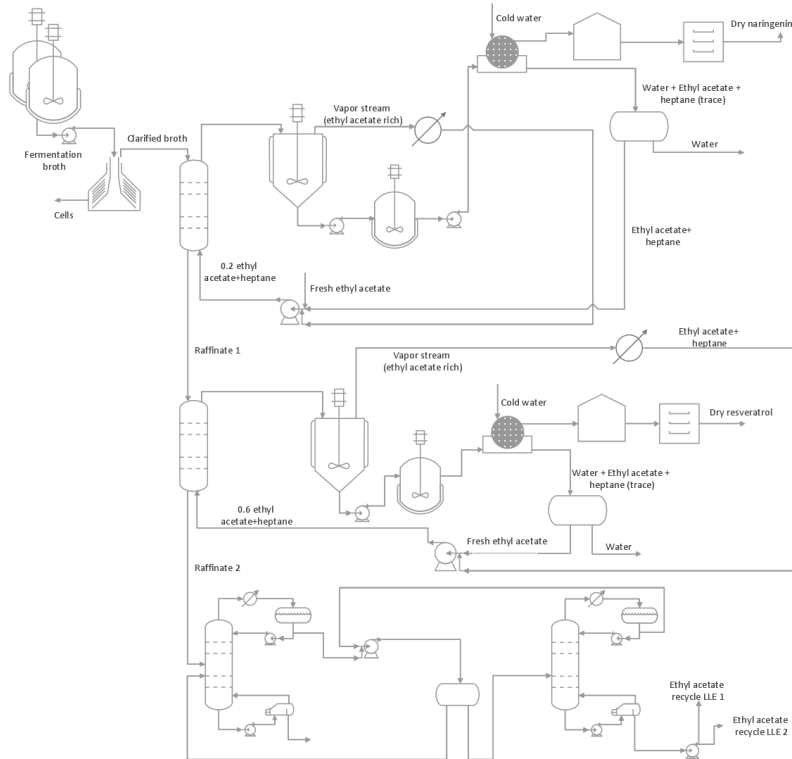**Figure 6.9 - Conceptual downstream process train for the recovery and purification of both *trans*-resveratrol and naringenin. In this scenario, the selective resin RENSA PY is used in each of the two adsorption columns used (which render the process continuously). After obtaining the two different pure fractions which are directed to holding tanks, the desired compounds are crystallized, filtered, washed and dried to obtain the final formulations. The solvent used for the washing, elution and regeneration steps (ethanol) is recovered by distillation and then recycled to the process.**

The streams coming from the holding tanks, and that have a significant ethanol content, are combined with the condensed vapor streams of the crystallizers and sent to a distillation column, where ethanol is recovered. As in all the previous cases, the detailed mass balance calculations are indicated in the appendix section (Appendix D4).

Due to the high degree of ethanol recovery, the required make-up stream of ethanol is greatly reduced, as indicated in Table 6.11.

For calculating the cost associated with the resin RENSA PY, its unitary price was taken from the supplier (Biotage) as 23 k$.kg^{-1} for 10 g. Its cost as a function of the quantity ordered was then obtained by the six-tenths rule.[14]

Table 6.11 - Quantity and cost of the different raw materials used in scenario 2-2

Raw material	Quantity (ton.y^{-1})	Price (k$.ton^{-1})	Total cost (k$.y^{-1})
Water	2700	-	n.s.
Ethanol	n.s.	1.14[†]	n.s.
RENSA PY resin	0.5	300	150

* n.s. means not significant

[†] The price was obtained from the ICIS public database of chemical prices.[18] Whenever the chemical had a price range, the average price was considered.

For this process, the E-factor is of 3.8 kg waste.kg product^{-1}, below the required criteria of 1 kg waste.kg product^{-1}.

The detailed calculation of the utility costs for this scenario are included in Appendix D. The discriminated costs are represented in Figure 6.10.
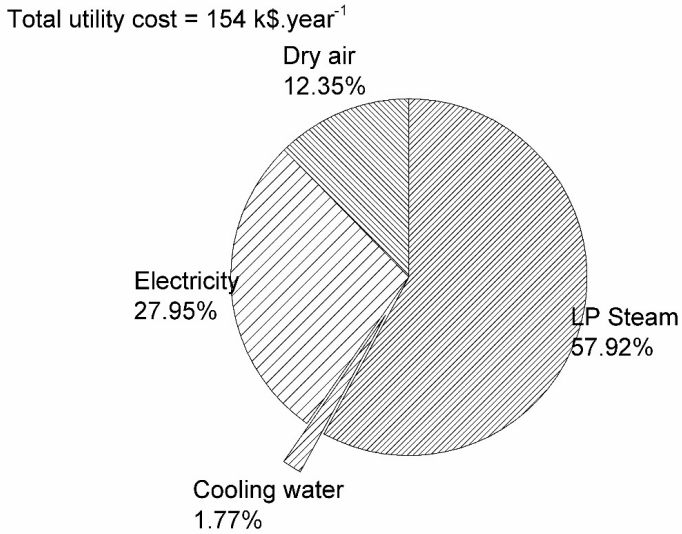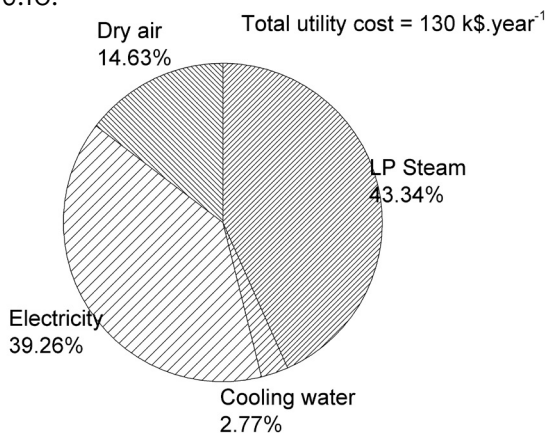

Figure 6.10 - Detailed utility costs used in scenario 2-2. All the costs specified are given as a percentage of the total value (130 k$.year^{-1}).

The total cost of equipment was calculated as mentioned in the previous section. The detailed costs are shown in Table 6.12.

Table 6.12 - Detailed costs for each equipment piece used in scenario 2-2.

Utility	Unitary cost (k\$.unit⁻¹)	# units	Total cost (k\$)
Adsorption column	49	2	100
Distillation column	112	1	112
Condensers*	5.1	1	5.1
Disk stack centrifuge	150	1	150
Holding tanks**	10	7	70
Silo†	7	2	14
Rotary vacuum filter	116.5	1	116.5
Evaporative crystallizer 1	17	1	17
Evaporative crystallizer 2	42	1	42
Tray dryer	23.8	1	23.8
Utility	Unitary cost (k\$.unit⁻¹)	# units	Total cost (k\$)
Centrifugal pumps	4.9	21	103
Vacuum pump	12.9	2	25.8
Total cost			780
Fixed capital investment (Lang factor of 4.8)			3750

* The contribution of each condenser to the total cost is given in Appendix D

** The cost per holding tank was taken as the cost of a 1 m³ vessel with agitation

† The cost per silo was taken as the cost of a 1 m³ vessel without agitation

6.3.2.2 Scenario 2-3

In the last scenario, preferential crystallization is applied to the purification of *trans*-resveratrol and naringenin. However, it is assumed that this technique can only be applied when the two polyphenols are relatively purified with respect to all the

remaining impurities in the fermentation broth. For that reason, a preliminary chromatography step is performed, using two XAD-16 resin packed columns (Figure 6.11).
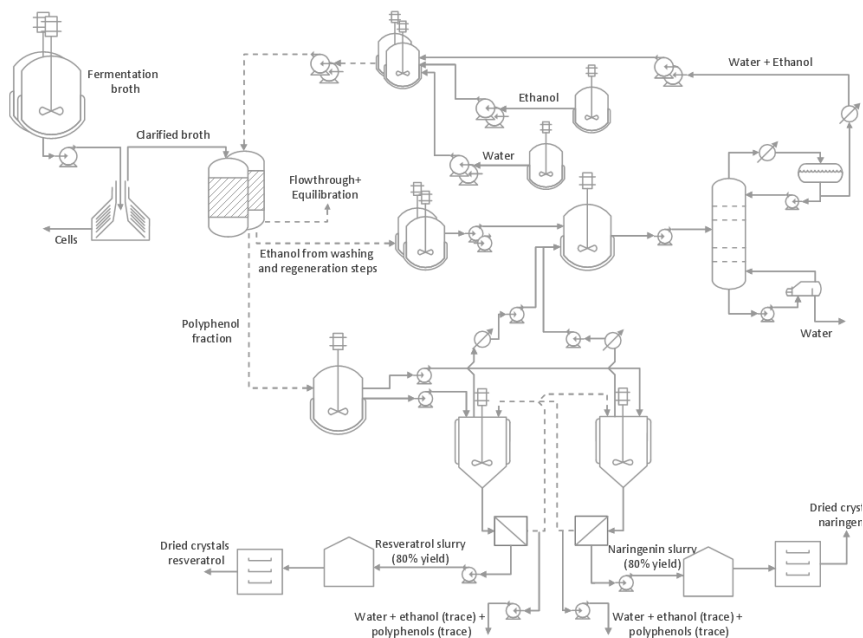
Figure 6.11 - Conceptual downstream process train for the recovery and purification of both *trans*-resveratrol and naringenin. In this scenario, the both polyphenols are purified from the remaining hydrophilic impurities using two columns loaded with XAD-16 resin (which render the process continuously). After obtaining the polyphenol fraction which is sent to a holding tanks, two separate stream are sent to two different crystallizers where each compound is preferentially crystallized. Afterwars, both polyphenols are filtered, washed and dried to obtain the final formulations. The solvent used for the washing, elution and regeneration steps (ethanol) is recovered by distillation and then recycled to the process.

The first chromatography step purifies the polyphenols (both *trans*-resveratrol and naringenin) from the rest of the broth components. The adsorption step is performed continuously,

by using two columns interchangeably. To have the preferential crystallization step running in continuous mode as well, and holding tank is used to collect the intermittent polyphenol fraction collected from the chromatography unit.

To be consistent with the previous scenarios, the crystallization step is taken to be an evaporative crystallization step. The ethanol evaporated from both crystallizers is condensed and combined with the ethanol that is used during the different chromatography steps, to be partially recovered by distillation (in order to minimize the solvent consumption). The detailed calculations involved in the different mass balances are indicated in the Appendix D5.

The cost of the raw materials used in this scenario are indicated in Table 6.13. The cost of the XAD-16 resin was taken from the literature as 23 $.kg^{-1}.[20] Similarly to what was performed for the RENSA PY resin, its cost as a function of the quantity ordered was obtained by the six-tenths rule.[14]

Table 6.13 - Quantity and cost of the different raw materials used in scenario 2-3.

Raw material	Quantity (ton.y^{-1})	Price (k$.ton^{-1})	Total cost (k$.y^{-1})
Water	4100	-	n.s.
Ethanol	n.s.	1.14[†]	n.s.
XAD-16 resin	0.5	1.9	0.95

* n.s. means not significant

[†] The price was obtained from the ICIS public database of chemical prices.[18] Whenever the chemical had a price range, the average price was considered.

For this process, the E-factor is of 3.8 kg waste.kg product^{-1}.

The detailed calculation of the utility costs for this scenario are included in Appendix D. The discriminated costs are represented in Figure 6.12.

6

Total utility cost = 195 k$.year^{-1}

Electricity
25.65%

LP Steam
59.93%

Dry air
9.75%

Cooling water
4.67%
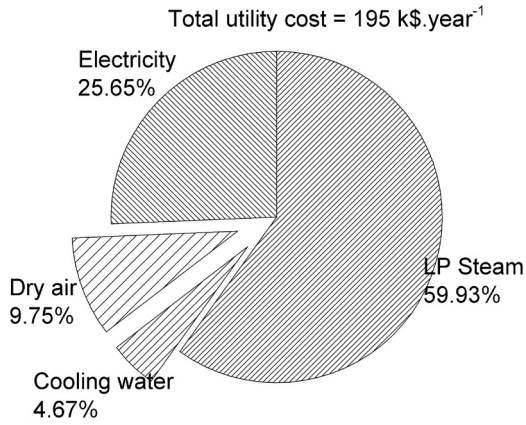
Figure 6.12 - Detailed utility costs used in scenario 2-3. All the costs specified are given as a percentage of the total value (195 k\$.year^{-1}).

The total discriminated equipment capital investment is indicated in Table 6.14.

Table 6.14 - Detailed costs for each equipment piece used in scenario 2-3.

Utility	Unitary cost (k\$.unit^{-1})	# units	Total cost (k\$)
Adsorption column	49	2	100
Distillation column	112	1	112
Disk stack centrifuge	150	1	150
Condensers*	23.3	1	23.3
Holding tanks**	10	7	70
Silo[†]	7	2	14
Rotary vacuum filter	116.5	1	116.5
Evaporative crystallizer 1	52	1	104
Evaporative crystallizer 2	47	1	47

6

Utility	Unitary cost (k$.unit⁻¹)	# units	Total cost (k$)
Tray dryer	23.8	1	23.8
Centrifugal pumps	4.5	22	99
Vacuum pump	12.9	2	25.8

Total cost	885
Fixed capital investment (Lang factor of 4.8)	4250

* The contribution of each condenser to the total cost is given in Appendix D

** The cost per holding tank was taken as the cost of a 1 m3 vessel with agitation

† The cost per silo was taken as the cost of a 1 m3 vessel without agitation

6.3.2.4 Scenario comparison for case-study 2

For the second case-scenario – the recovery and purification of both *trans*-resveratrol and naringenin from the fermentation broth – three strategies were compared: liquid-liquid extraction using an organic solvent mixture (heptane + ethyl acetate), reverse-phase adsorption with a selective resin (RENSA PY) and preferential crystallization after a preliminary adsorption step with the XAD-16 resin. In Figure 6.13, the CAPEX, OPEX and the E-factor are compared for the three proposed strategies.

6
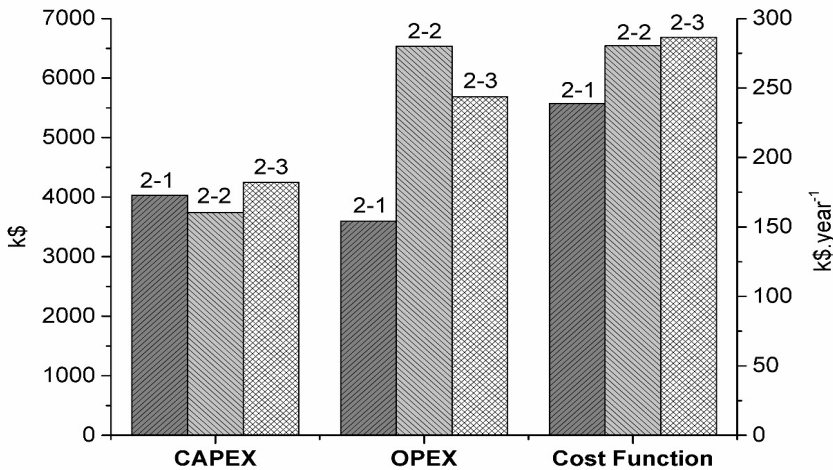
Figure 6.13 - Cost comparison between the different downstream process strategies studied for scenario 2. The OPEX should be read on the right axis and the CAPEX and Cost Function on the left axis.

One can observe that the CAPEX costs are almost similar in every scenario. However, it is again the operational costs that mostly contribute for the final cost function. It is interesting to note that, in this case, the scenario using LLE (2-1) became the cheapest one, presenting even lower costs than the previous scenario 1-1, which might look surprising. What happened in this case, is that by introducing heptane in the extraction, one is adding an anti-solvent which contributes to the crystallization of both *trans*-resveratrol and naringenin. By doing so, less steam is needed in the two crystallizers to recover both products in the solid phase.

6

Table 6.15 - Compilation of the OPEX and CAPEX values in each scenario addressing the second case-scenario. The cost function value is calculated according to eq. 6.24 and eq. 6.25.

Scenario	OPEX (k$.y^{-1})	OPEX' (k$.y^{-1})	CAPEX (k$)	Cost function value (k$)	Specific cost ($.kg product^{-1})
2-1	154	154	4000	5570	73
2-2	280	280	3750	6500	86
2-3	195	244	4250	6700	88

If scenario 2-2 could use the XAD-16 resin instead of the RENSA PY, that would be the optimal solution. However, in this case, the costs with the adsorbent dominate the operational costs (150 k$.y^{-1} are the annual costs associated with the resin). For that reason, this scenario became, along with the last 2-3 scenario, the most expensive options.

Scenario 2-3 is probably the one which shows largest potential to be improved. The biggest cause for the high cost associated with this option is due to the chromatography step. In this case, the stream containing the polyphenols was concentrated only 2.5 times after eluting. For that reason, a much larger aqueous stream had to be treated in the distillation column. Moreover, more heat was needed to evaporate the content of both evaporative crystallizers. Not only the stream is now more dilute, as the heat needed to evaporate water is much larger than the heat needed to vaporize either ethyl acetate or heptane (Table 6.16).

Table 6.16 - Vaporization enthalpies of the solvents used in this study.[21]

Solvent	$\Delta_{vap}H$ $(kJ.kg^{-1})$
Water	2260
Heptane	360
Ethyl acetate	400

Although the preliminary economic results indicate LLE as the cheapest option for scenario 2, other factors might play a role when selecting the most indicated scenario. First of all, the usage of an alkane like heptane might be restricted for food-grade

6

purposes (although listed as a Class 3 solvent according to the Q3C guidance). In that case, only scenarios 2-2 and 2-3 could be compared. If that would be the case, since 2-2 is constrained by the resin price, efforts could be directed in order to improve the costs associated with scenario 2-3. One of the possibilities might be eluting both polyphenols with a higher ethanol content. Less resolution is obtained, but the eluate stream would come more concentrated. Moreover, in the case the solubility curves of both polyphenols show a strong dependence on temperature, cooling crystallization could replace evaporative crystallization. This would immediately reduce operational costs by around 30%.

6.4 Conclusions

The goal of this chapter was to present, discuss and economically evaluate feasible downstream process alternatives for the recovery and purification of hydrophobic polyphenols from a fermentation broth. Two case-studies were introduced. In the first one, the goal was to recover and purify *trans*-resveratrol from hydrophilic impurities which are thought to be the main fermentation by-products (S1). In the second situation, naringenin and *trans*-resveratrol were to be separated and purified from a similar aqueous matrix (S2). Given the hydrophobicity of these compounds, three strategies were addressed: liquid-liquid extraction, reverse-phase adsorption (also considering functionalized resins) and crystallization.

The results obtained for S1 suggest that reverse-adsorption is the optimal scenario. Not only the usage of toxic solvents is avoided, as one less distillation column is needed and less steam is needed. For S2, liquid extraction was the cheapest option within the simulation conditions presented in this manuscript. The reason was that not only heptane could work as an anti-solvent in the crystallization of both polyphenols, as also ethyl acetate and heptane have lower vaporization enthalpies than water (present in large quantity in the other two scenarios). Using RP-adsorption in this case turned out to be too expensive, as the costs associated with the resin dominated the operational expenses. In the case of preferential crystallization, the bottleneck was the costs with energy. When using the XAD-16

6

resin, the collected fraction of both polyphenols was still too dilute. Owing to that, still a lot of steam was needed for the evaporative crystallization and for the distillation column. One of the possible options to lower its costs is to perform cooling crystallization instead, in case the solubility curves of both polyphenols show a significant dependency on temperature.

The main objective of this study was to obtain an order-of-magnitude estimation of the costs associated with the different DSP strategies and give valuable information that can assist in a preliminary design phase. Nonetheless, a more in-depth study of each alternative should be taken in order to have a more precise estimate of the associated costs. Aspects like process integration or heat integration were not considered. Moreover, the whole process was not optimized, but rather some individual unit operations like distillation or adsorption, in what may be called a greedy algorithm.

Of course not all polyphenols could be addressed in this study, as each one will have its own chemical characteristics and will claim for a slightly different purification approach. Despite that, we believe this work addresses some of the most complicated scenarios: when polyphenols are present in small concentrations in the liquid phase and when two similar ones might have to be purified from one another. In the case their titer increases, the DSP might even become simpler. In that situation, *in-situ* crystallization, for example, might be the logical strategy to use.

The findings presented in this work should give the reader a more tangible perspective of the benefits and disadvantages associated with the different DSP strategies shown. The results obtained, gave an overview of both fixed and operational costs associated with different DSP strategies which can guide future process design. This study also shown how the knowledge of polyphenol equilibrium properties can be used to solve the required mass and energy balances in Aspen Plus. Models developed in previous work, using the semi-predictive NRTL-SAC model to describe liquid-liquid partition or solubility or an exponential model describing how the adsorption isotherm initial slope varies with the concentration of modifier, can be extended to similar molecules and similar adsorbents.

6

The developed process selection methodology and the results obtained can be of value not only for a polyphenol focused process design, but may also be extended and applied to other similar molecules and produced by fermentation.

LIST OF SYMBOLS

Symbol	Description	Units
C_i	Concentration of component *i* in the liquid phase	$mg.L^{-1}$
x_i	Molar fraction of component *i* in the liquid phase	–
ϕ	Phase ratio	–
q_{i*}	Concentration of component *i* in the adsorbent	$mg.g\ resin^{-1}$
q_i	Equilibrium concentration of component *i* in the adsorbent	$mg.g\ resin^{-1}$
u	Linear velocity	$m.h^{-1}$
D_L	Axial dispersion coefficient	$m.s^{-2}$
z	Column height variable	m
H	Total column height	m
d_p	Resin particle diameter	m
ε	Column external porosity	–
ε_T	Column total porosity	–
k_m	Mass transfer coefficient	$m.s^{-1}$
C_{mod}	Modifier concentration in the liquid phase	$g.L^{-1}$
α_i	Coefficient for the	–
γ_i		–
C_i^{org}	Concentration of component *i* in an organic phase	$g.L^{-1}$
C_i^{aq}	Concentration of component *i* in an aqueous phase	$g.L^{-1}$
γ_i^{org}	Activity coefficient of component *i* in an organic phase	–
γ_i^{aq}	Activity coefficient of component *i* in an aqueous phase	–
$\log P$	Logarithm of the volumetric partition coefficient	–

$\log D$	Logarithm of the volumetric partition coefficient, dependent on the pH	−
ΔH_m	Melting enthalpy	$J.kg^{-1}$
T_m	Melting temperature	K
R	Universal gas constant	$J.K^{-1}.mol^{-1}$
U	Overall heat transfer coefficient	$m^{-2}.K^{-1}$
$v_R N_r$	Flow rate of filtrate	$m^3.s^{-1}$
A_D	Total area of the drum filter	m^2
Ψ_a	Air suction area fraction of drum filter	−
Ψ_f	Filtration area fraction of drum filter	−
Δp	Pressure difference	Pa
α	Cake specific resistance	$m.kg^{-1}$
ω	Solids concentration of stream entering the drum filter	$kg.m^{-3}$
μ	Viscosity	$Pa.s$
α/β'	Ratio of specific cake resistance in water and specific cake resistance in air	−
k	Air specific heat ratio (C_p / C_v)	−
ΔH_w^{vap}	Water vaporization enthalpy	$J.kg^{-1}$
m_v	Mass of vapor	kg
m_c	Mass rate of crystals formed	$kg.h^{-1}$
h	Convective heat transfer coefficient	$W.m^{-2}.K^{-1}$
T_d	Air dry bulb temperature	K
T_w	Air wet bulb temperature	K
G	Specific gas stream flow rate	$kg.m^{-2}.h^{-1}$
F_{cost}	Cost Function	−

List of abbreviations

Abbreviation	Description
DSP	Downstream process
LLE	Liquid-liquid equilibrium
VLE	Vapor-liquid equilibrium
OPEX	Operational expenditures
CAPEX	Capital expenditures
PC	Preferential crystallization
NRTL-SAC	Nonrandom Two-Liquid Segment Activity Coefficient
RPA	Reverse phase adsorption
USD	U.S. Dollar

Acknowledgements

Appendix C

C1. NRTL-SAC PARAMETERS FOR THE POLYPHENOLS USED IN THIS WORK

For calculation liquid-liquid partition coefficients and the solubility of *trans*-resveratrol and naringenin in heptane and ethyl acetate, the parameters indicated in Table C1.1 were used.

Table C1.1 – NRTL-SAC molecular descriptors and melting properties of the polyphenols considered in this work. These values were taken from chapter 2 of this thesis.

Molecule	X	Y^-	Y^+	Z	T_m (K)	H_m $(kJ \ mol^{-1})$
trans-resveratrol	0.427	1.768	3.057	0.000	541.3	30.6
p-coumaric acid	0.545	1.777	1.871	0.75	494.35	34.3
Naringenin	0.674	1.271	1.53	0.000	523.15	39.8

The parameters of the needed solvents were obtained from the literature.[22]

C2. PARAMETERS FOR THE DESCRIPTION OF ADSORPTION EQUILIBRIUM

For the XAD-16 resin, the capacity varies with the ethanol percentage. Since there is no model describing how that saturation capacity varies with the ethanol content, an empirical model is used. In this case, a logistic function will be used:

$$q_{max} = q_{max,0} + \frac{(q_{max,\infty} - q_{max,0})}{1 + e^{-k(c_{EtOH} - c_0)}} \tag{C.1}$$

The value $q_{max,\infty}$ is the saturation capacity when the ethanol volumetric percentage tends to 100%. Since the isotherms tend to be linear as the ethanol content increases, a randomly large value is defined for its value. The value $q_{max,\infty}$ is the saturation capacity when pure water is used. The parameters k and C_0 define where the logistic curve is centered and how rapidly the function attains $q_{max,\infty}$.

Table C2.1 – Parameters used for describing how the Langmuir isotherm parameters of the considered polyphenols vary with the modifier concentration. These values were applied to the simulations that used the XAD-16 resin.

Compound	$q_{max,0}$ (mg.g^{-1})	$q_{max,\infty}$ (mg.g^{-1})	k	C_0 (%v.v^{-1})	α	γ
trans-resveratrol	19.9	120	1.37	12.4459	9.9	-0.1786
p-coumaric acid*	-	-	-	-	0.01	-0.23
naringenin	18.8763	119	1.473	4.9075	13	-0.1882

For the RENSA PY, $q_{max,\infty}$ is constant.

Table C2.2 - Parameters used for describing how the Langmuir isotherm parameters of the considered polyphenols vary with the modifier concentration. These values were applied to the simulations that used the RENSA PY resin.

Compound	q_{max} (mg.g^{-1})	α	γ
trans-resveratrol	58	23	-0.197
naringenin	38	146	-0.18

APPENDIX D

D1. CALCULATIONS SCENARIO 1-1

According to the data available on the literature, the solubility of *trans*-resveratrol in ethyl acetate at 45°C is of 60.9 g.L^{-1}.[23]

The flow-rate of the stream coming out of the second evaporative crystallizer is of 3 L.h^{-1} and carries 380 g.h^{-1} of *trans*-resveratrol (obtained from Aspen Plus simulation), but the desired polyphenol is still dissolved. After the third evaporation, where the outlet stream has a flow-rate of 0.3 L.h^{-1}, the mass rate of crystals formed is calculated:

$$m_c = 380 \ g \cdot h^{-1} - 60.9 \ g \cdot L^{-1} \cdot 0.3 \ L \cdot h^{-1} = 362 \ g \cdot h^{-1} \qquad \text{(D1.1)}$$

This means a yield of 95% is obtained. The crystal slurry comes with a concentration of 889 kg crystals.m^{-3}.

The residence time inside the crystallizers is set to be 8 hours. Thus, for the first tank, which has an output of 45 L.h^{-1}, it corresponds to the following vessel volume (20% oversizing):

$$V = 1.2 \cdot 45 \frac{L}{h} \cdot 8h = 430 \ L \qquad \text{(D1.2)}$$

For calculating the crystallization tank cost, the price of a tank under vacuum was considered. The remaining crystallizers, having ten and hundred times less capacity than the first evaporator, were ignored for the purpose of the economical calculations.

After coming out of the crystallizers, the crystal slurry needs to be filtered and washed. By using eq. 17, it is calculated that at 0.33 rpm and a P of 12 kPa, approximately 276 kg.h^{-1} of dry cake can be

treated in a 1 m² rotary vacuum filter. Since this capacity is much more than what is needed (only 0.38 kg.h⁻¹ are needed), the slurry will be stored in a holding tank and the filtration will be performed once every month, during one hour. That will correspond to the desired average solid flow rate of 3 ton.y⁻¹:

$$F_c = \frac{276 \cdot 11}{1000} = 3 \; ton.\, y^{-1}$$

(D1.3)

The cold wash water flow rate is set as five times the mass of *trans*-resveratrol crystals, which is equivalent to an average of 1.9 kg water.h⁻¹.

For the holding tank capacity calculation, the slurry for 1 month (720 hours) at a rate of 0.3 L.h⁻¹, thus the needed tank volume is:

(D1.4)

$$F_c = \frac{276 \cdot 11}{1000} = 3 \; ton.\, y^{-1}$$

The power consumption of the vacuum pump in the rotary filter is obtained by applying eq. 6.19. Since the air flow rate at 66.3 kPa would be approximately 1 m³.h⁻¹, this makes the vacuum pump power consumption be lower than 1 kW. For that reason, this consumption was disregarded for the calculation of electricity costs.

According to the previous calculations, the tray dryer will have to cope with a mass of 276 kg dry crystals or 345 kg wet crystals every month, assuming they contain 20% moisture. For the tray dryer it is going to be assumed a loading of 45 kg.m⁻².[24] In this case, 8 m² of drying area are needed.

The mass of water to evaporate is given by:

$$0.2 \, V + 0.3 \, t_{load} = 0.8 \, V \Leftrightarrow V = 0.36 \; m^3$$

(D1.5)

Tray dimensions will be taken as 40.6 cm (length) x 81.3 (width) x 3.2 cm (height) (http://www.wintechpharmachem.com/tray-dryer-ovens.html). The tray area is then 0.33 m². 24 trays are used, giving the total desired area of 8 m².

$$m_v = 345 \cdot (0.2 - 0.01) = 66 \, kg \qquad \text{(D1.6)}$$

The cross section area in each tray is of 0.026 m². For 24 trays, a total cross section area of 0.6 m² is obtained. Thus, the total air flow-rate can be calculated:

$$t_c = \frac{(66/24) \cdot 2413 \cdot 1000}{43 \cdot (80 - 40) \cdot 0.33} = 3.2 \, h \qquad \text{(D1.7)}$$

Knowing that air enters at 1 atm and 80°C, this corresponds to 1.9 Nm³.s⁻¹ or 22000 Nm³.cycle⁻¹. The total year consumption is 11 times the obtained value, or 241 000 Nm³.y⁻¹.

The cost of the tray dryer with 8 m² (86 ft²) is of 17.2 k$.[15]

While the crystals of *trans*-resveratrol are filtered, washed and dried, the ethyl acetate present in the extract and raffinate streams of the liquid-liquid extraction column are sent to two separate distillation columns. These columns are able to separate water from ethyl acetate by an azeotropic distillation method.

D2. CALCULATIONS SCENARIO 1-2

For sizing the adsorption columns, a maximum pressure drop of 2 bar was defined. Usually, these type of columns are also sized taking into account the needed mass of compound that needs to be adsorbed. However, since in this case two columns are being used continuously, this criteria is not useful. If a taller column is defined, more resin is needed, but less cycles are performed. If the column is shorter, the opposite occurs.

For the purpose of these preliminary calculations, a loading time of 55 minutes was defined and both column dimensions could be obtained assuming that a 10% maximum breakthrough was acceptable.

The sized columns have a diameter of 0.195 m and a height of 1 m. Given that the feed flow rate is of 3.8 $m^3.h^{-1}$, the pressure drop was calculated using the Carman-Kozeny equation:

$$\Delta p = 150 \cdot \frac{H \cdot \mu \cdot u \cdot (1 - \varepsilon)^2}{d_p^2 \cdot \varepsilon^3} \qquad (D2.1)$$

In this equation, Δp is the pressure drop, H the column height, μ the viscosity of the mobile phase (taken as the one of water), u the linear velocity, d_p the particle diameter and ε the column external porosity. The obtained pressure drop was of 1.2 bar, which is lower than the imposed limit of 2 bar.

The steps involved in each column cycle are indicated in Table D2.1:

Table D2.1 – Description of each chromatographic cycle performed in each column belonging to scenario 1-2. Because the loading time is the bottleneck, it is possible to use two adsorption columns in order to run the downstream process continuously.

Step	Flow rate (m³.h⁻¹)	Time (min)	% EtOH (v.v⁻¹)
Loading	3.8	55	0
Washing	3.8	2.5	0
Elution	3.8	5	50
Regeneration	3.8	5	80
Equilibration	3.8	5	0

Given the time taken by each step, the two different holding tanks can be sized:

Table D2.2 - Design details of the holding tanks used after the adsorption columns. represents the period of time during which the tank is receiving content and is the time the tank is discharging while not receiving any incoming stream.

Step	(min)	(min)	(m³.h⁻¹)	(m³.h⁻¹)	(m³)
Regeneration	5	110	3.8	0.173	0.53
Elution	5	110	3.8	0.173	0.53

After loading the column, a washing step is performed with pure water (pH 7.0) which leads to the desorption of *p*-coumaric acid. The adsorbed *trans*-resveratrol is then eluted with a step of 50% ethanol. The column is regenerated with 80% ethanol and equilibrated afterwards with water. The predicted chromatogram is depicted in Figure D2.1.
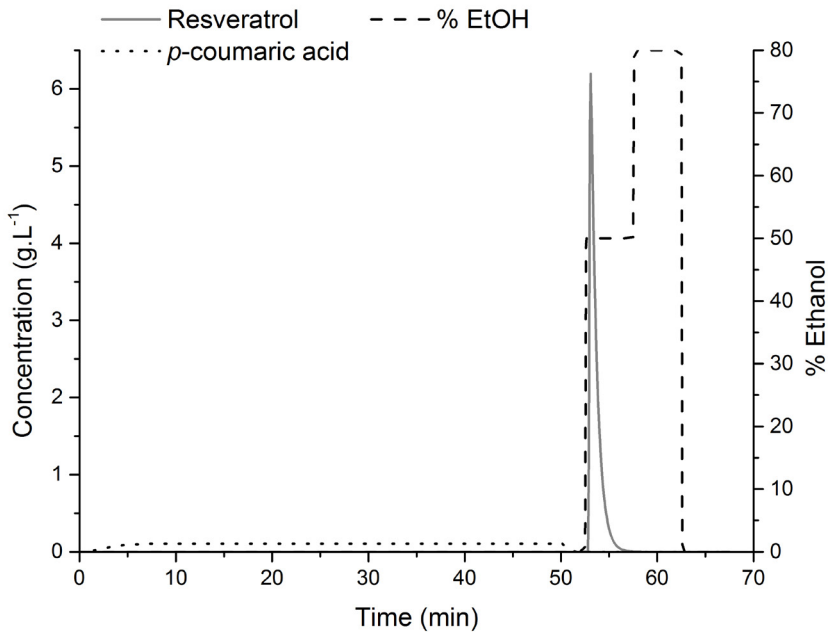
Figure D2.1 – Chromatogram obtained for the separation of *trans*-resveratrol from the remaining hydrophilic impurities (*p*-coumaric acid is expected to be the most similar to *trans*-resveratrol). After loading, a washing step with pure water is applied in order to remove *p*-coumaric acid. A elution step of 50% ethanol is used to elute *trans*-resveratrol from the column. Afterwards, a regeneration step with 80% ethanol is applied and the column is then equilibrated with pure water.

For the calculation of the adsorption column cost, the following equation was used:[25]

$$C_{col} = 8.57(V)^{0.77} = 8.57(0.03 \times 10^6)^{0.77} = 23.9 \ k\$ \qquad \text{(D2.2)}$$

Since the cost of the peripherals is taken to be 25 k\$,[25] the total cost per column is of 48.9 k\$.

Given that each column is used every 110 minutes, this means that each column performs 4320 cycles each year. Assuming that the packing is replaced every 300 cycles, this means that they are replaced 15 times each year. This corresponds to a XAD-16 resin quantity of 540 kg.y⁻¹.

After eluting *trans*-resveratrol with 50% ethanol, it is concentrated 11 times (the elution volume is 11 times smaller than the loading volume). Thus, *trans*-resveratrol comes out of the column with a concentration of:

$$C = 11 \cdot 0.38 = 4.2 \ kg.m^{-3}$$

(D2.3)

Knowing that the solubility of *trans*-resveratrol in 50% ethanol (0.24 molar fraction ethanol) is approximately 24 g.L⁻¹ (value was interpolated from available data in the literature[26]), it is present in the eluate fraction still below the solubility limit.

As indicated in Figure 6.4, after every elution step, the eluate is collected in a holding tank which then is able to continuously feed the crystallization unit. In this case, the stream coming out of the holding tank has a flow rate of 173 L.h⁻¹. This stream is then fed to an evaporative crystallizer, whose vapor fraction is set at 55% of the initial volume. Since ethanol partitions to the vapor phase, this will cause the final liquid stream to have a 0.05 molar fraction of ethanol (obtained by Aspen Plus). The solubility of *trans*-resveratrol in such a stream is of 1 g.L⁻¹ (value was interpolated from available data in the literature[26]). By mass balance, it is then possible to calculate the amount of polyphenol remaining in solution.

$$4.2 \frac{kg}{m^3} \cdot 0.173 \frac{m^3}{h} - \frac{1kg}{m^3} \cdot 0.063 \ m^3/h = 0.66 \ kg/h$$

(D2.4)

The recovery yield is then calculated to be:

$$100 \cdot \frac{0.66\ kg/h}{4.2\ kg/m^3 \cdot 0.173\ m^3/h} = 92\% \qquad \text{(D2.5)}$$

The obtained slurry has a solids concentration of 10.5 kg crystals.m^{-3}.

For sizing the crystallizer, a residence time of 8 hours was assumed as mentioned in the previous scenario.

This slurry needs to be filtered and washed in a rotary vacuum filter. By using eq. 6.17, it is calculated that at 2 rpm and a P of 60 kPa, approximately 68 kg.h^{-1} of dry cake can be treated in a 1 m^2 filter. Similarly to what was observed before, the vacuum pump needed for the filter operation would need such a lower power input, that its cost was disregarded for this economic analysis.

If the rotary vacuum filter is run every week, the annual production of 3 ton.y^{-1} is attained. Thus, as in the previous scenario, a holding tank is used to collect the crystal slurry which is going to be filtered once per week. The holding tank receives the slurry for 7 days (168 hours) at a rate of 0.063 m^3.h^{-1}, thus the needed tank volume is:

$$0.2\ V + 0.063\ t_{load} = 0.8\ V \Leftrightarrow V = 18\ m^3 \qquad \text{(D2.6)}$$

The dryer is again operated every month, as shown in scenario 1-1. Thus, the same equations used for sizing apply. The silo that holds the dry crystals needs to hold 270 kg. Assuming a porosity of 0.4 and that the tank is at 80% of its maximum capacity, a 500 L silo is needed:

$$0.8 \cdot (1 - 0.4) \cdot V = \frac{270\ kg}{1\ kg.L^{-1}} \Leftrightarrow V = 570\ L \qquad \text{(D2.7)}$$

D3. Calculations scenario 2-1

In the first crystallizer (crystallizing naringenin), the vapor fraction is of 45% of the initial volume (data obtained from Aspen Plus), leading to a 95% recovery and a slurry of 0.917 kg.m⁻³:

$$m_c = 372 \ g \cdot h^{-1} - 0.0477 \ g \cdot L^{-1} \cdot 386 \ L \cdot h^{-1} = 354 \ g \cdot h^{-1} \quad \text{(D3.1)}$$

The solvent consists of 0.88 molar fraction of heptane in ethyl acetate (data obtained from Aspen Plus).

In the second crystallizer (crystallizing *trans*-resveratrol) the vapor fraction is of 82% of the initial volume, leading to a 92% recovery and a slurry of 2.65 kg.m⁻³:

$$m_c = 376 \ g \cdot h^{-1} - 0.241 \ g \cdot L^{-1} \cdot 130 \ L \cdot h^{-1} = 345 \ g \cdot h^{-1} \quad \text{(D3.2)}$$

The solvent consists of 0.51 molar fraction of heptane in ethyl acetate.

By using eq. 6.17, the first rotary vacuum filter is run at 3 rpm and a ΔP of 80 kPa. The second rotary filter is run at 1.5 rpm and a ΔP of 55 kPa. In this way, if one 1m² unit is run each week for 1 hour, the annual capacity of 3 ton.y⁻¹ can be met for both cases. Thus, as in the previous scenario, a holding tank is used to collect the crystal slurry which is going to be filtered once per week.

One holding tank receives the slurry for 7 days (168 hours) at a rate of 0.386 m³.h⁻¹ and the second one at a rate of 0.130 m³.h⁻¹. Thus, one tank needs to have a volume of 110 m³ and the other one of 40 m³.

Both dryers will operate once per month, as mentioned previously. Thus, their volume will be of 570 L as well (they have to store the same amount of crystals).

As in the previous scenarios, the distillation columns are optimized (in terms of reflux ratio and distillate rate) to minimize solvent consumption (heptane and ethyl acetate in this case).

D4. Calculations scenario 2-2

For sizing the adsorption columns the same criteria as previously defined are used. The dimensions are fixed by defining a maximum pressure drop (2 bar) and a loading time until 10% breakthrough occurs (60 min). The sized columns have a diameter of 0.4 m and a height of 0.24 m. Given that the feed flow rate is of 3800 kg.h^{-1}, the pressure drop is calculated to be 1.7 bar (eq. D2.1).

Using eq. D2.2, the column cost, including peripherals, was calculated to be 49 k\$.unit^{-1}.

Since the columns are used every 120 minutes, they end up performing 3960 cycles.year^{-1}. Assuming the packing to be replaced every 300 cycles, 14 replacements will be needed per year. Since each column has 0.03 m^3 of volume, 500 kg of resin will be needed every year.

In Table D4.1, the steps performed in every adsorption cycle are indicated.

Table D4.1 - Description of each chromatographic cycle performed in each column belonging to scenario 2-2. Because the loading time is the bottleneck, it is possible to use two adsorption columns in order to run the downstream process continuously.

Step	Flow rate (m^3.h^{-1})	Time (min)	% EtOH (v.v^{-1})
Loading	3.8	60	-
Washing	3.8	5	10
Elution resveratrol	3.8	6	28
Elution naringenin	3.8	4	58
Regeneration	3.8	10	80
Equilibration	3.8	10	0

Given the time taken by each step, the four different holding tanks can be sized:

Table D4.2 - Design details of the holding tanks used after the adsorption columns. represents the period of time during which the tank is receiving content and is the time the tank is discharging while not receiving any incoming stream.

Step	(min)	(min)	(m³.h⁻¹)	(m³.h⁻¹)	(m³)
Washing	5	120	3.8	0.158	0.53
Regeneration	10	120	3.8	0.317	1.06
Elution resveratrol	6	120	3.8	0.190	0.67
Elution naringenin	4	120	3.8	0.126	0.42
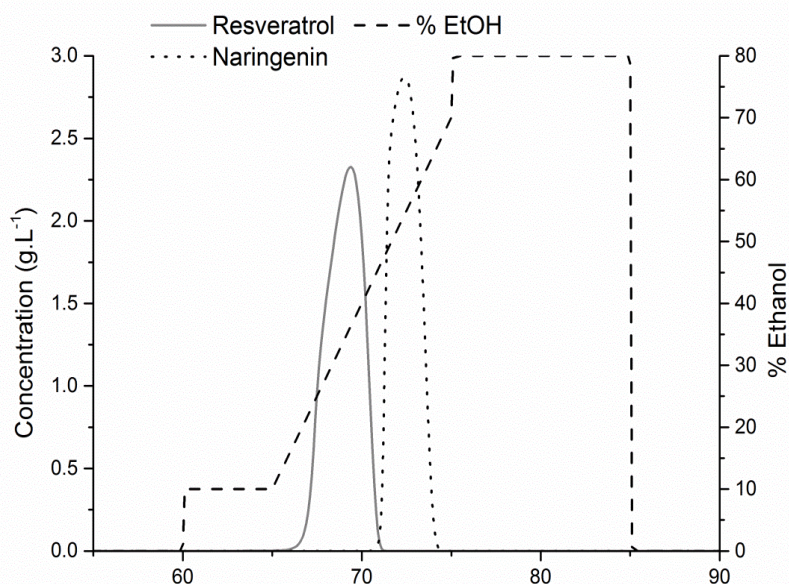
Figure D4.1 - Chromatogram obtained for the separation of *trans*-resveratrol from naringenin (assumed to be the most difficult separation). After loading, a washing step with 10% ethanol is applied in order to remove weakly bound impurities (e.g., *p*-coumaric acid). A gradient from 10 to 70% ethanol is applied to elute and resolve both *trans*-resveratrol and naringenin. Afterwards, a regeneration step with 80% ethanol is applied and the column is then equilibrated with pure water.

Coming out of the first fraction pool, *trans*-resveratrol is concentrated 10 times (to 3.8 g.L⁻¹). Naringenin is concentrated 15 times to 5.7 g.L⁻¹.

In the first crystallizer (crystallizing naringenin), the vapor fraction is of 85% of the initial volume, leading to a 94% recovery and a slurry of 25.6 kg.m⁻³:

$$m_c = 380\ g \cdot h^{-1} - 1.58\ g \cdot L^{-1} \cdot 14\ L \cdot h^{-1} = 358\ g \cdot h^{-1} \quad \text{(D4.1)}$$

The solvent consists of 0.037 molar fraction of ethanol in water.

In the second crystallizer (crystallizing *trans*-resveratrol) the vapor fraction is of 45% of the initial volume, leading to a 91% recovery and a slurry of 3.72 kg.m⁻³:

$$m_c = 380\ g \cdot h^{-1} - 0.370\ g \cdot L^{-1} \cdot 93\ L \cdot h^{-1} = 346\ g \cdot h^{-1} \quad \text{(D4.2)}$$

The solvent consists of 0.014 molar fraction of ethanol in water.

By using eq. 6.17, the first rotary vacuum filter is run at 3 rpm and a ΔP of 80 kPa. The second rotary filter is run at 1.5 rpm and a P of 55 kPa. In this way, if one 1m² unit is run each week for 1 hour, the annual capacity of 3 ton.y⁻¹ can be met for both cases. Thus, as in the previous scenario, a holding tank is used to collect the crystal slurry which is going to be filtered once per week.

One holding tank receives the slurry for 7 days (168 hours) at a rate of 0.386 m³.h⁻¹ and the second one at a rate of 0.130 m³.h⁻¹. Thus, one tank needs to have a volume of 110 m³ and the other one of 40 m³.

Both dryers will operate once per month, as mentioned previously. Thus, their volume will be of 570 L as well (they have to store the same amount of crystals).

D5. Calculations scenario 2-3

Each column is set to have a length of 1 m and a diameter of 0.195 m. Thus, the pressure drop is calculated to be 1.2 bar.

The description of each chromatographic cycle is shown in Table D5.1. An ethanol gradient from 20 to 70% ethanol was applied for 8 minutes in order to increase peak resolution. However, although the imposed conditions are expected to purify both polyphenols from the remaining hydrophilic impurities (e.g., sugars, proteins), they do not seem to be able to resolve the two peaks. Nonetheless, it was decided to keep the gradient as it is possibly the selected elution mode in an actual chromatographic separation.

Table D5.1 - Description of each chromatographic cycle performed in each column belonging to scenario 2-3. Because the loading time is the bottleneck, it is possible to use two adsorption columns in order to run the downstream process continuously.

Step	Flow rate ($m^3.h^{-1}$)	Time (min)	% EtOH ($v.v^{-1}$)
Loading	3.8	20	-
Washing	3.8	2.5	20
Elution	3.8	8	42.5
Regeneration	3.8	2.5	80
Equilibration	3.8	5	0

The predicted chromatogram is shown in Figure D5.1.
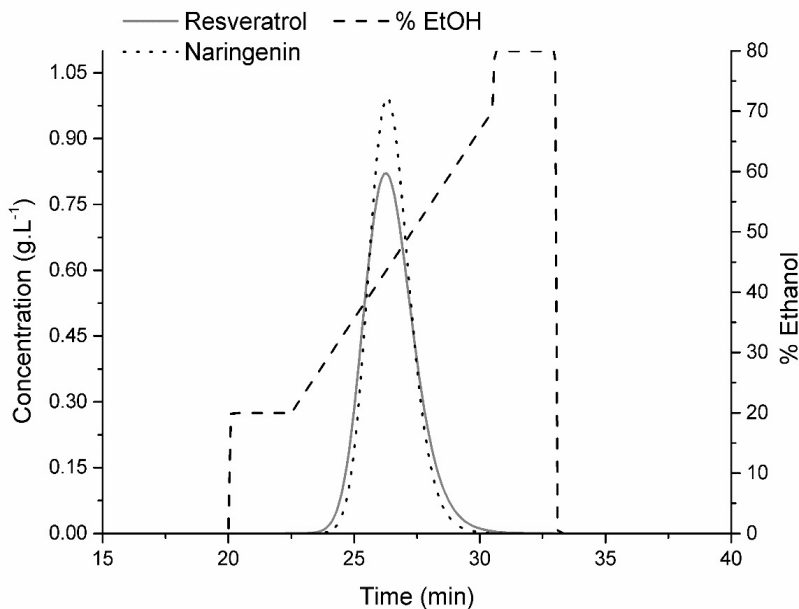
Figure D5.1 - Chromatogram obtained for the separation of *trans*-resveratrol from naringenin (assumed to be the most difficult separation). After loading, a washing step with 20% ethanol is applied in order to remove weakly bound impurities (e.g., *p*-coumaric acid). A gradient from 20 to 70% ethanol is applied to elute and try to resolve both *trans*-resveratrol and naringenin. Afterwards, a regeneration step with 80% ethanol is applied and the column is then equilibrated with pure water. Although the two polyphenols are not resolved, it is expected that most of the hydrophilic impurities are removed during the washing step.

In this scenario, since no purification could be obtained between *trans*-resveratrol and naringenin, the total elution fraction was collected in a holding tank. Given the time taken by each cycle step, the three different holding tanks were sized as indicated in Table D5.2.

Table D5.2 – Design details of the holding tanks used after the adsorption columns. represents the period of time during which the tank is receiving content and is the time the tank is discharging while not receiving any incoming stream.

Step	(min)	(min)	(m³.h⁻¹)	(m³.h⁻¹)	(m³)
Washing	2.5	40	3.8	0.238	0.26
Regeneration	2.5	40	3.8	0.238	0.26
Elution	8	40	3.8	0.760	0.84

In this scenario, preferential crystallization is used in order to purify both *trans*-resveratrol and naringenin. Although previous experiments with this set-up were performed with cooling crystallization,[5] evaporation will be used in this study instead, in order to have a more fair comparison with the previous scenarios. Moreover, it was assumed that only an 80% yield of each compound could be obtained in order to avoid the nucleation of the impurity in each vessel.

In order to operate the preferential crystallization set-up in a continuous mode, the filtration of the crystallized polyphenols in each vessel also has to be performed continuously (only liquid solution is exchanged between the reactors). Because the solid flow-rate needed (0.304 kg.h⁻¹) is so low, small-sized filters would suffice. However, in order to have a fair comparison with the remaining scenarios, it will be assumed that the same type and size of rotary drum filter was acquired (1 m² rotary vacuum drum filter).

Although a more detailed modelling would be needed to describe the crystallization process, a simpler approach was taken in this study. The following equations were defined in order to solve the mass and energy balances:

$$Yield_{resveratrol,s} = 80\% \quad\quad (D5.1)$$
$$Yield_{naringenin,s} = 80\%$$
$$R.\,supersaturation_{resveratrol,II} \leq 5$$
$$R.\,supersaturation_{naringenin,I} \leq 5$$
$$C_{resveratrol,l,I} = C_{s,resv}(ethanol)$$
$$C_{naringenin,l,II} = C_{s,nar}(ethanol)$$

The first two equations state that the desired yield of each polyphenol in the solid phase would be 80%. The third and fourth equations, limit the relative supersaturation of each polyphenol – as an impurity – in the vessel where the "pure" polyphenol is crystallized. For both cases, that value was set as 5. The last two equations just state that the concentration in the liquid phase of each polyphenol at the exit stream of their respective crystallizer, is their solubility – which depends on the ethanol molar fraction. The vapor fraction used in both crystallizers was allowed to be varied in order to minimize the total process ethanol consumption. The vessel crystallizing *trans*-resveratrol had a vapor fraction of 70% and the other one (crystallizing naringenin) had a vapor fraction of 63%.

As in the previous scenarios, both dryers will operate once per month. Despite now the amount of crystals to collect is slightly lower (only 80% yield), the same volume for the silos will be used - 570 L. As it will be shown afterwards, the goal is to take into account the difference in yield in the operating costs and not on the capital investment costs (assumed to be approximately the same).

Appendix E

In this appendix, the detailed calculations of the utility costs are described. For determining those costs, the unit price of electricity, steam, cooling water and dry air has to be given. For that purpose, previously developed models were used.[27] According to those, two main variables are needed to compute the utility costs: the CE PCI index (taken as 550) and the energy cost, considered to be 4.5 \$.GJ^{-1}. The determined costs are indicated in Table E1:

Table E1 – Unit cost for the utilities used in each of the downstream process strategies.

Utility	Unit price
Electricity	0.12 \$.kWh^{-1}
LP steam	0.0127 \$.kg^{-1}
Cooling water	0.0685 \$.m^{-3}
Dry air*	0.0394 \$.Nm^{-3}

* 1.9 Nm^3.s^{-1} and 5 bara

E1. Utility costs scenario 1-1

Heat exchangers

As previously mentioned, the dimensioning of the heat exchangers was performed using a minimum temperature approach of 10°C.

Heat exchanger 1 is the heat exchanger put after the distillation column reboiler. Heat exchanger 2 condenses the vapour stream coming from the evaporative crystallizer and heat exchanger 3 provides the heat to vaporize the liquid in the same crystallizer.

Table E1.1 – Parameters used for the sizing of the heat exchangers included in scenario 1-1. The amount of steam and cooling water used for the utility cost calculation is also indicated.

Heat exchanger	T_{in} (°C)	T_{out} (°C)	Energy (Gcal.h⁻¹)	Area (m²)	Cost (k$)	F_{cool} (kg.h⁻¹)	F_{steam} (kg.h⁻¹)
1	69.6	25	0.013	2.5	0.7	260	-
2	45*	45	0.04	4.6	1.6	1600	-
3	45**	45	0.04	1.1	0.3	-	73

* Cold fluid exits at 35°C

** Steam is condensed at 100°C

Distillation columns

For the first distillation columns, the following heating/cooling duties were determined in Aspen Plus:

Table E1.2 – Data used for the calculation of the needed quantities of cooling water and steam in the distillation columns used in scenario 1-1. The heating (cooling) duties and the temperatures in the condenser were obtained from Aspen Plus. The overall heat transfer coefficient was defined as mentioned in Table 6.1 and the condenser area was calculated by using the minimum approach temperature of 10°C.

Distillation column 1				
Piece	Heating duty (Gcal.h⁻¹)	Temperature (°C)	F_{cool} (kg.h⁻¹)	F_{steam} (kg.h⁻¹)
Condenser	-0.0687	68.6	1400	-
Reboiler	0.0825	-	-	153
Distillation column 2				
Piece	Heating duty (Gcal.h⁻¹)	Temperature (°C)	F_{cool} (kg.h⁻¹)	F_{steam} (kg.h⁻¹)
Condenser	-0.301	61.7	7200	-
Reboiler	0.605	-	-	1100

For the evaporative crystallizer a heating duty of 0.0394 Gcal.h⁻¹ was determined.

Electricity

In every scenario, a disk stack centrifuge was used in order to separate the cells from the fermentation broth. The electrical power consumption, obtained from the supplier, was determined to be 18 kW. Thus, for an annual operation, the consumption amounts to 147 000 kW.h.

For calculating the electricity consumption for the centrifugal pumps, an average flow-rate of 3.8 $m^3.h^{-1}$ and a pressure drop of 1 bar were defined. The power consumption per pump was then determined using the following equation:

(E2)

$$P = \frac{q \cdot \rho \cdot g \cdot h}{\eta \cdot 3.6 \times 10^6}$$

Where q is the flow-rate, ρ the liquid density (taken as the one of water), the gravity acceleration, g is the differential head and is the pump efficiency (defined as 60%).

For each pump, 0.17 kW of electricity are consumed. In this scenario, which includes 11 pumps, approximately 15000 kW.h are consumed.

Concerning the contribution of the mixing in the holding tanks, an average electricity consumption of 1 $kW.m^{-3}$ and an average liquid volume of 1 m^3 were assumed. The total consumption for this scenario was calculated to be 195 000 kW.h.

Dry air for the tray dryer

The flow-rate of dry air was already determined in the main body of this manuscript, and amounted to 241 000 $Nm^3.y^{-1}$. Using the utility costs in Table D1, the total yearly cost for this scenario is 9.5 $k\$.y^{-1}$.

E2. Utility costs scenario 1-2

Heat exchangers

Heat exchanger 1 is the heat exchanger put after the distillation column condenser. Heat exchanger 2 condenses the vapour stream coming from the evaporative crystallizer and heat exchanger 3 provides the heat to vaporize the liquid in the same crystallizer.

Table E2.1 – Parameters used for the sizing of the heat exchangers included in scenario 1-2. The amount of steam and cooling water used for the utility cost calculation is also indicated.

Heat exchanger	T_{in} (°C)	T_{out} (°C)	Energy (Gcal.h^{-1})	Area (m²)	Cost (k\$)	F_{cool} (kg.h^{-1})	F_{steam} (kg.h^{-1})
1	79.1	25	0.01	1.9	0.5	170	-
2	45*	45	0.04	4.4	1.5	1500	-
3	45**	45	0.04	1.2	0.3	-	77

* Cold fluid exits at 35°C

** Steam is condensed at 100°C

Distillation column

Table E2.2 - Data used for the calculation of the needed quantities of cooling water and steam in the distillation column used in scenario 1-2. The heating (cooling) duties and the temperatures in the condenser were obtained from Aspen Plus. The overall heat transfer coefficient was defined as mentioned in Table 6.1 and the condenser area was calculated by using the minimum approach temperature of 10°C.

Distillation column				
Piece	Heating duty (Gcal.h^{-1})	Temperature (°C)	F_{cool} (kg.h^{-1})	F_{steam} (kg.h^{-1})
Condenser	-0.13	79.1	2300	-
Reboiler	0.15	-	-	270

Electricity

The electricity costs were calculated as indicated in scenario 1-1. In this case, however, 12 pumps and 6 holding tanks were considered. The total consumption amounts to 210 000 kW.h.

Dry air for the tray dryer

The costs with dry air for this scenario are the same as in scenario 1-1.

E3. UTILITY COSTS SCENARIO 2-1

Heat exchangers

Heat exchanger 1 and 2 are the heat exchangers put after each of the crystallizers. Heat exchanger 3 and 4 are the ones associated with the evaporative crystallizers.

Table E3.1 – Parameters used for the sizing of the heat exchangers included in scenario 2-1. The amount of steam and cooling water used for the utility cost calculation is also indicated.

Heat exchanger	T_{in} (°C)	T_{out} (°C)	Energy (Gcal.h^{-1})	Area (m²)	Cost (k$)	F_{cool} (kg.h^{-1})	F_{steam} (kg.h^{-1})
1	45*	45	0.02	2.4	0.65	830	-
2	45*	45	0.04	5.0	1.8	1700	-
3	45**	45	0.02	0.7	0.12	-	44
4	45**	45	0.044	1.3	0.3	-	82

* Cold fluid exits at 35°C

** Steam is condensed at 100°C

Distillation columns

Table E3.2 - Data used for the calculation of the needed quantities of cooling water and steam in the distillation columns used in scenario 2-1. The heating (cooling) duties and the temperatures in the condenser were obtained from Aspen Plus. The overall heat transfer coefficient was defined as mentioned in Table 6.1 and the condenser area was calculated by using the minimum approach temperature of 10°C.

Distillation column 1				
Piece	Heating duty (Gcal.h^{-1})	Temperature (°C)	F_{cool} (kg.h^{-1})	F_{steam} (kg.h^{-1})
Condenser	-0.12	68.5	2500	-
Reboiler	0.41	-	-	760
Distillation column 2				
Piece	Heating duty (Gcal.h^{-1})	Temperature (°C)	F_{cool} (kg.h^{-1})	F_{steam} (kg.h^{-1})
Condenser	-0.0005	68.6	10.1	-
Reboiler	0.004	-	-	7.2

Electricity

The electricity costs were calculated as indicated in scenario 1-1. In this case, however, 12 pumps and 6 holding tanks were considered. The total consumption amounts to 210 000 kW.h.

Dry air for the tray dryer

The costs with dry air for this scenario are the double as in scenario 1-1, due to the fact that the try dryer is operated twice per month (one product more is being produced).

E4. Utility costs scenario 2-2

Heat exchangers

Heat exchanger 1 and 2 are the heat exchangers put after each of the crystallizers. Heat exchanger 3 and 4 are the ones associated with the evaporative crystallizers.

Table D4.1 – Parameters used for the sizing of the heat exchangers included in scenario 2-2. The amount of steam and cooling water used for the utility cost calculation is also indicated.

Heat exchanger	T_{in} (°C)	T_{out} (°C)	Energy (Gcal.h⁻¹)	Area (m²)	Cost (k$)	F_{cool} (kg.h⁻¹)	F_{steam} (kg.h⁻¹)
1	79.6	25	0.019	3.5	1.1	311	-
2	45*	45	0.02	4.8	1.7	1700	-
3	45*	45	0.04	4.8	1.7	1700	-
4	45**	45	0.045	1.3	0.3	-	83
5	45**	45	0.043	1.2	0.3	-	80

* Cold fluid exits at 35°C

** Steam is condensed at 100°C

Distillation column

Table E4.2 - Data used for the calculation of the needed quantities of cooling water and steam in the distillation column used in scenario 2-2. The heating (cooling) duties and the temperatures in the condenser were obtained from Aspen Plus. The overall heat transfer coefficient was defined as mentioned in Table 6.1 and the condenser area was calculated by using the minimum approach temperature of 10°C.

Distillation column 1				
Piece	Heating duty (Gcal.h⁻¹)	Temperature (°C)	F_{cool} (kg.h⁻¹)	F_{steam} (kg.h⁻¹)
Condenser	-0.177	79.5	3000	-
Reboiler	0.22	-	-	400

Electricity

The electricity costs were calculated as indicated in scenario 1-1. In this case, however, 21 pumps and 13 holding tanks were considered. The total consumption amounts to 280 000 kW.h.

Dry air for the tray dryer

The costs with dry air for this scenario are the double as in scenario 1-1, due to the fact that the try dryer is operated twice per month (one product more is being produced).

E5. Utility costs scenario 2-3

Heat exchangers

Heat exchanger 1 and 2 are the heat exchangers put after each of the crystallizers. Heat exchanger 3 and 4 are the ones associated with the evaporative crystallizers.

Table E5.1 – Parameters used for the sizing of the heat exchangers included in scenario 2-3. The amount of steam and cooling water used for the utility cost calculation is also indicated.

Heat exchanger	T_{in} (°C)	T_{out} (°C)	Energy (Gcal.h^{-1})	Area (m²)	Cost (k$)	F_{cool} (kg.h^{-1})	F_{steam} (kg.h^{-1})
1	79.0	25	0.027	5.0	1.8	450	-
2	45*	45	0.16	18	10	6300	-
3	45*	45	0.14	16	8.6	5500	-
4	45**	45	0.16	4.6	1.6	-	300
5	45**	45	0.14	4.0	1.3	-	270

* Cold fluid exits at 35°C

** Steam is condensed at 100°C

Distillation column

Table E5.2 - Data used for the calculation of the needed quantities of cooling water and steam in the distillation column used in scenario 2-3. The heating (cooling) duties and the temperatures in the condenser were obtained from Aspen Plus. The overall heat transfer coefficient was defined as mentioned in Table 6.1 and the condenser area was calculated by using the minimum approach temperature of 10°C.

Distillation column 1				
Piece	Heating duty (Gcal.h^{-1})	Temperature (°C)	F_{cool} (kg.h^{-1})	F_{steam} (kg.h^{-1})
Condenser	-0.27	79.0	4500	-
Reboiler	0.32	-	-	600

Electricity

The electricity costs were calculated as indicated in scenario 1-1. In this case, however, 22 pumps and 11 holding tanks were considered. The total consumption amounts to 265 000 kW.h.

Dry air for the tray dryer

The costs with dry air for this scenario are the double as in scenario 1-1, due to the fact that the try dryer is operated twice per month (one product more is being produced).

REFERENCES

1 Goszcz, K.; Deakin, S. J.; Duthie, G. G.; Stewart, D.; Leslie, S. J.; Megson, I. L., Antioxidants in Cardiovascular Therapy: Panacea or False Hope? *Front Cardiovasc Med.* **2015**, 2, 29.

2 Figueira, I.; Menezes, R.; Macedo, D.; Costa, I.; dos Santos, C. N., Polyphenols Beyond Barriers: A Glimpse into the Brain. *Current Neuropharmacology.* **2017**, 15, (4), 562-594.

3 Dudnik, A.; et al., BacHBerry: BACterial Hosts for production of Bioactive phenolics from bERRY fruits. *Phytochemistry Reviews.* **2017**, 17, (2), 291-326.

4 Braga, A.; Silva, M.; Oliveira, J.; Silva, R.; Ferreira, P.; Ottens, M.; Rocha, I.; Faria, N., An adsorptive bioprocess for production and recovery of resveratrol with Corynebacterium glutamicum. *Journal of Chemical Technology & Biotechnology.* **2017**.

5 Silva, M.; Vieira, B.; Ottens, M., Preferential crystallization for the purification of similar hydrophobic polyphenols. *Journal of Chemical Technology and Biotechnology.* **2018**, 93, (7), 1997-2010.

6 Myerson, A., *Handbook of Industrial Crystallization*; 2nd Edition ed.; Butterworth-Heinemann: 2002.

7 Silva, M.; Ottens, M. *BacHBerry Project Report D7.3. Techno-economic aspects of optimal fermentation based on large-scale process for phenolics production*; http://www.bachberry.eu, 2016.

8 Silva Ferreira, M.; Mouthaan, M.; Pereira, P. *GDP report: Techno-Economic Evaluation of Polyphenol Production and Purification on Industrial Scale*; TU Delft: 2016.

9 Felinger, A.; Guiochon, G., Comparison of the kinetic models of linear chromatography. *Chromatographia.* **2004**, 60, S175-S180.

10 Chung, S. F.; Wen, C. Y., Longitudinal Dispersion of Liquid Flowing through Fixed and Fluidized Beds. *Aiche Journal.* **1968**, 14, (6), 857-&.

11 Slater, M. J., *The Principles of Ion Exchange Technology*; Butterworth-Heinemann Lda.: Linacre House, Jordan Hill, Oxford OX2 8DP, 1991.

12 Guiochon, G., Attila Felinger, and Dean GG Shirazi, *Fundamentals of Preparative and Nonlinear Chromatography*; Academic Press: San Diego, CA, USA, 2006.

13 Sandler, S. I., *Chemical, biochemical, and engineering thermodynamics*; 5th Edition ed.; John Wiley & Sons: Hoboken, NJ, USA, 2017.

14 Peters, M. S.; Timmerhaus, K. D.; West, R. E., *Plant design and economics for chemical engineers*; 5th Edition ed.; McGraw-Hill: New York, USA, 2003.

15 Matches Matches' Process Equipment Cost Estimates. http://www.matche.com/equipcost/Default.html *(February 2018)*.

16 *Albright's chemical engineering handbook*; CRC Press: Boca Raton, FL, USA, 2008.

17 Henley, E. J.; Seader, J. D.; Roper, D. K., *Separation process principles*; Wiley: 2011.

18 ICIS Indicative Chemical Prices A-Z. https://www.icis.com/chemicals/channel-info-chemicals-a-z/ (3 September 2018).

19 M. Walas, S., Costs of Individual Equipment. In *Chemical Process Equipment*, Butterworth-Heinemann, Ed. Elsevier Inc.: 1988.

20 Schouten, N.; van der Ham, L. G.; Euverink, G. J.; de Haan, A. B., Selection and evaluation of adsorbents for the removal of anionic surfactants from laundry rinsing water. *Water Res.* **2007**, 41, (18), 4233-41.

21 Green, D.; Perry, R., *Perry's Chemical Engineers' Handbook, Eighth Edition*; McGraw-Hill Education: 2007.

22 Chen, C.-C.; Crafts, P. A., Correlation and prediction of drug molecule solubility in mixed solvent systems with the nonrandom two-liquid segment activity coefficient (NRTL-SAC) model. *Industrial & engineering chemistry research.* **2006**, 45, (13), 4816-4824.

23 Sun, X.; Peng, B.; Yan, W., Measurement and correlation of solubility of trans-resveratrol in 11 solvents at T=(278.2, 288.2, 298.2, 308.2, and 318.2)K. *The Journal of Chemical Thermodynamics.* **2008**, 40, (4), 735-738.

24 Baker, C. G. J., *Industrial Drying of Foods*; 1st Edition ed.; Springer US: 1997.

25 Peskin, A. P.; Rudge, S. R., Optimization of Large-Scale Chromatography for Biotechnological Applications. *Applied Biochemistry and Biotechnology.* **1992**, 34-5, 49-59.

26 Sun, X. L.; Shao, Y. D.; Yan, W. D., Measurement and Correlation of Solubilities of trans-Resveratrol in Ethanol plus Water and Acetone plus Water Mixed Solvents at Different Temperatures. *Journal of Chemical and Engineering Data.* **2008**, 53, (11), 2562-2566.

27 Ulrich, G. D.; Vasudevan, P. T. How to Estimate Utility Costs. https://terpconnect. umd.edu/~nsw/chbe446/HowToEstimateUtilityCosts-UlrichVasudevan2006.pdf (18 October 2016).

7

Conclusions and outlook

This thesis dealt with the study of different downstream process strategies for the recovery and purification of polyphenols from a fermentation broth.

The work performed in this thesis aimed to improve the following points:

- Provide the necessary thermodynamic models for the description of polyphenol equilibrium data (e.g., solubility, liquid-liquid partition, adsorption);

- Present systematic studies that enable the selection of the proper solvents and adsorbents for different purification tasks involving polyphenols;

- Provide a wide spectrum of different downstream process alternatives (e.g., adsorption, liquid extraction, preferential crystallization) that can be applied to different polyphenols and fermentation conditions under slight modifications.

Liquid-liquid extraction was the first option explored (chapter 2). With the lack of polyphenol partition data in the literature (most of the data reports to the octanol/water partition coefficient), there was a need to efficiently screen a large database of solvents. For that purpose, thermodynamic models like UNIFAC or NRTL-SAC are very useful tools. One of the issues with the UNIFAC model is the problem with describing polyphenols. Not only there is a lack of parameters describing specific chemical groups present in those molecules (MPP-UNIFAC came to correct this), but treating polyphenols with group-contribution models might not be the best option. This is mostly because those molecules present a lot of resonance and have many functional groups attached to their aromatic

rings. Those factors may change the partial charge associated with every "chemical group" in the molecule, meaning that the assumption of a molecule-independent energy interaction parameter might not be as valid as in other, simpler molecules.

NRTL-SAC comes then as a more robust option, although at the expense of a fully predictive activity coefficient. The NRTL-SAC model proved to be very suitable not only to describe the solubility trend, but also the liquid-liquid partition coefficients. One of the major issues was with the description of naringin, a glycosylated polyphenol. Since it does not form a crystalline structure, the thermodynamic equation relating solubility with melting temperature and melting enthalpy, is not valid anymore. In that case, a more detailed model should be used, taking into account that some molecules do not have a defined melting point.

Another explored possibility for the purification of polyphenols was reverse-phase adsorption. The study performed in chapter 3 – that focused on food-grade resins – meant to provide a new systematic study on which resins could be applied to the recovery and purification of polyphenols. Given that non-functionalized resins, like the XAD series, might not provide enough selectivity in more challenging purification scenarios, the effect of functional groups (e.g., pyridine, imidazole) attached to same polystyrenic backbone was investigated. The obtained results suggest that those chemical groups might interact with polyphenols by hydrogen bonding, providing an interaction mechanism similar to what is displayed by mixed-mode resins. In this case, adsorption affinity is obtained through a combined effect of hydrophobicity and the degree of hydrogen bonding (related with the number of hydroxyl groups in each polyphenol). Not only high affinities could be obtained with such resins, as elution was also proved to be possible by acidifying the medium and decreasing the hydrogen bonding strength (Chapter 3).

In chapter 4, the same technique – reverse-phase adsorption – was studied. However, in this case, the goal was to test it in a continuous recovery process, integrating fermentation with the adsorption column, mediated by an ultrafiltration unit. The results showed that a lower titer

7

was obtained when the product (*trans*-resveratrol) was continuously adsorbed. Nonetheless, the ratio of extracellular product to total product increased from 75% to 95%. This observation was justified by the fact that hydrophobic polyphenols tend to accumulate in the cell membrane (they have high lipophilicity) and by continuously removing them from the broth, a driving force for their excretion to the extracellular medium is created. One of the indicated reasons for the total production to be lower might be associated with the co-adsorption (although much weaker) of the precursor *p*-coumaric acid, essential for the synthesis of *trans*-resveratrol.

Preferential crystallization was also investigated as a possible unit operation for the purification of polyphenols (chapter 5). The rationale behind this technique is to promote purification based on the different crystallization kinetics of the two similar polyphenols, by the usage of seed crystals of the desired compound.

Using this unit operation lead to very pure products – naringenin and *trans*-resveratrol - in their solid forms (almost 100% purity), although still at the expense of some yield (maximum obtained was 81% for *trans*-resveratrol). A better approach was tried by coupling two crystallization vessels, in order to maximize the minimum yield. However, some challenges were observed: needle crystals were able to pass through the inlet filter (despite being larger than their pore size); the presence of an inline filter led to the formation of a solid cake on its surface, leading to increased pressure drop and yield loss; when those unpredicted factors came into play, the applied controls (temperature and flow-rates), were not the optimal ones, since they were based on model predictive control. Probably, among all the scenarios studied in this thesis, this is the one where there is much more room for further investigation and improvement. Still, when using the coupled vessels, the obtained yields were 63% for naringenin and 44% for *trans*-resveratrol, both with almost complete purity.

The final part of this thesis focused on the economical evaluation of the different downstream process strategies for the purification of model polyphenols from a typical *C. glutamicum* fermentation broth, under

7

aerobic conditions. This analysis, which assumed a titer of 100 mg.L^{-1} (based on current available data), led to the following conclusions:

The utility cost was the most important factor when distinguishing different process alternatives;

- The energy cost associated with solvent recovery, through distillation, was among the utilities (steam, in this case), the most important parameter to take into account. The higher number of distillation columns and boilup rate in the case of the scenarios involving liquid-extraction, makes them the most expensive option when only taking the cost of steam for distillation into account.

- If a more challenging purification scenario is intended, and adsorption is the desired approach, only the previously tested functionalized resins can provide the desired selectivity. In that case, the annual costs with resin (around 150 k\$.y^{-1} for a 3 ton.y^{-1} production rate), was found to be a very important factor. Owing to that, this approach is expected to be the most costly. When using preferential crystallization, the costs were dominated by the needed steam for the evaporative crystallizers. For all these reasons, liquid extraction was found to be a cheaper option. However, in the cases where crystallization can be performed by cooling the medium (as in the case of preferential crystallization for trans-resveratrol and naringenin), this scenario becomes the preferred one. Moreover, the usage of more harmful organic solvents – which should be food-grade and present low toxicity – is avoided.

Although this thesis focused on the assumption of a relatively low polyphenol titer (in the 100 mg.L^{-1} range), it is very likely that if the product is meant to sell as nutraceutical, that concentration has to increase in order to obtain an interesting return on investment. That change in the fermentation conditions might influence the optimal downstream process design. For example, if a titer in the g.L^{-1} range is reached, *in-situ* crystallization (inside the fermenter) might be a better option. Moreover, if no continuous product removal is applied during the fermentation, most of the polyphenols, being highly hydrophobic, will spontaneously precipitate inside the vessel. Recovering the product from the solid phase then becomes unavoidable. Techniques

7

such as liquid-liquid extraction or reverse-phase adsorption then only make sense if applied in an integrated production/purification process or if they are intended as a polishing step, after the solid-liquid separation.

The major goal of this work was to investigate different alternatives to the recovery and purification of polyphenols from a fermentation broth. However, being downstream process development highly product-dependent and fermentation-dependent (e.g., titer dependence), the different scenarios proposed here should be further explored, optimized and compared. Nonetheless, we are confident that with this work, new approaches and new tools can help polyphenols and similar metabolites to reach market sooner by means of cheaper and more environmentally-friendly processes.

7

Acknowledgements

The development and writing of this thesis was only possible because of the support, scientific or not, of many people.

In the first place, I would have never have arrived at this point of my life without my family, namely my parents and my brother. They were the ones always supporting me in every situation and – most importantly – passing values on to me that I am proud to keep. Those are infinitely more important than any education degree.

A special word also to all the teachers I had during my life - I learned with all of them. If anyone of them ends up finding this thesis, I hope they are aware that they are partly responsible for what I am today – as a person and engineer/scientist.

My acknowledgments then move to the moment I started my PhD. Obviously, I have to give a special word to my promotor, Marcel Ottens. He was the one deciding to hire me for this project and believing I would end up doing a good job. Moreover I must specially thank him for allowing me to develop and test the idea that ended up becoming the fifth chapter of this thesis.

I need also to thank my promotor, Luuk van der Wielen, for the ideas exchanged during our meetings, especially in the beginning of this PhD when the tackling approaches for this project were still being defined.

During this thesis, I also had the luck of working with master students and PDEng's. Joan Cortada-García, Leydi Castellanos, Briana Vieira, Tiago Silva (I kind of adopted you :p) (master students at the time) and Maikel Mouthaan, Marcelo Ferreira and Pedro Pereira (PDEng's at that time), they all helped shape this work. Thank you for your commitment to our projects and for all the ideas that we exchanged.

From the people that were directly involved with this project, I move to all the persons that contributed to the nice atmosphere I lived in the BPE group. Not only the people who I shared the office with: David, Shima,

Rita, Joan, Floor, but also all the other group members who I hope can now call friends: Silvia, Joana (we started this journey at the same time!), Carlos, Mónica, Bianca.

Still within the BPE group, I wanted to thank all the staff that helped in the most diverse situations: Max ("Bonjour!"), Stef and Song (I'm glad you came to our group!).

One of my last references, but not less important (for sure not), goes to all my friends living in Portugal. You made my trips back to Portugal much nicer, whenever I needed to reload batteries and spend very good moments!

The last reference goes to Ana, my girlfriend. I put it in last, because I needed to make it special. Now, they will be the last words I will have written in this thesis. I told you more than one time that I would have never finished my PhD if I did not have you. If every time I had issues, feeling tired or not motivated, I did not have someone I loved sharing the same house, I would have probably quitted or, at least, the work I have done here would not make me as proud.

I also did not want to finish leaving with the feeling that "behind a great man there is always a great woman", as that kind of implies always a secondary role for women. I want you to know that the way you supported me, I will always support you, so you can achieve the goals you want and deserve. Your happiness will always be my happiness.

List of Publications

Full papers

Silva, Marcelo, Joan Cortada García, and Marcel Ottens. "Polyphenol Liquid-Liquid Extraction Process Development using NRTL-SAC." *Industrial & Engineering Chemistry Research* (2018).

Silva, Marcelo, Leydi Castellanos, and Marcel Ottens. "Capture and purification of polyphenols using functionalized hydrophobic resins." *Industrial & engineering chemistry research* 57.15 (2018): 5359-5369.

Braga, Adelaide, et al. "An adsorptive bioprocess for production and recovery of resveratrol with Corynebacterium glutamicum." *Journal of Chemical Technology & Biotechnology* 93.6 (2018): 1661-1668.

Silva, Marcelo, Briana Vieira, and Marcel Ottens. "Preferential crystallization for the purification of similar hydrophobic polyphenols." *Journal of Chemical Technology & Biotechnology* 93.7 (2018): 1997-2010.

Dudnik, Alexey, et al. "BacHBerry: BACterial Hosts for production of Bioactive phenolics from bERRY fruits." *Phytochemistry Reviews* 17.2 (2018): 291-326.

Duarte, Pedro, et al. "Liquid mixtures involving hydrogenated and fluorinated chains:(p, ρ, T, X) surface of (ethanol+ 2, 2, 2-trifluoroethanol), Experimental and Simulation." *The Journal of Physical Chemistry B* 117.33 (2013): 9709-9717.

Conference papers

Tellen D., Stamati I., **Silva M.**, Logist F., Van Impe, Jan F.M. *Optimal experiment design for model discrimination of nonlinear biochemical systems using the sigma point method*, European Symposium on Computer Aided Process Engineering (ESCAPE24) (2014).

Curriculum Vitae

Marcelo David Henriques da Silva was born in Lisbon, Portugal in 1989. After completing high-school in Queluz, Lisbon in 2007, he started his studies in Biological Engineering at Instituto Superior Técnico, Lisbon in that same year. During his degree, he worked at Centro de Química Estrutural (CQE) with prof. Eduardo Filipe, studying physical properties of fluorinated molecules using molecular dynamics.

Between September 2012 and April 2013 he wrote his Master thesis in Leuven, Belgium under the supervision of dr. Filip Logist and Prof. Jan Van Impe. The work concerned the application of optimal experimental design to the discrimination of two microbial growth models (CTMI and aCTMI).

After completing his Master's degree, he worked between Sep. 2013 – Dec. 2013 at Laboratório Nacional de Energia e Geologia (LNEG), Lisbon. His research, under the supervision of dr. Isabel Marques, was related with the anaerobic digestion of microalgae for the production of biogas.

In Feb. 2014 he came to the Netherlands to start his PhD position at the Bioprocess Engineering group of the Technical University of Delft, under Dr. ir. Marcel Ottens and Prof. dr. ir. Luuk van der Wielen. The thesis, inserted in the BacHBerry European Project, concerned the study and evaluation of different downstream process strategies for the purification of polyphenols, produced by fermentation.